INSTITUTO TECNOLOGICO Y DE ESTUDIOS SUPERIORES DE MONTERREY

MONTERREY CAMPUS

GRADUATE PROGRAM IN MECHATRONICS AND INFORMATION TECHNOLOGIES

TECNOLÓGICO DE MONTERREY

COMPARISON OF MAGNETO-RHEOLOGICAL DAMPER MODELS

THESIS

PRESENTED IN PARTIAL FULFILLMENT OF THE REQUIREMENTS FOR THE DEGREE OF:

MASTER OF SCIENCE IN AUTOMATION

BY:

JAVIER ANTONIO RUIZ CABRERA

MONTERREY, NUEVO LEON, MEXICO DECEMBER 2010

INSTITUTO TECNOLOGICO Y DE ESTUDIOS SUPERIORES DE MONTERREY

MONTERREY CAMPUS

GRADUATE PROGRAM IN MECHATRONICS AND INFORMATION TECHNOLOGIES

TECNOLÓGICO DE MONTERREY

COMPARISON OF MAGNETO-RHEOLOGICAL DAMPER MODELS

THESIS

PRESENTED IN PARTIAL FULFILLMENT OF THE REQUIREMENTS FOR THE DEGREE OF:

MASTER OF SCIENCE IN AUTOMATION

BY:

JAVIER ANTONIO RUIZ CABRERA

MONTERREY, NUEVO LEON, MEXICO DECEMBER 2010

INSTITUTO TECNOLÓGICO Y DE ESTUDIOS
SUPERIORES DE MONTERREY

MONTERREY CAMPUS

GRADUATE PROGRAM IN MECHATRONICS AND
INFORMATION TECHNOLOGIES

COMPARISON OF MAGNETO-RHEOLOGICAL DAMPER MODELS

THESIS

PRESENTED IN PARTIAL FULFILLMENT OF THE REQUIREMENTS FOR THE
DEGREE OF:

MASTER OF SCIENCE IN AUTOMATION

BY

JAVIER ANTONIO RUIZ CABRERA

MONTERREY, NUEVO LEÓN, MÉXICO, DECEMBER 2010

Comparison of Magneto-Rheological Damper Models

BY

Javier Antonio Ruiz Cabrera

THESIS

Presented to the Graduate Program in Mechatronics and Information Technologies

This Thesis is a partial requirement for the degree of

MASTER OF SCIENCE IN AUTOMATION

INSTITUTO TECNOLÓGICO Y DE ESTUDIOS SUPERIORES DE MONTERREY

MONTERREY, NUEVO LEÓN, MÉXICO, DECEMBER 2010

Dedication

A Dios:
A quien debo todos mis logros.

A mis papás:
Quienes siempre me enseñaron el camino correcto.
Gracias por su amor y apoyo incondicional.
Mis logros son un reflejo de su trabajo.

A Valerie:
Mi amada compañera.
Gracias por ser parte de mis sueños.
Tu amor me da fuerzas para conseguir nuestras metas.

A toda mi familia:
Porque puedo contar con ustedes.
Siempre los llevo en el corazón.

Acknowledgements

I would like to thank Dr. Rubén Morales, whose encouragement and valuable guidance enabled me to complete my research work. In addition, I would like to offer my regards to Jorge Lozoya for providing the experimental data for this work and to Dr. Luis Garza and Dr. Ricardo Ramírez for their time and contributions to the present report.

Lastly, I thank all of those who supported me in any respect during the completion of my degree and final research. Thanks to my fellow classmates for their invaluable friendship and the unforgettable times we shared.

- Javier Antonio Ruiz Cabrera

Abstract

The design of automotive suspension systems is concerned with ride comfort and handling performance of the vehicle. In the last decade, semi-active suspension systems have been greatly analyzed for automotive applications as they offer the reliability of passive devices, but maintain the versatility and adaptability of active systems. Semi-active Magneto-Rheological (*MR*) dampers present a viable choice for suspension systems. In an *MR* damper, the damping characteristics can be modified with the application of a magnetic field to the coil inside the tube of the device. Although *MR* dampers are greatly promising for the control of vehicle suspension systems, their major drawback lies on their non-linear and hysteretic behavior. This behavior makes it a challenge to develop a model for the system. Furthermore, the first step in designing a control strategy for a suspension system is modeling the behavior of the damper in an accurate manner.

The present research is focused on the modeling of an *MR* damper. The problem statement is centered on what type of model of an *MR* damper can be developed, which can accurately predict the highly non-linear behavior of the system and can be optimal for online control. For this purpose, various sets of experimental data were obtained from an industrial *MR* damper. Then, four state-of-the-art *MR* damper models were trained, analyzed and compared using quantitative and qualitative techniques. Each of the models was selected from four main modeling approaches, phenomenological, semi-phenomenological, black-box, and fuzzy-based. By the end of the research, a novel model for an *MR* damper was presented, which combined fuzzy techniques with semi-phenomenological modeling. The results showed that the proposed structure was able to accurately predict the behavior of the *MR* damper and was suitable for control purposes. The final results can be greatly applicable to the automotive industry, where better comfort and handling control systems could be developed. In addition, the results could be useful to the vast number of industries and applications where *MR* dampers are employed.

Contents

List of Tables

Table 1. Description of variables. The variables are shown in order of appearance.

Variable	Description	Model	Units
$x(t)$	Linear displacement of the *MR* damper		In
$\dot{x}$(t)	Linear velocity of the *MR* damper		In/s
$\ddot{x}$(t)	Linear acceleration of the *MR* damper		In/s^2
$i(t)$	Electric current on the coil of the *MR* damper		A
$V(t)$	*MR* damper voltage		V
$F(t)$	*MR* damper output force		lbf
$\hat{F}(t)$, F_{est}	Estimated *MR* damper force		lbf
$\ddot{F}(t)$	Second derivative of $F(t)$		lbf/s^2
$\dot{F}(t)$	First derivative of $F(t)$		lbf/s
$F^5(t)$	Fifth power of $F(t)$		lbf^5
$F^3(t)$	Third power of $F(t)$		lbf^3
κ	Discrete sample		-
T	Total number of discrete samples		-
p_j	Parameters for the model	Eq. 2.1	-
s_j	Parameters for the model	Eq. 2.2	-
c_0	Coefficient for the viscous damping at large velocities	Eq. 2.2	lbf · s/in
c_1	Damping coefficient for the roll-off at low velocities	Eq. 2.2	lbf · s/in
k_0	Stiffness control coefficient for large velocities	Eq. 2.2	N/cm
k_1	Accumulator stiffness coefficient	Eq. 2.2	N/cm
x_0	Initial displacement of spring k_1	Eq. 2.2	N/cm
$z(t), y(t)$	Evolutionary coefficients for the model	Eq. 2.2	-
A_1	Dynamic yield force coefficient	Eq. 2.3	-
A_2	Post-yield viscous damping coefficient	Eq. 2.3	-
A_3	Pre-yield viscous damping coefficient	Eq. 2.3	-
V_0	Hysteretic critical velocity coefficient	Eq. 2.3	-
X_0	Hysteretic critical displacement coefficient	Eq. 2.3	-
c_w	Viscous coefficient for the model	Eq. 2.4	lbf · s/in
k_w	Stiffness coefficient for the model	Eq. 2.4	lbf/in
$z_w(t)$	Hysteretic variable	Eq. 2.4	-
α	Scale factor of hysteresis	Eq. 2.4	-
f_0	Damper force offset coefficient	Eq. 2.4	-
β	Hysteretic slope coefficient	Eq. 2.4	-
δ	Hysteretic width coefficient	Eq. 2.4	-
L_{jp}	Positive acceleration parameters for the model	Eq. 2.5	-
L_{jn}	Negative acceleration parameters for the model	Eq. 2.5	-
k_L	Stiffness coefficient	Eq. 2.5	lbf/in
$F_p(t)$	Positive acceleration *MR* damper force	Eq. 2.5	lbf
$F_n(t)$	Negative acceleration *MR* damper force	Eq. 2.5	lbf
f_e	Coefficient for the pre-load of the accumulator	Eq. 2.6	-
c_b	Coefficient for the viscous damping	Eq. 2.6	lbf · s/in

Table 2. Description of variables continued

Variable	Description	Model	Units
f_y	Yielding force coefficient	Eq. 2.6	lbf
k_b	Shape coefficient for the model	Eq. 2.6	-
$\dot{x}_0$	Hysteretic velocity coefficient	Eq. 2.6	in/s
m	Virtual mass coefficient for the model	Eq. 2.6	lb
b_{1j}, b_{2j}	Coefficients for the model	Eq. 2.7	-
F_{k-j}	Discrete value of the force of the *MR* damper at sample $k-j$		lbf
x_{k-j}	Discrete value of the displacement of the *MR* damper at sample $k-j$		in
$\dot{x}_{k-j}$	Discrete value of the velocity of the *MR* damper at sample $k-j$		in/s
a_j	Coefficients for the model	Eq. 2.8	-
L_{INj}	Input layer neurons of the neural network	Fig. 2.4	-
L_{1j}	First hidden layer neurons of the neural network	Fig. 2.4	-
L_{2j}	Second hidden layer neurons of the neural network	Fig. 2.4	-
L_{Oj}	Output layer neurons of the neural network	Fig. 2.4	-
M_{Aj}	Fuzzy sets for the first input of the fuzzy-based model	Fig. 2.6	-
M_{Bj}	Fuzzy sets for the second input of the fuzzy-based model	Fig. 2.6	-
M_{Cj}	Fuzzy sets for the third input of the fuzzy-based model	Fig. 2.6	-
$f_j(x, \dot{x}, i, t)$	Output functions of the fuzzy model	Fig. 2.6	-
W_j	Degree of fitness of the fuzzy rules	Fig. 2.6	-
Wn_j	Normalized degree of fitness of the fuzzy rules	Fig. 2.6	-
o_j, q_j, r_1, u_j	Output parameters of the model	Fig. 2.6	-
$e(t)$	Uniformly distributed white noise	Eq. 3.1	-
N_{ICPS}	Number of constant amplitude samples	Eq. 3.1	-
μ	Normally distributed random number	Eq. 3.2	-
α	Probability variable	Eq. 3.2	-
$S(f)$	Power spectral density of the elevation of the road profile	Eq. 3.3	Hz
C_r	Roughness coefficient of the road profile	Eq. 3.3	$ft^2/cycles/ft$
N_{cr}	Constant coefficient corresponding to the roughness of the road profile	Eq. 3.3	-
v_c	Speed of the vehicle	Eq. 3.3	in/s
ω_x	Number of cycles per feet	Eq. 3.3	cycles/ft
ϕ_j	Random phase angle normally distributed between 0 - 2π	Eq. 3.4	-
ω_j	Frequency within the interval of $S(f)$	Eq. 3.4	-
$\Delta\omega$	Frequency increment	Eq. 3.4	-
ω_{min}	Minimum frequency for the spectrum	Eq. 3.4	-
ω_{max}	Maximum frequency for the spectrum	Eq. 3.4	-
N_f	Total number of frequency intervals within $\omega_{min} - \omega_{max}$	Eq. 3.4	-
$G_{LPF}(s)$	Transfer function for the low-pass filter	Eq. 3.5	-
M_{Fj}	Fuzzy sets for the non-linear fuzzy-based model	Fig. 4.13	-
W_{Fj}	Degree of fitness of the fuzzy rules	Fig. 4.13	-
$f_j(x, \dot{x}, t)$	Output functions of the non-linear fuzzy model	Fig. 4.13	-

List of Figures

Chapter 1

Introduction

1.1 Presentation

With the development of science and technology for automobiles and the continuously increasing need for safety and comfort, great attention has been drawn to automotive suspension systems. The primary concerns that a suspension system has to address are ride comfort and handling performance of the vehicle. Ride is primarily associated with the ability of a suspension system to accommodate vertical inputs. On the other hand, handling relates more to horizontal forces acting through the center of gravity and moments acting through the wheels.

Among automotive suspensions, three main groups can be identified. The first, passive suspension systems, are the most widely used systems in vehicles. As their name suggests, the role of a passive suspension system is to withstand perturbations without the use of an external power supply or feedback control system. Thus, passive suspensions are designed as a compromise between ride comfort and handling performance. The second group is active suspension systems. Active systems are meant to provide independent treatment of perturbations using inertial forces through active control of some of the suspension system functions. In theory this means that the mentioned compromise in passive suspension systems can be eliminated. Active suspension systems, however, usually involve a continuous power supply, fast-acting mechanical devices, complex control algorithms, and closed-loop control systems. The final group is that of semi-active suspension systems. These systems offer the reliability of passive devices, but maintain the versatility and adaptability of active systems. A semi-active suspension can be adjusted in real time, but cannot input energy into the system being controlled. Hence, the force delivered by the suspension is constrained to be proportional and opposite to the elongation speed of the damper. Nonetheless, the power requirement of these systems is considerably lower than that of an active system.

In semi-active suspension systems for vehicles, the most commonly used damping devices are mono-tube dampers. A widely investigated mono-tube semi-active damper is the one denominated Magneto-Rheological (*MR*) damper. An *MR* damper is a non-linear dynamical system where the inputs can be the elongation speed and an electric current. The electric current is the control input that modulates the damping characteristic of the *MR* fluid through the variation of a magnetic field. The output is the force delivered by the damper. Fig. 1.1 illustrates the main components of an *MR* damper.

MR fluids are non-colloidal suspensions of particles with a size on the order of a few microns [4]. These fluids are unique due to their ability to change their properties reversibly between fluid and solid-like states upon the

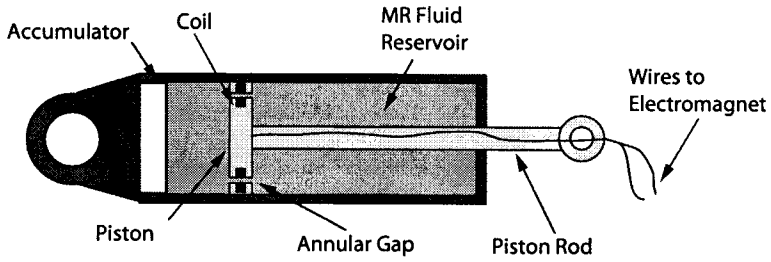

Figure. 1.1. *MR* damper configuration. The coil is connected to an external power supply. The *MR* fluid is energized as it passes through the annular gaps.

application of a magnetic field. As discussed in [5], when a certain magnetic field is applied to an *MR* fluid, the particles in the fluid become polarized and form polarization chains in the direction parallel to the applied field. The mechanical energy needed to yield these chain-like structures increases proportional to the applied magnetic field, resulting in a field dependent yield stress. This region is referred to as the pre-yield region. When the external shear stress is increased and exceeds a certain value, the polarization chains will be broken and *MR* fluids start to flow like regular Newtonian fluids. This last region is referred to as the post-yield region. If the shear stress is gradually decreased again, the broken polarization chains will tend to reform, but with a stress value less than the one with which they were broken. Thus, a hysteretic behavior is observed on the material. Fig. 1.2 shows the force-velocity behavior of an industrial *MR* damper under various constant electric current inputs.

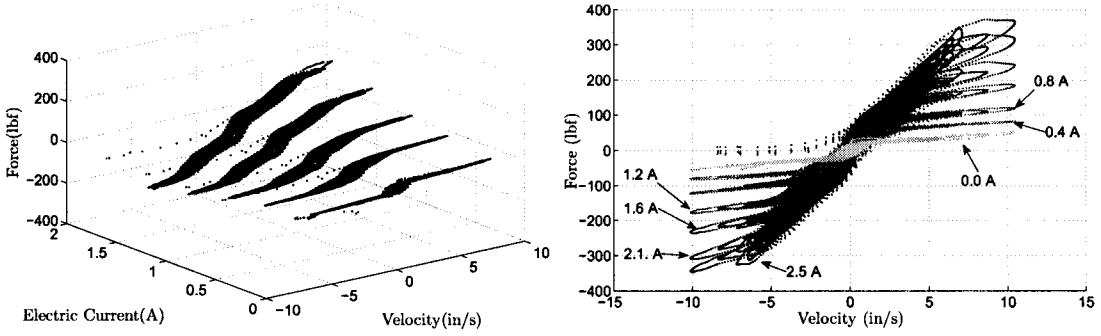

Figure. 1.2. Force-velocity behavior of an industrial *MR* damper. On the left side, the force is plotted against the velocity and electric current. On the right side, the force is plotted against the velocity for various constant electric current inputs.

As mentioned in [1], in the past decade there has been an increasing interest of scientists and engineers on *MR* fluid dampers and their applications. *MR* dampers have been utilized in a broad range of areas. Large *MR*

damping systems have been studied for civil engineering applications when damping is required to withstand the high vibrations generated by earthquakes [6]. Also, vibration control systems that include *MR* dampers have been developed for railcar comfort [7]. On the biotechnological side, *MR* dampers are being studied as part of intelligent prosthesis [8] and bionic legs [9]. According to [10], concerning the automotive industry *MR* fluids are appealing for vehicle suspension systems since they can operate at temperatures ranging from 40 to 150 °C with only slight variations in the yield stress. Additionally, *MR* fluids are almost insensitive to impurities and can be controlled with low voltages (12-24 V) and a current driven power supply outputting 1-2 A .

1.2 Problem Statement

Although *MR* dampers are greatly promising for the control of vehicle suspension systems, their major drawback lies on their non-linear and hysteretic behavior. Furthermore, the first step in designing a control strategy for a suspension system is modeling the behavior of the damper in an accurate manner. High-accuracy black-box and semi-phenomenological models have been developed recently. The models utilize displacement, velocity, electric current, and, many times, old values of the damping force as process variables in order to predict the output force of the *MR* damper. Nonetheless, to accurately predict the output force of the *MR* damper, the models are required to include a high number of parameters or complex mathematical functions. Thus, the computational necessities of those models become non-practical for commercial online application.

Due to the aforementioned, what type of model of an *MR* damper can be developed, which can accurately predict the highly non-linear and hysteretic behavior of the system and be suitable for online implementation of a control system? To answer this question, a broad spectrum of modeling techniques will be analyzed and employed. To obtain experimental data sets, a series of experiments will be carried out on a commercial *MR* damper [1]. The experiments will be designed to test the behavior of the damper under various input profiles. Then, various *MR* damper models will be tested and validated using the experimental data. At the end of the research, an *MR* damper model will be proposed.

1.3 Objectives

1.3.1 General Objective

The general objective of the present research is to explore various models and modeling techniques for an *MR* damper in order to compare them and analyze their strengths and weaknesses based on experimental data.

1.3.2 Specific Objectives

1. Perform experiments on an industrial *MR* damper in order to obtain real data and useful information for model identification.
2. Test models that describe in a precise and simple manner the behavior of an *MR* damper.
3. Compare how the models predict the behavior of an *MR* damper, using established criteria.
4. Identify input patterns that allow a better identification of models for the *MR* damper.
5. Present novel techniques to model an *MR* damper.

[1] Thanks to Metalsa www.metalsa.com.mx

1.4 Justification

As mentioned before, the areas where *MR* dampers can be utilized abound. Over the past decade, sustained interest in *MR* devices has increased due to the controllable interface provided by the *MR* fluid inside the damper. This fluid enables the mechanical system to interact with an electronic controller, which can be used to continuously adjust the mechanical properties of the damper. Some examples of devices in which *MR* fluids have been employed include dampers, clutches, brakes, and transmissions [11].

Nonetheless, the development of an effective control algorithm is reliant on the accurate modeling of the system to be controlled. The *MR* damper system includes both the process and the actuator. Thus, the adequate characterization of this system has shown to be a challenge due to its highly nonlinear dynamic response [12].

The present research is motivated by the aforementioned challenge that involves the correct modeling of an *MR* damping system. Various models and modeling techniques will be analyzed in order to compare their strengths and weaknesses. In addition, the training input patterns utilized for the identification of models will be discussed. Moreover, a new model for an *MR* damper will be proposed. The obtained results could be applicable to the automotive industry, where better comfort and handling control systems could be developed. Also, the results could be useful to the vast number of industries and applications where *MR* dampers are employed.

1.5 Hypothesis

The present research seeks to propose and compare models and modeling techniques for an *MR* damper. In consequence and based on the elements discussed in the previous sections, the following thesis statements are proposed.

1. Models for an *MR* damper can be developed, which can precisely describe its behavior.
2. There are certain modeling techniques that outperform the rest and help to develop precise and optimal models of an *MR* damper.
3. There are certain experimental input patterns that facilitate the identification of models for an *MR* damper.

1.6 Research Strategy

The present research will be divided into four main areas.

1. First, the previous work done on modeling of *MR* dampers will be revised. Then, the literature review will be centered on the various modeling approaches and techniques that have already been used for modeling *MR* dampers. The review will be the starting point for selecting various models for comparison.
2. Second, experiments to be performed on a commercially available *MR* damper will be designed. Once the experiments have been defined, experimental data will be obtained using an industrial *MR* damper.
3. Third, various models for the *MR* damper will be trained using the generated experimental data. The models will be compared against each other by using various performance indexes and qualitative indicators. After comparing the models, a set of different modeling techniques will be analyzed and new models for the *MR* damper may be developed.
4. Fourth, based on the results, a novel modeling technique for the *MR* damper will be documented.

1.7 Thesis Outline

The present work is divided into six chapters and five appendixes. This chapter presented the introduction, problem definition, and general outline of the research. In Chapter 2, a literature review on the modeling of *MR* dampers is discussed. In Chapter 3, the design of experiments and experimental setup are described. In Chapter 4, the results obtained on the comparison of *MR* damper models are presented. In Chapter 5, the obtained results are analyzed and discussed. Finally, in Chapter 6 the final conclusions of the research are presented.

Chapter 2

Literature Review

A literature review on the modeling of *MR* dampers is presented. In the first section, the state-of-the-art models of *MR* dampers are discussed according to various modeling approaches. Next, a summary of previous work done on comparing *MR* damper models and training patterns is presented.

2.1 State-of-the-Art Models

The models were divided into four different approaches: Phenomenological, Semi-Phenomenological, Black-Box, and Fuzzy-Based.

2.1.1 Phenomenological (P) Models

Phenomenological models are obtained by analyzing the physical characteristics of the systems they seek to model. Thus, in this type of models the parameters can be said to have a physical interpretation.

The model presented in [5] represents a phenomenological model based on the phase shifting dynamics of *MR* fluids. The authors based the analysis on the differential equations that characterize the behavior of the *MR* fluid as it flowed through the gap between the piston and the cylinder in the *MR* damper. The proposed model is shown in equation 2.1.

$$\dot{x}(t) = p_1\ddot{F}(t) + p_2\dot{F}(t) + p_3F(t) + p_4F(t)^3 + p_5F(t)^5 \tag{2.1}$$

where the five parameters p_j need to be determined under a given loading velocity $\dot{x}(t)$; $F(t)$ is the generated force; $\dot{F}(t)$ and $\ddot{F}(t)$ are the first and second derivatives of the force, respectively; and $F(t)^3$ and $F(t)^5$ are the third and fifth powers of the force, respectively. Notice that the model is a second order differential equation, with five parameters, that uses the velocity and force as inputs.

Using the experimental data employed in [1] (specified in the next section), the parameters for the model were identified using nonlinear least-squares approximation. After numerical experimentation, the authors concluded that the model that was constructed captured the hysteretic behavior of the damper precisely. In addition, hysteresis loops with various loading frequencies, applied field intensities, and excitation amplitudes were all modeled successfully by the proposed model. The authors commented that in the model, all the coefficients are to be assumed to be

dependent on the applied electrical current. That is, the coefficients should be functions of the applied magnetic field. This dependency is to be approximated by a polynomial of order 2 and must be identified from experimental data.

2.1.2 Semi-Phenomenological (S-P) Models

Semi-phenomenological models combine the analysis of the physical characteristics of the systems and various mathematical techniques in order to model those systems.

The model presented in [1] has been widely used to compare models for *MR* dampers. The authors modified a previously proposed structure in order to include the regions where the acceleration and velocity have opposite signs. The structure of the model is shown in Fig. 2.1 and in equation 2.2.

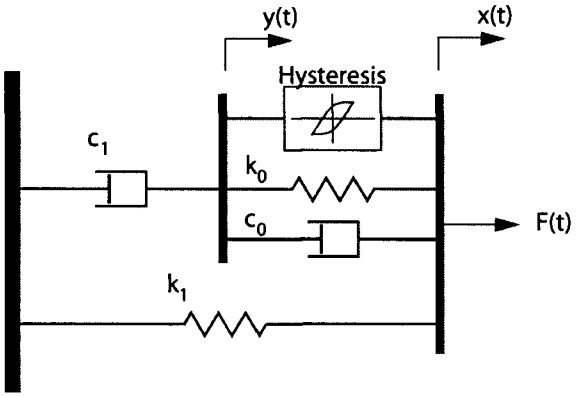

Figure. 2.1. Diagram of the semi-phenomenological model presented in [1].

$$
\begin{aligned}
F(t) &= c_0(\dot{x}(t) - \dot{y}(t)) + k_0(x(t) - y(t)) + k_1(x(t) - x_0) + s_1 z \\
\dot{y}(t) &= \frac{1}{c_0 + c_1}\left(s_1\, z + c_0\dot{x}(t) + k_0 x(t) - y(t)\right) \\
\dot{z}(t) &= -s_2|\dot{x}(t) - \dot{y}(t)|z(t)|z(t)^{s_3-1}| - s_4\left(\dot{x}(t) - \dot{y}(t)\right)|z(t)|^{s_3} + s_5\left(\dot{x}(t) - \dot{y}(t)\right)
\end{aligned} \tag{2.2}
$$

where c_0 and k_0 represent the viscous damping and stiffness characteristics at large velocities, respectively. c_1 is the damping coefficient for the roll-off induced at low velocities. k_1 and x_0 represent the accumulator stiffness and its initial displacement, respectively. s_j represents coefficients that are to be determined from experimental data. In addition, $z(t)$ and $y(t)$ are evolutionary coefficients for the model. The model can be seen to include 10 parameters, and be dependent on the displacement and the velocity. To validate the proposed structure, the authors calculated the prediction error as a function of time, displacement, and velocity. The experimental data explored sinusoidal, step, triangle, and pseudo-random displacement patterns with frequencies lower than 3 Hz. The electric current pattern was constant stepped increments. The model was capable of exhibiting a wide variety of hysteretic behaviors. Moreover, the model could be effectively employed for control algorithm development and for system evaluation. Nonetheless, the model does not include the effect of the varying electric current.

Continuing in the search of semi-phenomenological models, the one presented in [2] has been greatly analyzed in the past years. The proposed model is said to describe the bi-viscous and hysteretic behaviors of the *MR* damper with high precision. The structure is described in Fig. 2.2 and in equation 2.3,

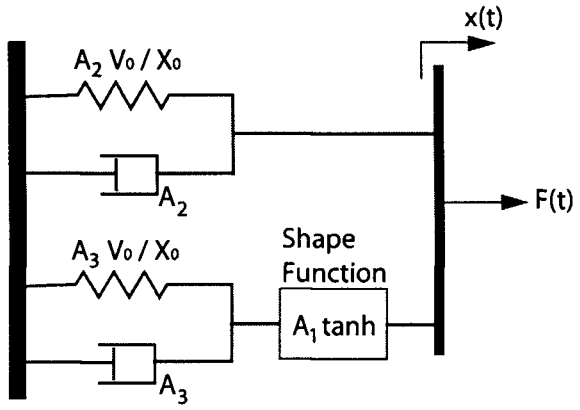

Figure. 2.2. Diagram of the semi-phenomenological model presented in [2].

$$F(t) = A_1 tanh\left(A_3(\dot{x}(t) + \frac{V_0}{X_0}\, x(t))\right) + A_2\left(\dot{x}(t) + \frac{V_0}{X_0}\, x(t)\right) \tag{2.3}$$

where A_1 represents the dynamic yield force of the *MR* fluid. A_2 and A_3 are parameters related to post-yield and pre-yield viscous damping coefficients respectively. V_0 and X_0 denote the absolute value of hysteretic critical velocity and hysteretic critical displacement, respectively. In the equation, the model can be seen to use the displacement and velocity as inputs and only depend on five parameters. The experiments performed on the *MR* damper consisted on sinusoidal sweeps for the displacement and constant steps for the electric current. The authors used a non-linear least-squares algorithm in order to identify the coefficients of the model. The results obtained in the experimentation were said to prove the correctness of the proposed structure. In addition, the concise form of the model was mentioned as its best feature. Nevertheless, the authors did not use experiments in which the current varied over time to prove the effectiveness of the model under varying current scenarios. Although, the authors noted that parameter A_3 could be said to be independent from the applied electrical current.

Another semi-phenomenological model that is to be considered is the one presented in [3]. The model is intended to include the hysteretic force-velocity characteristic of the *MR* damper. The authors employed a component-wise additive strategy that captured the viscous damping, spring stiffness, and hysteretic behavior of the *MR* damper. The model is presented in 2.3 and in 2.4.

$$\begin{aligned} F(t) &= c_w\, \dot{x}(t) + k_w\, x(t) + \alpha\, z(t) + f_0 \\ z_w(t) &= tanh\left(\beta\, \dot{x}(t) + \delta\, sign(x(t))\right) \end{aligned} \tag{2.4}$$

where, c_w and k_w are the viscous and stiffness coefficients, respectively. α is the scale factor of the hysteresis, $z_w(t)$ is the hysteretic variable given by the hyperbolic tangent function, and f_0 represents the damper force offset. Also, β and δ define the slope and width of the hysteretic loop, respectively. Notice that the model only depends on six parameters and uses the displacement and velocity as inputs.

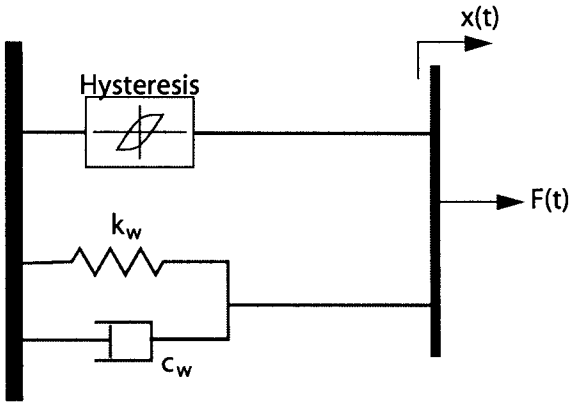

Figure. 2.3. Diagram of the semi-phenomenological model presented in [3].

Experimental data was obtained by a series of experiments performed on a commercially available *MR* damper. Sinusoidal displacement patterns of frequencies between 1 and 2 Hz were used. Also, the electric current was applied to the damper as constant steps. A performance-enhanced technique, based on particle swarm optimization, was proposed to identify the coefficients of the model. In order to make the model depend on the applied electrical current, the authors made the coefficients equal to a linear time function of that current. According to the authors, the results obtained by the new model showed highly satisfactory coincidence with the experimental data, and also proved the effectiveness of the proposed identification technique. In addition, as the proposed model contained only a simple hyperbolic tangent function it was said to be computationally efficient in the context of parameter identification and its subsequent inclusion in controller design and implementation.

Along the same modeling approach, in [9] a sigmoidal model of the *MR* damper was proposed. The authors took a previously proposed model and divided it into two parts corresponding to positive and negative acceleration, respectively. The model is presented in equation 2.5.

$$\begin{aligned} F_p(t) &= L_{1p}\frac{1-e^{-L_{2p}(\dot{x}(t)-L_{3p})}}{1+e^{-L_{2p}(\dot{x}(t)-L_{3p})}} + L_{4p}\dot{x}(t) + k_L x(t) \\ F_n(t) &= L_{1n}\frac{1-e^{-L_{2n}(\dot{x}(t)-L_{3n})}}{1+e^{-L_{2n}(\dot{x}(t)-L_{3n})}} + L_{4n}\dot{x}(t) + k_L x(t) \end{aligned} \tag{2.5}$$

where k_L is said to be the rigidity coefficient and the parameters L_j must be identified from experimental data. Additionally, the subscript p denotes the positive acceleration region and n the negative acceleration one. As shown, the model uses the velocity as input and depends on 10 parameters, five per equation. Unspecified experimental data was employed to test the proposed model. The identification of the coefficients was done using nonlinear least squares. The resulting model was tested and proved to match the behavior of the *MR* damper. In order to introduce the electric current to the model, every parameter was made equal to a linear time function of the electric current. The model was further used to successfully design and test a control scheme for an intelligent bionic leg.

Finally, in [13] a model that modified the one in [2] was presented. The authors included a nonlinear stiffness term, in addition to an inertial force part. The model is shown in equation2.6.

$$F(t) = f_b + c_b + \dot{x}(t) + \frac{2}{\pi} f_y \, tan^{-1} \left(k_b (\dot{x}(t) - \dot{x}_0 sgn(\ddot{x}(t))) \right) + m\ddot{x}(t) \tag{2.6}$$

where f_e is said to be the pre-load of the accumulator, c_b the coefficient of viscous damping, f_y the yielding force, k_b the shape coefficient, $\dot{x}_0$ the hysteretic velocity, and m represents a virtual mass. It can be seen that the model depends on the velocity and acceleration of the *MR* damper and it has six coefficients. Experiments that employed sinusoidal displacement patterns between 0.6 and 2.55 Hz were selected. The electric current was applied as constant stepped increments of 0.2 A. In order to identify the coefficients of the model, nonlinear least squares was used. The performance of the model was analyzed by calculating the error functions used by [1]. The proposed model could successfully be used to describe the behavior of the damper and to develop control algorithms. In respect to the model in [2], the modified one is said to predict the hysteresis to a higher degree of accuracy. As for other models, the analysis never included varying electric current scenarios.

2.1.3 Black-Box Models

Black-Box models utilize polynomials, recurrence relations, or artificial neural networks (*ANN*) to emulate the behavior of a system. This usually implies that the coefficients of such models do not have a physical interpretation. There are two fundamental objectives in the development of nonlinear black-box modeling of MR-dampers: improved model numerical stability at low-integration step rate for real-time embedded applications and generalized model structure for a wide range of dynamics [6].

In [14], a polynomial model was proposed and analyzed to predict the behavior of an *MR* damper. The structure of the model is shown in equation 2.7.

$$F(t) = \sum_{j=0}^{6} \left(b_{1j} + b_{2j} \, i(t) \right) \dot{x}(t)^j \tag{2.7}$$

where b_{1j} and b_{2j} are the coefficients that are to be learned from experimental data. It can be seen that the model has the velocity and electric current as inputs and depends on 14 parameters. To validate the model, experiments were performed using sinusoidal displacement patterns and constant electric current steps. The coefficients were estimated via nonlinear least squares. According to the authors, the proposed polynomial structure predicted fairly well the non-linear and hysteretic behavior of the *MR* damper. In addition, an inverse version of the model was tested in order to track a desired damping force. The reported results were equally successful when an open-loop controller was tested.

In [10], an *Autoregressive with eXogenous* (*ARX*) term model for an *MR* damper was proposed. The model is shown in equation 2.8,

$$\begin{aligned} F_k &= a_1 F_{k-1} + a_2 F_{k-2} + a_3 x_k + a_4 x_{k-1} \\ &\quad + a_5 \dot{x}_k + a_6 \dot{x}_{k-1} \end{aligned} \tag{2.8}$$

where F_k, x_k, and $\dot{x}_k$ represent the discrete force, displacement, and velocity values at instant k, respectively. In the same manner, the subscripts $k-1$ and $k-2$ represent old values of the respective variables. Additionally, a_j are the coefficients that ought to be learned from experimental data. Thus, the model uses present and old values of the displacement, velocity and force as inputs and depends on six coefficients.

The selected experimental data employed constant and random electric current input patterns. The most important regressors of the model were found to be the ones for $\dot{x}$ and the old values of F. If those two regressors were used, the role played by the regressors of x was negligible. In addition, old values of F were said to be extremely important for the quality of the model. If only $\dot{x}$ and x were used, the model quality remained very poor even if a great number of old values was employed. When the model was to be made dependent on the electric current, the authors added two regressors to the proposed structure, corresponding to the present and past values of the electric current, respectively. The results obtained showed that the *ARX* model was able to predict, with high precision, the behavior of the *MR* damper. Furthermore, for the varying current case the *ARX* model was said to outperform by far other phenomenological models.

Among Black-Box modeling, *ANNs* have been greatly exploited recently. As mentioned in [15], a *ANN* is a mathematical model inspired from the basic understanding of biological nervous systems. They are devices that can accept multiple inputs and be trained exclusively from experimental data using various learning techniques. Artificial neurons are the elementary units in an *ANN*. Incoming information is in the form of signals that are passed between neurons through connection links. Each connection link has a proper weight that multiplies the transmitted signal. Each neuron has an internal action resulting in an activation function being applied to the weighted sum of the input signals to produce an output signal.

Fig. 2.4 depicts a three layer *ANN* with three inputs and one output. It is to note that each connecting arrow has a multiplicative weight that is determined by the learning algorithm. In the figure, the L_{1j}, L_{2j}, L_{Oj} neurons represent the first hidden, second hidden, and output layers of the network, respectively.

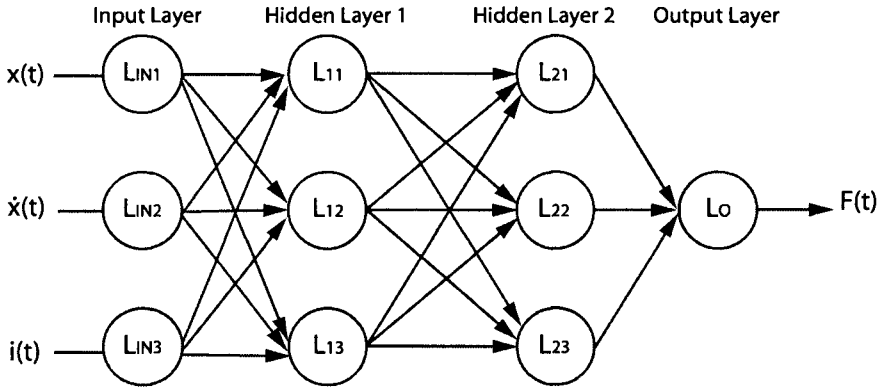

Figure. 2.4. Three layer *ANN* with three inputs and one output. Two hidden layers are presented, which are hidden in the sense that their direct output cannot be accessed. From input patterns, one can only observe the output pattern from the output layer.

In [16] an *ANN* was proposed in order to model the direct and inverse dynamics of an *MR* damper. For the direct model, a recurrent *ANN*) was used, in which the output is delayed and fed back to the input layer. Fifteen input layer neurons, five for each input (displacement, velocity, and force) were utilized. Additionally, 15 hidden layer neurons and one output layer neuron were selected. The form of the input and hidden layers was sigmoidal and that of the output layer was linear. To train the *ANN*, the Levenberg-Marquardt algorithm was utilized. To test the correctness of the proposed structure, the authors compared the predicted force with that predicted by the model propose in [1].

After the validation, the authors noted that the trained *ANN* could reasonably predict the damping force of the *MR* damper. Nonetheless, the effect of the commanding electric current was never considered.

An additional study on modeling using *ANNs* was presented in [17]. The structure employed the displacement, velocity, and electric current as inputs to predict the *MR* damping force. The selected experimental data was obtained by using sinusoidal displacement patterns with frequency of 6 Hz and constant steps of 0.2 A increments for the electric current. It was proposed to train the *ANN* using *Recursive Lazy Learning*. To validate the results, the error functions presented in [1] were utilized. It was concluded that the proposed model satisfactorily emulated the *MR* damper. The model could be adjusted when new data was present and it could be used for the design of control algorithms.

One more research of modeling with *ANN* can be found in [18]. Here, a 25 hidden-layer *ANN* structure that employs the present and one past value of the displacement, velocity, and electric current as inputs, in addition to the past value of the damping force was proposed. Hence, the structure had seven inputs and one output. Experimental data was obtained using sinusoidal displacement input patterns of frequencies between 0.5 and 4 Hz. The electric current was held constant at various values. To train the structure, a back-propagation algorithm was employed. The validation procedure confirmed that the proposed *ANN* model was able to accurately predict the behavior of the *MR* damper. In addition, a reversed structure was proposed in order to predict the necessary electric current to obtain a desired damping force. As for the forward model the reported results showed great accuracy between predicted and experimental data.

2.1.4 Fuzzy-Based Models

Fuzzy systems have been recently employed for modeling and control of physical processes. Said systems have very strong functional capabilities and may, if properly designed, satisfy the universal approximation property [19]. A fuzzy system is a static nonlinear mapping between inputs and outputs. Fig. 2.5 presents a block diagram of a general fuzzy system. The inputs and outputs of the system are crisp, that is, they are real numbers and not fuzzy sets. The fuzzyfication block converts the crisp inputs to fuzzy sets (membership functions) the inference mechanism uses the fuzzy rules in the rule-base to produce fuzzy conclusions, and the defuzzification block converts these fuzzy conclusions into the crisp outputs.

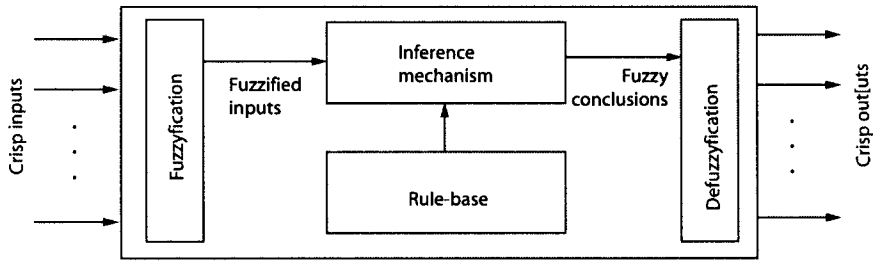

Figure. 2.5. Fuzzy system block diagram.

Among fuzzy systems, a Takagi-Sugeno-Kang (*TSK*) fuzzy system is one whose output conclusions are linear functions. A *TSK* fuzzy system can be selected for modeling complex systems. The fuzzy rules of the model can be determined by adaptively generating them based on input and output data or by selecting them by hand. The total output of the system is calculated using the weighted average of the output functions [20]. Unlike *ANNs*, fuzzy

systems can include human knowledge in the form of fuzzy rules. Nonetheless, it may take a considerable amount of time to design and tune pure fuzzy models by hand. In this regard and as mentioned in [15], *NN* learning techniques can automate the learning process of a fuzzy model by extracting rules directly from experimental data.

If a first-order *TSK* model consists of three inputs (with three membership functions each) and one output (described by linear output functions), and only three fuzzy rules are selected as shown in equations 2.9 - 2.11,

$$\begin{aligned} &If\ x(t)\ is\ M_{A1}\ and\ \dot{x}(t)\ is\ M_{B1}\ and\ i(t)\ is\ M_{C1} \\ &then\ f_1(t) = o_1 x(t) + q_1 \dot{x}(t) + r_1 i(t) + u_1 \end{aligned} \tag{2.9}$$

$$\begin{aligned} &If\ x(t)\ is\ M_{A2}\ and\ \dot{x}(t)\ is\ M_{B2}\ and\ i(t)\ is\ M_{C2} \\ &then\ f_2(t) = o_2 x(t) + q_2 \dot{x}(t) + r_2 i(t) + u_2 \end{aligned} \tag{2.10}$$

$$\begin{aligned} &If\ x(t)\ is\ M_{A3}\ and\ \dot{x}(t)\ is\ M_{B3}\ and\ i(t)\ is\ M_{C3} \\ &then\ f_3(t) = o_3 x(t) + q_3 \dot{x}(t) + r_3 i(t) + u_3 \end{aligned} \tag{2.11}$$

where $x(t)$, $\dot{x}(t)$, and $i(t)$ are input language variables; M_{Aj}, M_{Bj}, and M_{Cj} are fuzzy sets; $f_1(t)$, $f_2(t)$ and $f_3(t)$ are output language variables; o_j, q_j, r_1, and u_j are the output parameters of the fuzzy conclusions, then Fig. 2.6 would represent the *TSK* structure for the first-order fuzzy system. The W_j and Wn_j represent the degree of fitness and the normalized fitness of the fuzzy rules, respectively. For simplicity, the example considers only three of the 27 possible fuzzy rules.

A system as the one shown in the figure can use a hybrid learning algorithm that combines the backpropagation gradient descent and least squares methods. A *TSK* fuzzy model trained in this manner is often named Adaptive Neuro-Fuzzy Inference System (*ANFIS*). In general, the *ANFIS* learning algorithm consists of adjusting the parameters of the structure from sample data. Many other learning techniques, including Genetic Algorithms (*GA*), can be selected and will be discussed in detail when required.

In [12], *ANFIS* is used to determine the parameters of a *TSK* model of the *MR* damper. The selected fuzzy structure was similar to the one in 2.6. It utilized three inputs (displacement, velocity, and voltage) and one output (damping force). Two, four, and three membership functions were selected for the displacement, velocity, and control voltage, respectively. The total number of fuzzy rules was 27 and the output functions were linear.

The data selected for training and validating the model was generated from numerical simulation of the model presented in [1]. To validate the accuracy of the fuzzy-based structure, it was compared to the mathematical model when subjected to an identical input. The results showed excellent performance of the proposed model except for the low frequency damper dynamics. Nonetheless, the error was regarded as conservative for vibration control purposes.

In [7], the authors designed, fabricated, and modeled an *MR* damper for a railcar. The later was done by employing fuzzy logic. As the model before, the selected structure employed the displacement, velocity, and voltage as inputs with three, two, and four bell membership functions, respectively. A total of 27 fuzzy rules combined

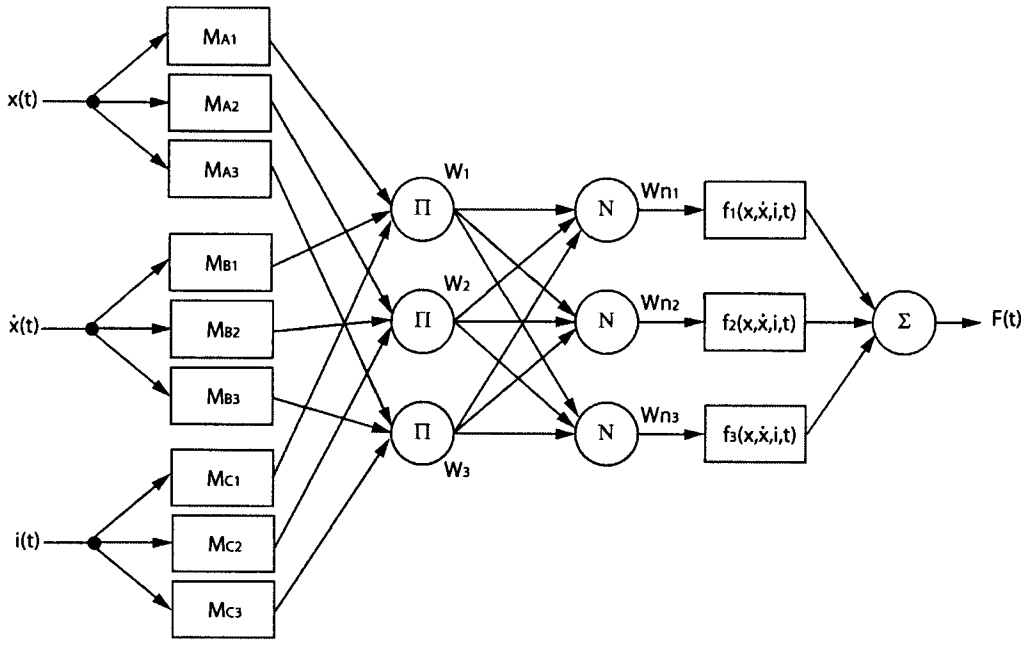

Figure. 2.6. Structure of a first-order *TSK* fuzzy-based model with three inputs and one output. For simplicity, only three fuzzy rules, out of the 27 possible combinations are considered. Each of the inputs is evaluated by the membership functions and their outputs are combined according to the defined fuzzy rules. Each output from the rules is then combined according to the selected sum method.

with linear output functions of the force were selected. The validation process was done by using experimental data obtained with the fabricated *MR* damper. Sinusoidal and random displacement signals were utilized with constant and sinusoidal voltages. The displacement frequencies were always kept lower than 3 Hz. To assess the performance of the model, the error functions employed in [1] were selected. The results confirmed the correctness of the proposed fuzzy model and it was labeled as computationally efficient. Additionally, the authors highlighted the structure as being a suitable option for real time control.

A similar approach was followed in [21]. The inputs for the fuzzy structure were selected as displacement, velocity, and control voltage, while the output was the damping force. The structure was trained using a *GA* that simultaneously evolved the membership function parameters. Hence, the proposed structure was regarded as an evolutionary fuzzy model. In this case, the authors also generated simulated data for the training of a *TSK* model of the *MR* damper using the model presented in [1]. The performance of the evolutionary fuzzy model was validated against the damping force generated by the mathematical model. The results showed that the structure emulated the behavior of the *MR* damper quite well. Additionally, the fuzzy model was tested using an unknown input pattern for which the results were very acceptable.

A self-tuning fuzzy structure was analyzed in [22] to model an *MR* damper. As inputs for the model were selected the displacement, velocity, and electric current with five triangular membership functions each. The output functions were selected as constants combined using the centroid method. To validate the model, experimental data were obtained. Both the displacement and electric current patterns were sinusoidal, the first with frequencies between 1 and 2.5 Hz. The training algorithm of choice was back-propagation. The proposed structure modeled the

hysteresis of the damper better than a physical model. As for other fuzzy models, the suitability of the structure for real time control was mentioned.

In [20], direct and inverse fuzzy models of the *MR* damper were identified using *ANFIS*. The identification data was obtained using a mathematical model of the damper. The fuzzy structure for the direct model resembled the one in Fig. 2.6, with velocity, acceleration, and control voltage as inputs and damping force as output. On the other hand, for the inverse model the control voltage and damping force were swapped with respect to the direct one. For both models, three membership functions for each input were selected as the best compromise between simplicity and performance. The results obtained with both fuzzy models proved that the proposed structures could accurately model the behavior of the *MR* damper.

2.1.5 Comparison

Table 2.1 summarizes the state-of-the-art models of *MR* dampers. The selected columns portray the main descriptions of the proposed or studied models. The column *Parameters* compares the number of parameters of the proposed models. In the case of phenomenological, semi-phenomenological, and non-*ANN* black-box models, the column represents the number of coefficients in the model. For the *ANN* black-box structures, the column describes the number of hidden layers in the network. For the fuzzy-based models, the column represents the number of membership functions per input. Additionally, the column *Validation Data* specifies whether the model presented by the authors was validated using experimental or simulated data.

The phenomenological model presented in [5] presents a good option for modeling the *MR* damper. Nonetheless, the dependency on the variable electric current would need to be added to the model, which would increase significantly the number of parameters. An additional consideration relies on the fact that, to compute the damping force, the model requires a non-linear differential function with four inputs that depend on the same force. This consideration could make the model impractical for online implementation.

Among the semi-phenomenological models, the ones presented in [2], [3], and [13] stand out due to their low number of parameters. Nonetheless, in order to include the dependency on the electric current to the models the number of parameters would be increased. On the other hand, the model presented in [1] has been greatly employed for comparison of new models for *MR* dampers, even when it employs 10 or more parameters. For all the analyzed semi-phenomenological models, their major drawback lies on the use of complex mathematical functions that resemble the behavior of the *MR* damper..

For black-box structures proposed to model the *MR* damper, the *ARX* structure presented in [10] appears to be the more compact one. Nevertheless, its dependency on old values of the damping force may be a challenge for implementation. On the other hand, *ANNs* propose a feasible modeling approach. Although, a high number of inputs and hidden layers may be required in order to obtain acceptable results.

Finally, fuzzy-based models stand as an interesting option for modeling the *MR* damper. All the analyzed models employed three inputs, including the control variable (voltage or electric current). The selection of inputs, fuzzy sets, and output functions may require a deep knowledge of the behavior of the system, buy may be alleviated by the use of *ANFIS* and *GA*. As for *ANNs*, a high number of fuzzy sets and fuzzy rules may be required in order to successfully model the *MR* damper.

Table 2.1. Comparison of Models. The state-of-the-art models are compared by modeling approach, number of inputs and parameters, and the type of validation data employed.

Modeling Approach	Authors	Inputs	Number of Parameters	Validation Data	Year
P	L. Wang and H. Kamath	$\dot{x}(t), \ddot{F}(t), \dot{F}(t),$	5	Experimental	2006
	...	$F^3(t), F^5(t)$	...	...	...
$S-P$	B. Spencer *et al.*	$x(t), \dot{x}(t)$	10	Experimental	1996
	S. Guo *et al.*	$x(t), \dot{x}(t)$	5	Experimental	2006
	N. Kwok *et al.*	$x(t), \dot{x}(t)$	6	Experimental	2006
	F. Li *et al.*	$x(t), \dot{x}(t)$	10	Experimental	2009
	S. Çesmeci and T. Engin	$\dot{x}(t), \ddot{x}(t)$	6	Experimental	2010
Black-Box	S. Choi *et al.*	$\dot{x}(t), i(t)$	14	Experimental	2001
	D. Wang and W. Liao	$x_k, \dot{x}_k, F_{k-1}$	15	Simulated	2001
	S. Savaresi *et al.*	$x_k, x_{k-1}, \dot{x}_k,$	6	Experimental	2005
	...	$\dot{x}_{k-1}, F_{k-1}, F_{k-2}$	...	...	...
	M. Boada	$x(t), \dot{x}(t), i(t)$	N/S	Experimental	2008
	E. Chen '	$x_k, x_{k-1}, \dot{x}_k,$	25	Experimental	2009
	...	$\dot{x}_{k-1}, i_k, i_{k-1}, F_{k-1}$	...	...	...
Fuzzy	C. Schurter and P. Roschke	$x(t), \dot{x}(t), V(t)$	2, 4, 3	Simulated	2000
	V. Atray	$x(t), \dot{x}(t), V(t)$	3, 2, 4	Experimental	2003
	H. Du and N. Zhang	$x(t), \dot{x}(t), V(t)$	N/S	Simulated	2006
	K. Ahn	$x(t), \dot{x}(t), i(t)$	5, 5, 5	Experimental	2008
	H. Wang and H. Hu	$\dot{x}(t), \ddot{x}(t), i(t)$	3, 3, 3	Simulated	2009

2.2 Previous Work

The research done in [10] compared the semi-phenomenological modified Bouc-Wen model presented by [1] in equation 2.2 and an *ARX* structure as in equation 2.8. The selected performance index for comparing the results was the *Error to Signal Ratio* (*ESR*), defined later in equation 4.2. The authors first compared the models using the three experimental data sets in which the electrical current was held constant. For those data sets, both models were reported to obtain very low error values. For varying electric current scenarios, the reported results showed that the semi-phenomenological model was not able to predict the behavior of the damper and obtained high error values. On the other hand, the *ARX* model was reported to obtain error values as low as for the constant electric current experiments. In relation to the input patterns selected, the authors did not comment on the effect of those patterns on the identification process of the models.

In [23], the work from [10] was continued. Three models of an *MR* damper were selected and compared. The author divided the experiments performed into two groups. The first group employed constant displacement and constant electric current inputs. The second group of tests employed constant velocity patterns. Once the velocity was measured stable and constant, a constant electrical current was applied to the damper. To compare the models, the *ESR* index was utilized. The author selected the same two models used in [10] and added to the research the semi-phenomenological model presented in [2]. The dependency on the electric current was added to the models by making their coefficients equal to time varying functions of the current or by adding regressors in the case of the

ARX one. In this case, the author selected a polynomial of order five instead of a linear function. After identifying the models, the author concluded that the model presented in [2] obtained the best compromise between exactness and overall simplicity. Nonetheless, the other two models were reported to obtain acceptable results. At the end of the research, the effect of the input patterns on the identification process was not analyzed.

In the thesis work presented in [24], linear, non-linear, and probabilistic models for an *MR* damper were analyzed. Experimental data was obtained using an industrial *MR* damper. The selected input patterns were designed to be bounded according to real-life scenarios. The velocity and displacement patterns were selected as uniform random distributions. The electric current input was also continuously varied according to a uniform random distribution. To compare the *MR* damper models, force-time and force-velocity plots were employed. The general conclusion of the research was that a deterministic model was insufficient to model the behavior of an *MR* damper. In addition, it was said that the number of parameters required for a phenomenological model that includes all the dynamic effects would be too high to be implementable. For the non-linear model, the addition of a hysteresis term was observed to dramatically improve its performance.

In [25], various input patterns for *MR* damper modeling were analyzed. A neural network that emulated the behavior of an *MR* damper modeled by an *ARX* structure was used. The objective of the research was to determine which experimental input pattern allowed the adaptation mechanism of the neural network to be more precise on its prediction of the behavior of the damper. The authors concluded that a sinusoidal displacement with modulated frequency and constant amplitude, plus an Increased Clock Period Signal (*ICPS*) current pattern between 0 and 4 *A* provided the best combination for model identification. For the *ICPS* signal, the authors noted that the amplitude duration was to be held constant and that the duration of each step was to be at least equal to the settling time of the *MR* damper force step response. Additionally, the authors proposed a modification to the model presented in [2] in order to make it dependent on the electric current. The resulting model was successfully compared against simulated experimental data sets.

2.3 Opportunities

After reviewing the state of the art, the following areas of opportunity were identified.

- There is a need for an extensive quantitative and qualitative comparison of *MR* damper models. This comparison should take into account the performance of the models, as well as their overall complexity and ease of implementation. The present work is meant to fulfill this need by selecting various state-of-the-art models and presenting an in depth comparison.
- There is a need for *MR* damper models that can precisely model the hysteretic and non-linear behavior of the system. The present work is determined to analyze how various *MR* damper models mimic the behavior of the system.
- There is a need for *MR* damper models that can accurately characterize the role of the electric current without being excessively complex. In the present work, a novel method for introducing the electric current dependency to models will be presented.

2.4 Summary

The chapter presented a literature review on the modeling of MR dampers. The first section various state-of-the-art *MR* damper models were summarized according to four modeling approaches: phenomenological, semi-phenomenological, black-box, and fuzzy-based. The following section discussed previous work done on the comparison of *MR* damper models and training patterns. Later, Table 2.1 presented a chronological synthesis of the latest contributions to *MR* damper modeling. At the end, the areas of opportunity in *MR* damper modeling were identified.

Chapter 3

Experiments

The description of the design of experiments, experimental setup, and experimental results is discussed in the following sections. In order to model a dynamical system, such as the *MR* damper, experimental data was obtained from an industrial damper. A set of experiments was designed in order to test the behavior of the system under various input patterns. The experimental setup consisted of measuring devices, electric current controllers, and displacement actuators.

3.1 Design of Experiments

Experiments were designed in order to generate displacement and electric current input patterns that would characterize the behavior of an *MR* damper for automotive applications. Special attention was placed on the proper frequency content of the displacement signals. Additionally, the patterns were selected in order to aid the modeling process of the system. The experiments were based on the work presented in [26], where a set of training patterns was reviewed and designed for the identification of *MR* dampers.

3.1.1 Electric Current Patterns

Electric current patterns are very important for the correct identification of the *MR* damper. The selection of these patterns is to take into account the settling time of the electric circuit involved in the coil, the electric current input limits of the *MR* damper, and the capabilities of the experimental setup. The electric current input patterns selected for the experimental tests are described as follows.

Increased Clock Period Signal (*ICPS*)

For an *ICPS* signal, the amplitude is modified randomly at a constant period of time. Due to its random content, this signal is rich in frequencies. According to [27], the signal can be calculated as shown in equation 3.1,

$$i(t) = e\left(\left\lfloor \frac{t-1}{N_{ICPS}} \right\rfloor + 1\right) \tag{3.1}$$

where $\lfloor q \rfloor$ represents the integer part of q; $e(t)$ is a uniformly distributed white noise signal; N_{ICPS} represents the number of samples for which the amplitude of the signal is to be held constant; and t is time.

As mentioned in [27], *ICPS* signals provide various advantages over white noise signals for system identification purposes. First, for an *ICPS* signal the amplitude is held constant over long periods of time. This is significantly important, as the measured data would approximately contain information for a transient analysis of the system. Second, an *ICPS* signal is advantageous for processes where the wearing of the actuators is a main concern, as the input to the system is not continuously varying. For the *MR* damper, the *ICPS* signal is employed to extract the steady and transient behavior of the damper by a constant excitation of the *MR* fluid. The period at which the value of the signal is changed is to be greater than the settling time of the *MR* damper.

For the present work, the *ICPS* signal was designed to contain electric current values between 0 and 2.5 A, uniformly distributed. The period for which the amplitude of the signal was held constant was set to 0.20 s, according to the typical settling time of an *MR* damper. Thus, the value of N_{ICPS} was calculated for a sampling frequency of 512 Hz. Additionally, the uniformly distributed signal $e(t)$ was obtained in *MATLAB*^{TM} by means of the *rand* function.

Pseudo-Random Binary Signal (*PRBS*)

A *PRBS* signal is very common for system identification. The amplitude of the signal is shifted between two values, with a certain period of time. The duration of every step is governed by a binary algorithm that is to be dependent on the settling time of the system to identify. As mentioned in [27], a *PRBS* is a purely deterministic signal. This is, future states can be computed exactly. Nonetheless, the correlation function of the signal resembles one of white random noise.

In order to compute the *PRBS* signal, the *idinput* function from the *System Identification Toolbox* in *MATLAB*^{TM} was selected. The function computes a maximum length *PRBS* based on the desired length of the signal, the minimum constant interval, and the two levels at which the signal is to shift. For the present work, a *PRBS* signal of 30 s (a total of 15360 samples, base on a sampling frequency of 512 Hz) was employed. The minimum constant interval was set to 0.195 s (a total of 100 samples, based on a sampling frequency of 512 Hz). In addition, the electric current values were bound between 0 and 2.5 A.

Amplitude Pseudo-Random Binary Signal (*APRBS*)

An *APRBS* signal is one in which the amplitude is randomly modified every certain period of time. The signal can be defined as shown in equation 3.2,

$$i(t) = \begin{cases} \mu & \text{if } t = 0 \\ i(t-1) with\ probability\ \alpha & \text{if } t > 0 \\ \mu\ with\ probability\ 1-\alpha & \text{if } t > 0 \end{cases} \tag{3.2}$$

where μ is a normally distributed random number and α is a number between 0 and 1 that specifies the probability of $i(t)$ being equal to $i(t-1)$. If α is one, the amplitude of the signal becomes constant. If α is zero, the amplitude of the signal becomes normally distributed white noise. *APRBS* signals were employed in [10] to train *ANNs* in order to model an *MR* damper.

For the present work, the algorithm to compute the *APRBS* signal was programmed in *MATLAB*^{TM}. In order to obtain a signal with normally distributed amplitude, the value of α was set to 0.01. In addition, the electric current values were bound between 0 and 2.5 A.

Stepped Increments Signal (*SC*)

A *SC* signal is one in which the amplitude is held constant for a predetermined period of time. At the end of the period, the value of the signal is incremented to a different constant value. The purpose of the signal is to identify the various operational zones of the *MR* damper. In the present work, the electric current values were held constant for 30 seconds. Constant steps of 0.0, 0.4, 0.8, 1.2, 1.6, 2.1, and 2.5 A were employed.

3.1.2 Displacement Pattern

As mentioned in [28], it is common to employ sine waves, step functions, or triangular waves as displacement patterns for vehicle testing. While these inputs provide a basis for comparative evaluation of various designs, they do not serve as a valid basis for studying the real ride behavior of a suspension system since surface profiles are rarely of simple forms. In consequence, it is found that road profiles are more realistically resembled by random functions. As discussed in [29] and [30], these random functions can be generally described by means of their frequency composition. According to the *ISO 8606:1995* standard, there are eight different degrees of road roughness according to their power spectral density. Based on the work in [28], equation 3.3 describes the power spectral density of a road profile,

$$S(f) = \frac{C_r \, \omega_x^{N_{cr}}}{v_c} \tag{3.3}$$

where $S(f)$ represents the power spectral density of the elevation of the surface profile, f is a frequency in Hz, C_r is the roughness coefficient of the road, ω_x is the number of cycles per feet, N_{cr} is a constant corresponding to the roughness coefficient, and v_c is the speed at which the vehicle is traveling.

Table 3.1 presents the values for C_r and N_{cr} depending on the desired road profile.

Table 3.1. Roughness coefficients for power spectral density functions of road profiles. Taken from [28].

Description	N_{cr}	C_r $(ft^2/cycles/ft)$
Smooth runway	3.8	1.6 x 10^{-11}
Rough runway	2.1	2.3 x 10^{-5}
Smooth highway	2.1	1.2 x 10^{-6}
Highway with gravel	2.1	1.1 x 10^{-5}
Pasture	1.6	1.6 x 10^{-3}
Plowed field	1.6	3.4 x 10^{-3}

Once a roughness coefficient has been selected, according to [30] the road profile $x(t)$ can be generated based on a standard procedure as the sum of a series of harmonics. Equation 3.4 presents the calculation of a road profile,

$$x(t) = \sum_{j=1}^{N_f} \sqrt{2\Delta\omega\, S(f)\, \omega_j}\, cos(\omega_j t - \phi_j) \tag{3.4}$$

where ϕ_j is a random phase angle normally distributed in the interval 0 - 2π; ω_j is a frequency within the interval at which $S(f)$ is defined and calculated as $\omega_j = \omega_{min} + \Delta\omega(j-1)$; the frequency increment $\Delta\omega$ is defined as $\Delta\omega = (\omega_{max} - \omega_{min})/N_f$; N_f is the total number of frequency increments in the interval $\omega_{min} - \omega_{max}$; the term inside the square root represents the amplitude of the harmonics; ω_{min} and ω_{max} are the minimum and maximum frequencies at which the spectrum is defined; and t represents the time.

In the present work, road profile (*RP*) displacement patterns were chosen for all tests. The employed roughness coefficient was that of a smooth highway. The number of harmonics was selected as 100 with minimum and maximum frequencies of 0.2 and 20.5 Hz, respectively. The number of cycles per feet was set to 0.5 and the speed of the vehicle was selected as 440 in/s (25 mi/h). The values were employed in order to recreate the displacement pattern of a highway under standard conditions and contain a time-changing frequency with peak values around 6 Hz. In order to obtain the signals, the algorithm was programmed in *MATLAB*^{TM}. *RP* signals were employed in [31] to test passive suspension systems and in [10] to train *ANNs* in order to model the behavior of an *MR* damper.

3.2 Experimental Setup

The selected experimental system can be divided into four parts: an *MR* damper, the actuators, the control system, and the data acquisition system. An ACDelco^{TM}*MR* damper, part of a *Delphi MagneRide*^{TM} suspension from a Cadillac 2008, was employed. An *MTS*^{TM}*GT* controller testing system was used to control the position of the damper. A *Flextest*^{TM} data acquisition system commanded the controller and recorded the position and force of the *MR* damper, as well as the electric current on the coil. A sampling frequency of 512 Hz was used. The displacement actuator was a hydraulic servo-controlled piston of 3000 psi and displacement bandwidth of 15 Hz. The displacement and electric current ranges were: 0 - 1.6 in, and 0 - 2.5 A, respectively. The damping force was measured using an *Instron* load cell and the measured span was 0 - 640 lbf. The experimental setup was controlled and monitored by a Human-Machine Interface (*HMI*) developed in *LabView*^{TM}. A block diagram of the experimental setup is shown in Fig. 3.1.

3.3 Signal Conditioning

3.3.1 Noise Filter

The measured signals were observed to be highly permeated by noise. In order to remove the undesired noise frequencies, a filter was designed as a second order low-pass filter with a cutoff frequency of 20 Hz. Equation 3.5 presents the transfer function for the designed filter.

$$G_{LPF}(s) = \frac{1}{(0.5\pi\, s + 1)^2} \tag{3.5}$$

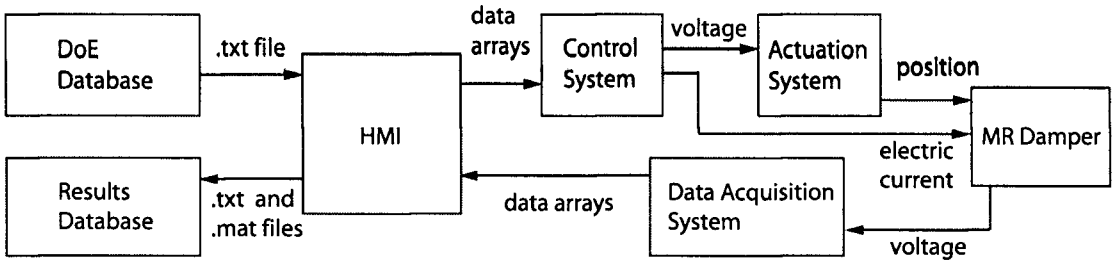

Figure. 3.1. Block diagram of the experimental setup. The designed experiments are loaded as text files to the *HMI*. The *HMI* converts the files and sends the patterns to the control system. Then, a voltage respective to the desired position is sent to the actuation system, at the same time that the desired electric current is sent to the *MR* damper. The position, force, and temperature measurements are sent to the data acquisition system and are then passed to the *HMI* in the appropriate format. Finally, the *HMI* is in charge of formatting and saving the data.

3.3.2 Discrete Derivative

In order to compute the velocity of the *MR* damper, a discrete-time derivative was employed after the displacement signal was filtered. The calculations were performed using *Simulink* (see appendix A).

3.4 Experimental Results

Eight sets of experimental data were obtained for the identification of *MR* damper models. In the selected experiments, the electric current patterns were *CS*, *ICPS*, *PRBS*, and *APRBS* signals. On the other hand, *RP* patterns were employed as the displacement input. Three 30 s experiments were performed for the highly varying electric current patterns. In addition, two 600 s experiments with *APRBS* and *ICPS* electric current patterns were performed in order to test the behavior of the *MR* damper as the temperature of the device increased. Finally, three 210 s experiments were carried out employing *SC* electric current patterns. Various replicates of the experiments were performed and used as validation data.

The specific patterns of the eight experiments are shown in Table 3.2, where the experiments have been labeled according to the patterns employed. The table specifies the utilized input patterns, the number of replicates performed, the duration of the experiments, the maximum displacement frequency, and the displacement span. Moreover, figures 3.2 and 3.3 show 20 and 100 second windows of the patterns employed for the first and last experiments, respectively. In addition, 30 and 60 second windows present the frequency content of the experiments. See Appendix A for a complete comparison of the experimental data sets .

3.5 Summary

A description of the design of experiments, experimental setup, and resulting data sets was presented in this chapter. Various electric current patterns were selected in order to characterize the behavior of the *MR* damper. On the other hand, displacement patterns that resembled usual operating conditions of an automotive suspension system were chosen. The experimental setup and process were specifically described. At the end, eight experimental data sets were obtained in order to be used as training patterns for models of an industrial *MR* damper.

Table 3.2. Experimental data sets

Experiment Name	Displacement Pattern	E. Current Pattern	Number of Replicates	Duration (sec)	Max. Frequency Value (Hz)	Displacement Span (in)
RP-ICPS	RP	ICPS	11	30	5.5	1.04
RP-APRBS	RP	APRBS	11	30	4.5	1.08
RP-PRBS	RP	PRBS	11	30	4.2	1.17
RP-APRBS-L	Long RP	APRBS	3	600	4.5	1.08
RP-ICPS-L	Long RP	ICPS	4	600	5.5	1.02
RP1-CS	RP	CS	1	210	5.5	1.32
RP2-CS	RP	CS	1	210	4.5	1.31
RP3-CS	RP	CS	1	210	4.5	1.42

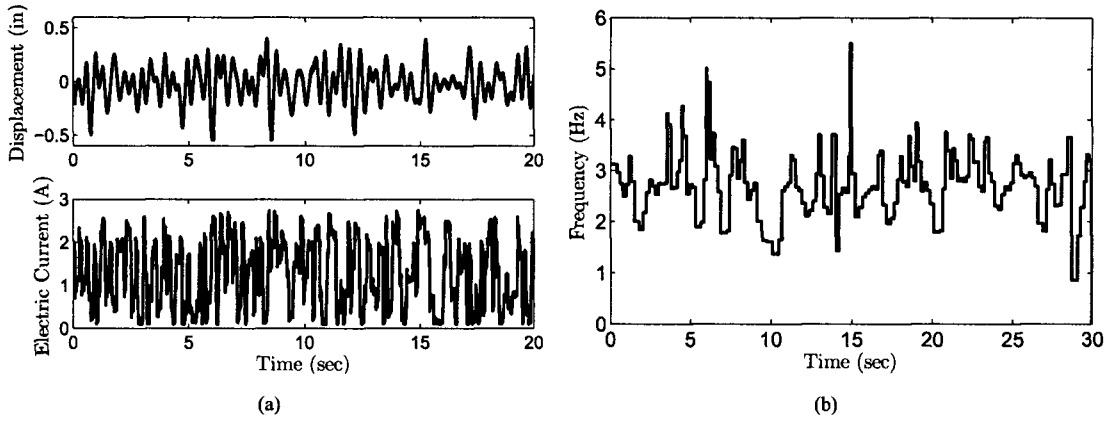

Figure. 3.2. Description of experiment *RP-ICPS*. Displacement and electric current patterns (left). Frequency content (right).

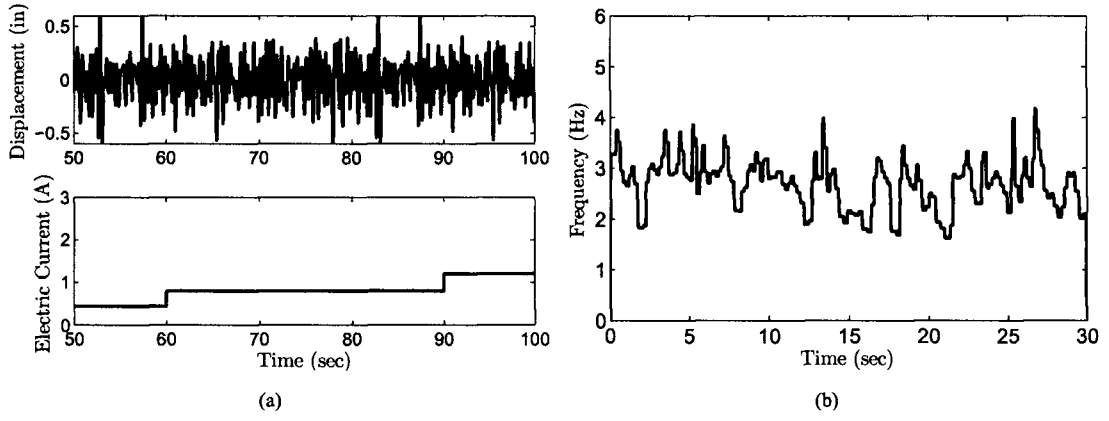

Figure. 3.3. Description of experiment *RP3-CS*. Displacement and electric current patterns (left). Frequency content (right).

Chapter 4

Results

An extensive comparison of *MR* damper models is presented. The study is motivated on the challenge that involves the correct modeling of an *MR* damping system. Four models were selected among the state of the art, one from each modeling technique presented in the previous chapter. The models were trained using eight sets of experimental data and two error indexes were calculated. The results are presented by means of box-and-whisker diagram plots.

4.1 Error Calculation

Among the state of the art, the selected models were the ones presented in [5], [32], a black-box model structure used in [10] and [33], and a fuzzy model that uses *ANFIS* as presented in [12] and [20]. The models were compared against each other by using the *Square Root of the Sum of the Squared Errors* (*RSSE*) and the *Error to Signal Ratio* (*ESR*) indexes. The *RSSE* and *ESR* are presented in equations 4.1 and 4.2, respectively. The *RSSE* presents the square root of the sum of the errors between the predicted and experimental output forces normalized by the total number of samples. The *ESR* is the ratio of the sum of squared errors and the variance of the experimental force. This last index is equal to one if the model is trivial and zero if the model is perfect.

$$RSSE = \sqrt{\frac{1}{T}\sum_{t=1}^{T}\left(F(t) - \hat{F}(t)\right)^2} \tag{4.1}$$

$$ESR = \frac{(RSSE)^2}{\frac{1}{T}\sum_{t=1}^{T}\left(F(t) - \left(\frac{1}{T}\sum_{j=1}^{T}F(j)\right)\right)^2} \tag{4.2}$$

The eight selected sets of experimental data discussed in the previous chapter were employed to train the structures. The models were identified using the first replicate of each experiment and cross validated with the remaining ones. The first three models were first identified in their passive form. This is, no electric current dependency was included. Then, the models were identified in their semi-active form. This is, the electric current was taken into account. The fuzzy-based structure was only identified in its semi-active form. At the end of the chapter, a non-linear fuzzy structure is proposed as an alternative for modeling an *MR* damper.

4.2 *ARX* Model

The *ARX* structure shown in 2.8 was modified to consider three regressors for each input variable ($x(t)$, $\dot{x}(t)$, $F(t)$) instead of two (see equation 4.3). Using the first replicate of each experiment, the nine coefficients of the model were identified with *MATLAB*^{TM} using a nonlinear least squares algorithm. Then, the *RSSE* and *ESR* were calculated by comparing the experimental force with the force predicted by the models. The coefficients were randomly initialized 25 times and the lowest error value was recorded. The resulting identification errors are shown in Table 4.1. The identified coefficients for the different *ARX* structures can be seen in Appendix B.

$$\begin{aligned} F_k &= a_1F_{k-1} + a_2F_{k-2} + a_3F_{k-3} + a_4x_k + a_5x_{k-1} + a_6x_{k-2} \\ &\quad + a_7\dot{x}_k + a_8\dot{x}_{k-1} + a_9\dot{x}_{k-2} \end{aligned} \tag{4.3}$$

Table 4.1. Identification *RSSE* and *ESR* for the passive *ARX* model.

Model Training	RSSE (lbf)	ESR
RP-ICPS	11.19	0.0146
RP-APRBS	9.87	0.0112
RP-PRBS	11.02	0.0211
RP-APRBS-L	10.47	0.0124
RP-ICPS-L	11.42	0.0152
RP1-CS	0.84	0.0002
RP2-CS	1.28	0.0002
RP3-CS	1.24	0.0002

Notice that for every *ARX* model identified, the *RSSE* and *ESR* lie below 12 lbf and 0.03, respectively even for the experiments with high electric current variations. In addition, a marked improvement can be seen for the models trained with the experiments that use constant steps of the electric current. Next, the eight identified models were validated using the remaining replicates and experiments. The resulting *RSSE* and *ESR* values by model are depicted in Figs. 4.1 and 4.2, respectively. The figures present a box and whisker plot with one box for each *ARX* model. The boxes have lines at the lower quartile, median, and upper quartile values. The whiskers are lines extending from each end of the boxes to show the extent of the rest of the data. Outliers are data with values beyond the ends of the whiskers. The models are named according to the experiments with which they were trained.

From the figure, it can been seen that the models trained with the experimental data sets with constant electric current obtained various *RSSE* and *ESR* values over 20 lbf and 0.10, respectively. On the other hand, the *ARX* models identified with experiments that contain varying electric current can be observed to have less error values overall.

In order to include the variant electric current in the model, the *ARX* structure was modified by adding three regressors. Equation 4.4 shows the final structure.

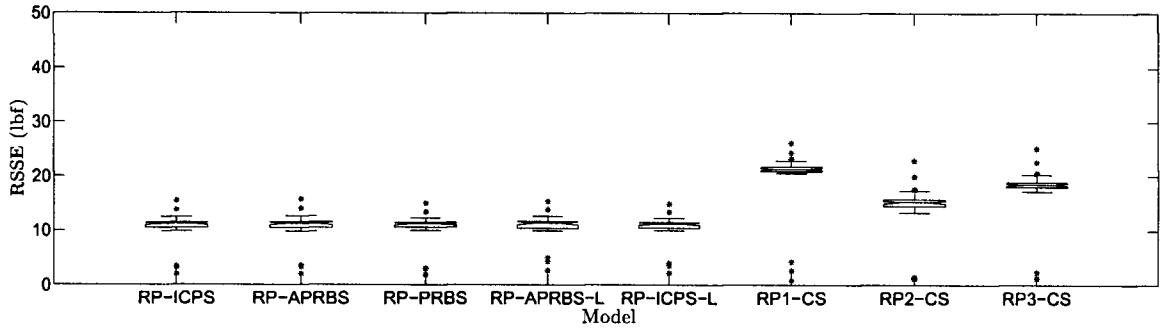

Figure. 4.1. *RSSE* results for the passive *ARX* model

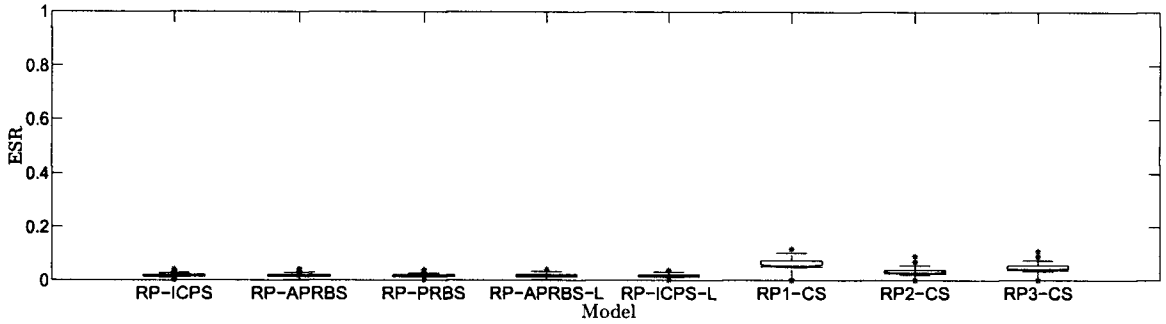

Figure. 4.2. *ESR* results for the passive *ARX* model

$$\begin{aligned} F_k &= a_1 F_{k-1} + a_2 F_{k-2} + a_3 F_{k-3} \\ &\quad + a_4 x_k + a_5 x_{k-1} + a_6 x_{k-2} \\ &\quad + a_7 \dot{x}_k + a_8 \dot{x}_{k-1} + a_9 \dot{x}_{k-2} \\ &\quad + a_{10} i_k + a_{11} i_{k-1} + a_{12} i_{k-2} \end{aligned} \tag{4.4}$$

As for the passive model, the modified *ARX* semi-active model was trained using the first replicate of each of the eight sets of experimental data. As for the passive structure, 25 random initializations of the 12 coefficients were performed and the lowest error was recorded. The resulting identification errors are shown in Table 4.2. The identified coefficients for the different *ARX* structures can be seen in Appendix B.

It should be noted that the addition of the three electric current regressors improved only slightly the performance of the *ARX* models. To further analyze the performance, the eight identified semi-active models were cross validated using the remaining replicates and experiments. The resulting *RSSE* and *ESR* values by model are depicted in Figs. 4.3 and 4.4, respectively.

It can be observed that the results are nearly identical to the results obtained with the passive *ARX* model for the first five models. Nonetheless, for the models trained with experiments that held the electric current constant, the validation results were not satisfactory.

Table 4.2. Identification *RSSE* and *ESR* for the semi-active *ARX* model.

Model Training	RSSE (lbf)	ESR
RP-ICPS	11.18	0.0145
RP-APRBS	9.86	0.0112
RP-PRBS	11.02	0.0210
RP-APRBS-L	10.46	0.0124
RP-ICPS-L	11.40	0.0152
RP1-CS	0.84	0.0002
RP2-CS	1.22	0.0002
RP3-CS	1.09	0.0001

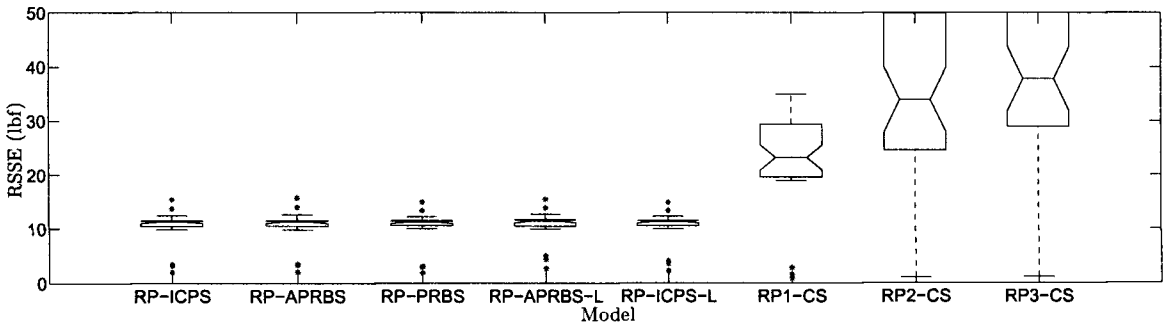

Figure. 4.3. *RSSE* results for the semi-active *ARX* model.

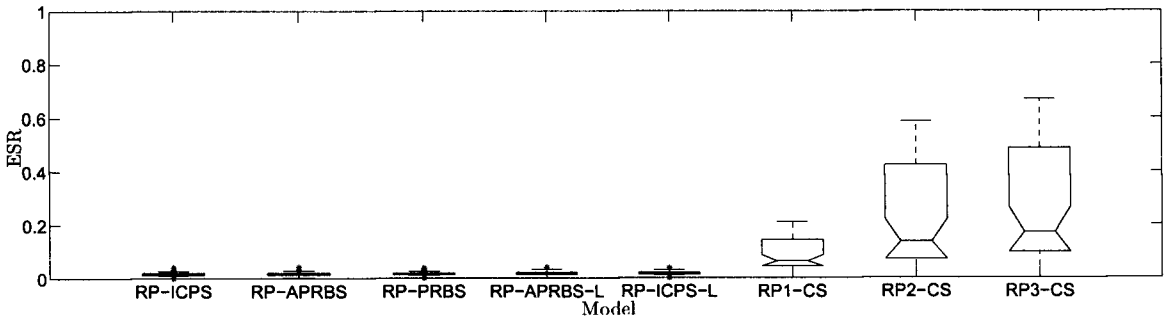

Figure. 4.4. *ESR* results for the semi-active *ARX* model.

4.3 Semi-Phenomenological (*S-P*) Model

The model shown in equation 2.3 was identified for the first replicate of each of the eight sets of experiments aforementioned. The identification algorithm was chosen as non-linear least squares. The five coefficients of the model were randomly initialized 25 times and the lowest error value was recorded. The resulting identification errors are shown in Table 4.3. Again, the identified coefficients are specified in Appendix B.

Table 4.3. Identification *RSSE* and *ESR* for the passive *S-P* model.

Model Training	RSSE (lbf)	ESR
RP-ICPS	38.35	0.1681
RP-APRBS	31.23	0.1098
RP-PRBS	44.74	0.3410
RP-APRBS-L	27.27	0.0837
RP-ICPS-L	35.95	0.1472
RP1-CS	43.18	0.2073
RP2-CS	45.16	0.2264
RP3-CS	44.79	0.2105

It can be noticed that the passive *S-P* model obtained high identification errors for most of the experiments. A later cross validation was performed using all the data sets and replicates. This validation confirmed that the passive *S-P* model was not able to predict the damping force in an accurate manner. Even for the models that obtained the lowest identification errors, *RSSE* and *ESR* values of more than 50 lbf and 0.30, respectively were observed.

In order to include the electric current into the model, each of the parameters (A_1, A_2, A_3, V_0, and X_0) was made equal to a second order polynomial dependent on the electric current. Thus, the *S-P* model, now semi-active, is represented in equation 4.5.

$$\begin{aligned} F(t) = {} & \left(A_{11} + A_{12}i(t) + A_{13}i(t)^2\right) \cdot \\ & tanh\left(\left(A_{21} + A_{22}i(t) + A_{23}i(t)^2\right)\left(\dot{x}(t) + \frac{\left(V_{01} + V_{02}i(t) + V_{03}i(t)^2\right)}{\left(X_{01} + X_{02}i(t) + X_{03}i(t)^2\right)}\, x(t)\right)\right) \\ & + \left(A_{31} + A_{32}i(t) + A_{33}i(t)^2\right)\left(\dot{x}(t) + \frac{\left(V_{01} + V_{02}i(t) + V_{03}i(t)^2\right)}{\left(X_{01} + X_{02}i(t) + X_{03}i(t)^2\right)}\, x(t)\right) \end{aligned} \tag{4.5}$$

The structure depends on 15 coefficients that were identified for the first replicate of each of the eight sets of experimental data. One more time, 25 random initializations of the coefficients were done and the lowest error values were recorded. The resulting identification errors for the semi-active *S-P* model are shown in Table 4.4.

Contrary to the passive one, the semi-active *S-P* model was able to obtain lower error values for all the experimental data sets. A considerable decrease in error was seen for the models trained using experiments with constant electric current. As for the passive model, a cross validation was performed using the semi-active version. Figs. 4.5 and 4.6 present the *RSSE* and *ESR* by model, respectively.

Table 4.4. Identification *RSSE* and *ESR* for the semi-active *S-P* model.

Model Training	RSSE (lbf)	ESR
RP-ICPS	26.47	0.0801
RP-APRBS	23.72	0.0633
RP-PRBS	22.39	0.0826
RP-APRBS-L	23.04	0.0597
RP-ICPS-L	24.55	0.0666
RP1-CS	21.65	0.0521
RP2-CS	22.96	0.0588
RP3-CS	20.98	0.0463

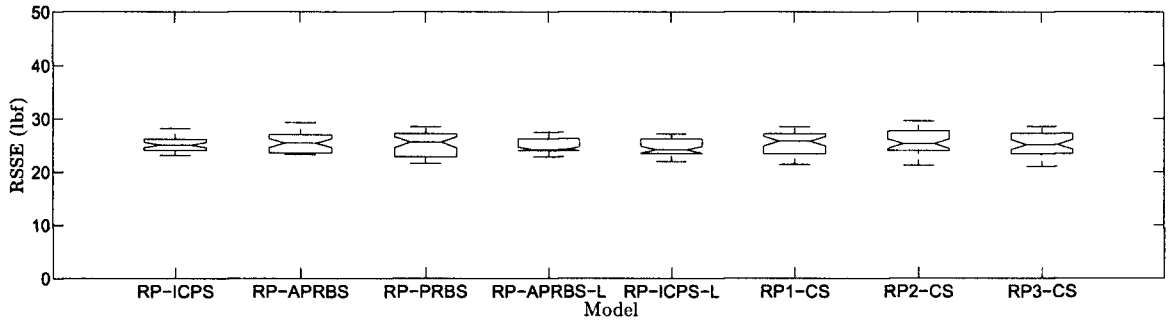

Figure. 4.5. *RSSE* results for the semi-active *S-P* model.

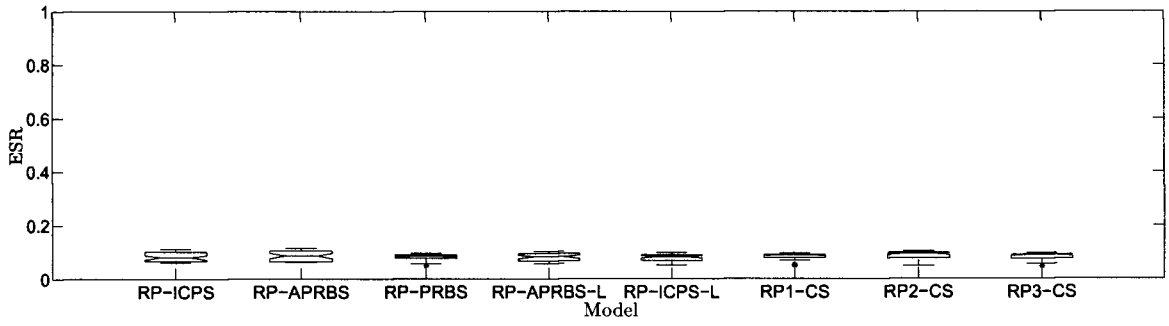

Figure. 4.6. *ESR* results for the semi-active *S-P* model.

The figures show that for all the identified semi-active *S-P* structures, the median of the *RSSE* laid around 25 lbf, while the median for the *ESR* was 0.09. Thus, the addition of the electric current parameters significantly improved the performance of the model.

4.4 Phenomenological (*P*) Model

The model previously shown in equation 2.1 was identified for the first replicate of each of the eight data sets using *MATLAB*^{TM} and a least squares optimization algorithm. The relationship shown in equation 4.6 was utilized as the objective function in order to capture the dynamics of the damper.

$$F(t) = p_1\dot{x}(t) + p_2\dot{F}(t) + p_3\ddot{F}(t) + p_4F(t)^3 + p_5F(t)^5 \tag{4.6}$$

The coefficients of the model were randomly initialized 25 times and the lowest error values were recorded. The identification errors for the passive *P* model are shown in Table 4.5.

Table 4.5. Identification *RSSE* and *ESR* for the passive *P* model.

Model Training	RSSE (lbf)	ESR
RP-ICPS	27.06	0.0832
RP-APRBS	24.89	0.0682
RP-PRBS	22.76	0.0854
RP-APRBS-L	21.23	0.0499
RP-ICPS-L	23.06	0.0606
RP1-CS	27.17	0.0821
RP2-CS	29.57	0.0975
RP3-CS	26.01	0.0712

It can be seen that the passive *P* model obtained low identification error values for all the experimental data sets, even for the ones with highly variant electric current. A cross validation was employed to further compare the performance of the model in different scenarios. The validation can be seen in Figs. 4.7 and 4.8. Notice that *RSSE* and *ESR* outliers of more than 35 lbf and 0.15 were observed for the models identified with highly variant electric current experiments.

Afterwards, in order to make the model dependent on the electric current, each coefficient in equation 4.6 was replaced by a second order polynomial electric current equation (see equation 4.7). This modified model was again identified using the first replicate of each of the eight experimental data sets. The obtained identification errors are displayed in Table. 4.6.

$$\begin{aligned} F(t) = {} & \left(p_{11} + p_{12}i(t) + p_{13}i(t)^2\right)\dot{x}(t) + \left(p_{21} + p_{22}i(t) + p_{23}i(t)^2\right)\dot{F}(t) \\ & + \left(p_{31} + p_{32}i(t) + p_{33}i(t)^2\right)\ddot{F}(t) + \left(p_{41} + p_{42}i(t) + p_{43}i(t)^2\right)F(t)^3 \\ & + \left(p_{51} + p_{52}i(t) + p_{53}i(t)^2\right)F(t)^5 \end{aligned} \tag{4.7}$$

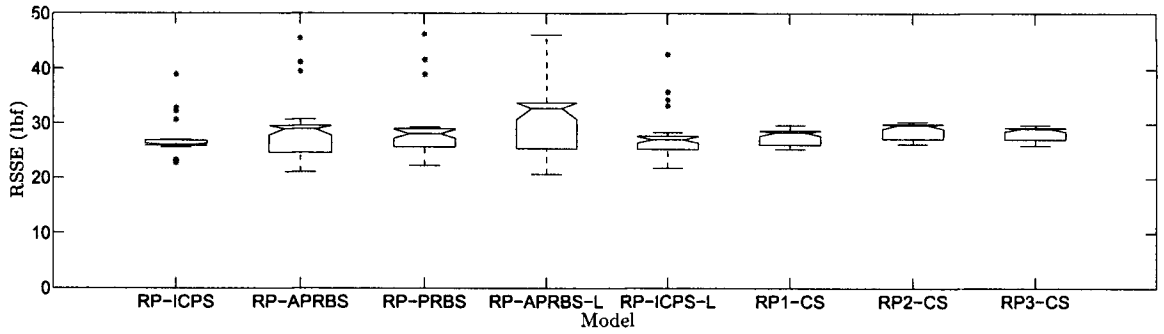

Figure. 4.7. *RSSE* results for the passive *P* model.

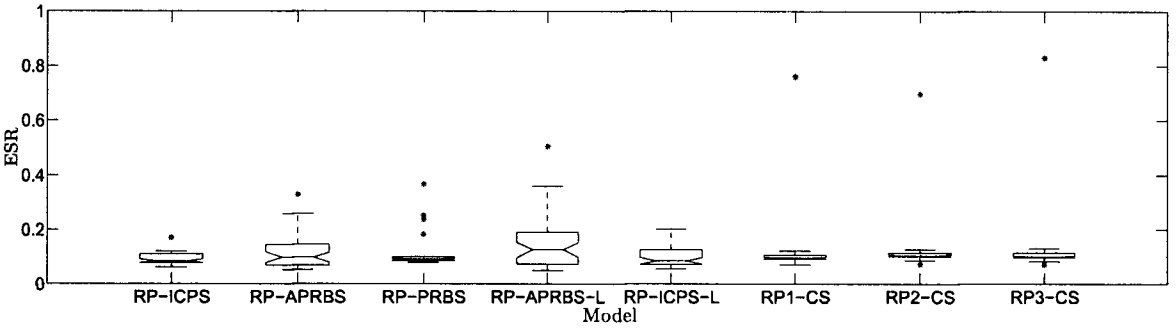

Figure. 4.8. *ESR* results for the passive *P* model.

Table 4.6. Identification *RSSE* and *ESR* for the semi-active *P* model.

Model Training	RSSE (lbf)	ESR
RP-ICPS	25.08	0.0713
RP-APRBS	22.60	0.0564
RP-PRBS	18.62	0.0576
RP-APRBS-L	22.29	0.0560
RP-ICPS-L	25.59	0.0749
RP1-CS	22.26	0.0551
RP2-CS	21.65	0.0522
RP3-CS	13.32	0.0187

It is important to mention that the semi-active *P* model outperformed the passive one for all the experiments when comparing the identification errors, except for experiment *RP-ICPS-L*. For this last one, the *RSSE* increased by 2 lbf. The cross validation performed using the semi-active *P* model is shown in Figs. 4.9 and 4.10.

Notice that, even when the semi-active *P* model obtained low identification errors for most experimental data sets, the validation results do not show a significant improvement with respect to the passive model.

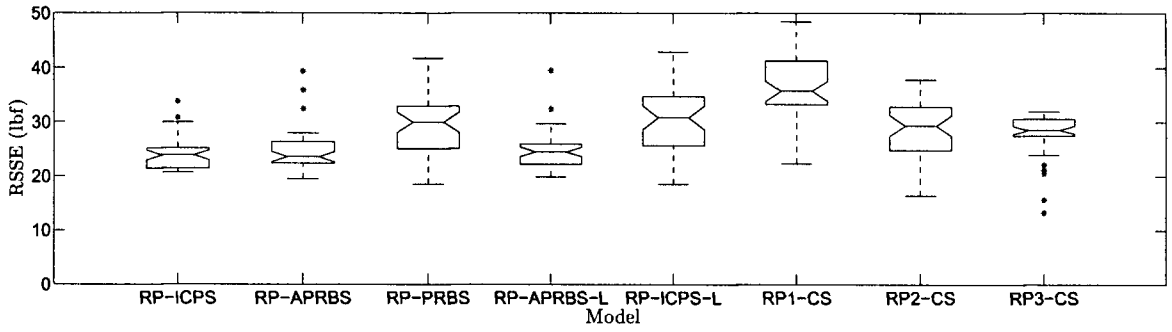

Figure. 4.9. *RSSE* results for the semi-active *P* model.

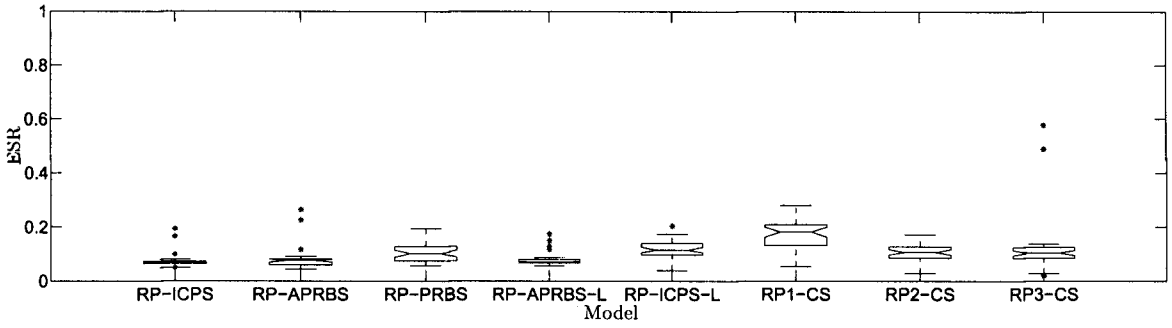

Figure. 4.10. *ESR* results for the semi-active *P* model.

4.5 Fuzzy-Based Model

A *TSK* fuzzy-based model that used *ANFIS* was analyzed for modeling the *MR* damper. Displacement, velocity, and electric current were used as inputs, and the damper force was the output. The model resembled the one in Fig. 2.6, but contained 27 fuzzy rules for all possible combinations of inputs. Three Gaussian membership functions were utilized for each input and the outputs of the system were selected as 27 linear functions.

One fuzzy-based model was trained using the first replicate of each set of experimental data after being normalized. A hybrid learning algorithm was selected to train the structure by means of the *ANFIS* toolbox in *MATLAB*^{TM}. The training was performed 50 times or until the error decreased by less than a threshold. After the training, the *RSSE* and *ESR* were calculated in *Simulink* as specified in Appendix C. The identification errors are shown in Table 4.7.

Notice that the fuzzy-based model obtained low identification errors when trained with all the experimental data sets, especially for the ones with constant electric current patterns. A cross validation was performed using the rest of the experimental data sets to further analyze the structure . Figs. 4.11 and 4.12 present the obtained *RSSE* and *ESR* values by model, respectively.

It can be seen that the models trained using experimental data with constant electric current steps outperformed those trained with highly variant electric current by far.

Table 4.7. Identification *RSSE* and *ESR* for the fuzzy-based model.

Model Training	RSSE (lbf)	ESR
RP-ICPS	26.27	0.0729
RP-APRBS	23.43	0.0565
RP-PRBS	22.64	0.0781
RP-APRBS-L	24.50	0.0645
RP-ICPS-L	25.43	0.0718
RP1-CS	21.69	0.0523
RP2-CS	22.07	0.0543
RP3-CS	20.68	0.0450

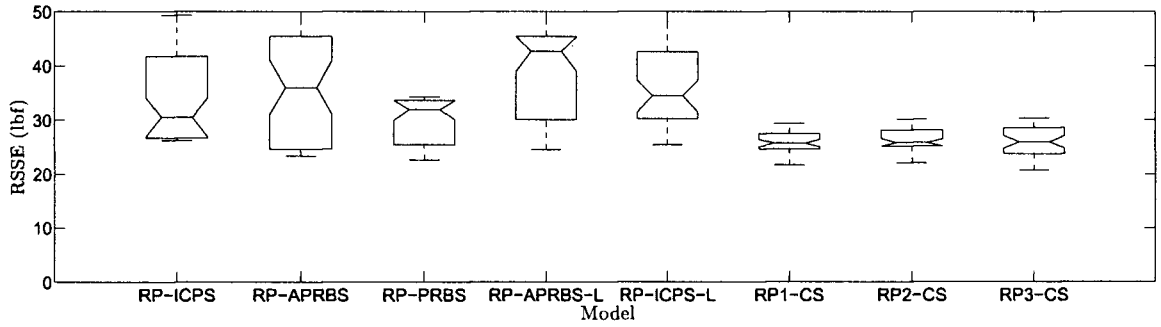

Figure. 4.11. *RSSE* results for the fuzzy-based model.

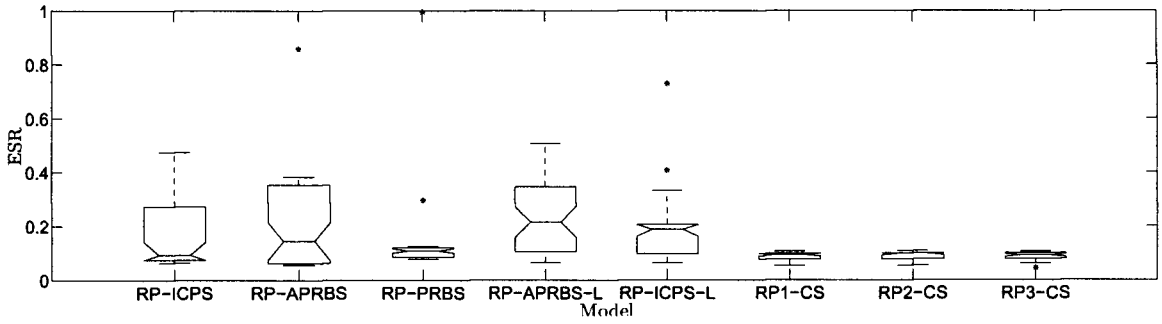

Figure. 4.12. *ESR* results for the fuzzy-based model.

4.6 Non-Linear Fuzzy-Based Model

A non-linear fuzzy-based model is proposed in the present work in order to model the behavior of an *MR* damper. The structure can be regarded as a fuzzy-based method to introduce the dependency on the electric current to a non-linear model of an *MR* damper. The model uses the electric current as input, and the fuzzy rules are defined as specified in equation 4.8.

$$If\ i(t)\ is\ M_{Fj}\ then\ f_j(t)\ =\ g_j(x(t),\dot{x}(t)) \tag{4.8}$$

Notice that each output function $f_j(t)$ depends on the displacement and the velocity of the *MR* damper. M_{Fj} are fuzzy sets of $i(t)$. The output functions for the model were selected to be of the form of the semi-phenomenological model of the *MR* damper presented in [2] and shown again in equation 4.9,

$$\begin{aligned} f_j(t) = d_{1j}\ tanh\left(d_{2j}\ (\dot{x}(t) + d_{3j}\ x(t))\right) \\ +d_{4j}\ (\dot{x}(t) + d_{3j}\ x(t)) \end{aligned} \tag{4.9}$$

where the coefficients d_{1j}, d_{2j}, d_{3j}, and d_{4j} are to be determined from experimental data.

The overall output force of the damper was selected to be computed as specified by equation 4.10,

$$F(t) = \frac{\sum_{j=1}^{7} W_{Fj}(i(t))\ f_j(t)}{\sum_{j=1}^{7} W_{Fj}(i(t))} \tag{4.10}$$

where W_j represents the membership degree of $i(t)$ on each of the membership functions. Fig. 4.13 depicts the proposed non-linear fuzzy-based structure.

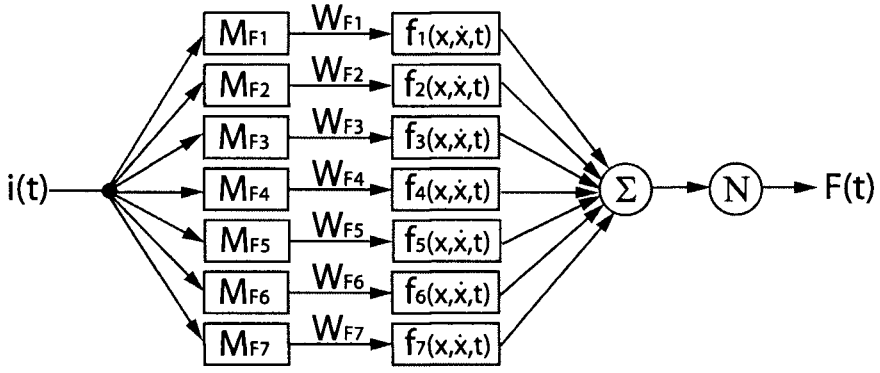

Figure. 4.13. Non-linear fuzzy-based model.

As equation 4.9 only depends on the displacement and velocity of the damper, the experimental data sets where the electric current was employed as constant step increments were selected as identification sets. Each experimental data set (*RC1-CS*, *RC2-CS*, and *RC3-CS*) was broken into seven subsets, each corresponding to a time span with

constant electric current values. Then, coefficients were identified using non-linear least squares and yielded one non-linear equation for each of the seven electric current stepped increments on the experiments. In this manner, one non-linear fuzzy-based model with seven output functions was obtained from experiment *RC1-CS*, one from experiment *RC2-CS*, and one from experiment *RC3-CS*. The fuzzy-based models were labeled according to the experiments with which they were trained.

The input membership functions for each model were defined as seven Gaussian functions with variance equal to 0.2 and means of 0, 0.4, 0.8, 1.2, 1.6, 2.1, and 2.5 A, respectively. Additionally, seven output functions were selected in the form of equation 4.9 with coefficients previously identified (see Appendix B).

Once the three structures were trained, a cross validation was performed using the eight sets of experimental data. Figs. 4.14 and 4.15 present the resulting *RSSE* and *ESR* by model, respectively. Notice that the models trained with the three experimental data sets obtained validation errors with medians below 29 lbf and 0.1. The details of the calculations for the proposed structure can be seen in Appendix D.

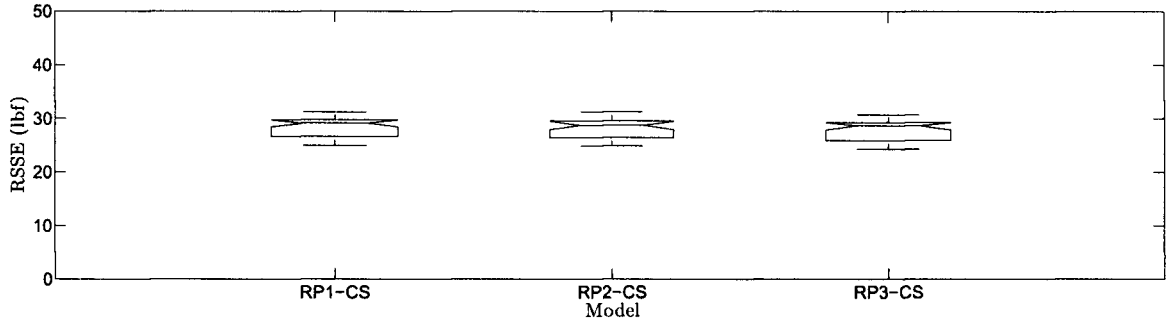

Figure. 4.14. *RSSE* results for the non-linear fuzzy model.

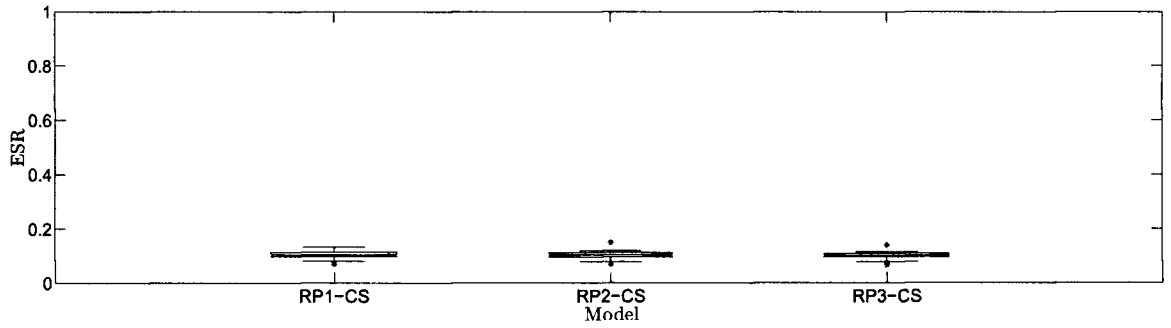

Figure. 4.15. *ESR* results for the non-linear fuzzy model.

4.7 Summary

This chapter presented an extensive comparison of four models for *MR* dampers. The models were trained using eight different sets of experimental data and the *RSSE* and *ESR* were computed. Box plots were utilized in order

to compare the performance of the structures under different input patterns. At the end of the chapter, a non-linear fuzzy-based model was proposed, identified, and tested.

Chapter 5

Analysis and Comparison of Results

An analysis of the identification results for *MR* damper models is presented. The models that obtained the lowest average validation errors were selected and then further compared by means of force-time and force-velocity plots. Experiment *RP-APRBS* was employed to test the models in the time domain, due to its variant electric current content. Experiment *RP1-SC* was employed to test the models in the force-velocity behavior, due to its constant electric current increments.

5.1 Best Models

The average *RSSE* and *ESR* values were calculated for each of the models presented in the previous chapter. The errors are shown in Tables 5.1 and 5.2 by model and divided according to the experimental data set with which they were identified.

Table 5.1. Average *RSSE* (lbf) by model and experimental data set.

Model/Exp.	RP-ICPS	RP-APRBS	RP-PRBS	RP-APRBS-L	RP-ICPS-L	RP1-CS	RP2-CS	RP3-CS
Passive ARX	10.99	11.06	10.99	11.11	10.98	20.98	15.18	18.36
Semi-Active ARX	10.99	11.06	10.98	11.13	10.98	24.21	37.51	41.32
Passive S-P	40.45	41.16	44.49	41.32	40.23	39.86	40.20	39.92
Semi-Active S-P	25.10	25.45	25.27	24.75	24.56	25.40	25.66	25.15
Passive P	26.50	28.93	29.11	32.66	26.96	27.57	28.79	28.30
Semi-Active P	23.96	24.82	34.15	24.82	36.07	45.66	35.66	29.50
Fuzzy-Based	36.12	38.55	38.19	40.11	37.96	25.94	26.32	26.12
N-L Fuzzy-Based	-	-	-	-	-	28.41	28.21	27.82

It can be noticed from the tables that the *ESR* values are almost proportional to the *RSSE* ones for all the models.

Table 5.2. Average *ESR* by model and experimental data set.

Model/Exp.	RP-ICPS	RP-APRBS	RP-PRBS	RP-APRBS-L	RP-ICPS-L	RP1-CS	RP2-CS	RP3-CS
Passive ARX	0.0164	0.0167	0.0163	0.0168	0.0164	0.0592	0.0314	0.0456
Semi-Active ARX	0.0164	0.0167	0.0163	0.0169	0.0163	0.0841	0.2104	0.2525
Passive S-P	0.2279	0.2378	0.2574	0.2400	0.2252	0.2161	0.2196	0.2169
Semi-Active S-P	0.0813	0.0838	0.0807	0.0786	0.0771	0.0816	0.0840	0.0803
Passive P	0.0875	0.1046	0.1029	0.1337	0.0911	0.0941	0.1029	0.0996
Semi-Active P	0.0723	0.0782	0.1603	0.0764	0.1815	0.3051	0.1827	0.1145
Fuzzy-Based	0.1655	0.1956	0.1607	0.2148	0.1736	0.0864	0.0879	0.0875
N-L Fuzzy-Based	-	-	-	-	-	0.1035	0.1024	0.0993

5.1.1 ARX Model

The *ARX* model obtained the lowest validation errors when trained with experiments with highly variant electric current patterns. The inclusion of regressors for the electric current was not seen to improve the results. In fact, when the model was trained with experimental data sets that employed constant increments of the electric current, the errors were observed to significantly increase for the semi-active version. This phenomenon confirmed that the *ARX* structure depends greatly on the damping force regressors and not on the electric current ones. Moreover, the addition of three electric current regressors only complicated the identification process. Based on the average error calculations, the semi-active *ARX* model trained with experiment *RP-ICPS-L* was selected as the best one among the *ARX* structures, with *RSSE* and *ESR* values of 10.9766 lbf and 0.0163, respectively.

Fig. 5.1 presents a two second window that compares the experimental force and the force estimated by the model. Fig. 5.2 compares the force-velocity behavior of the experimental and estimated damper force at six different constant electric current values. The experimental data was taken from experiments *RP-APRBS* and *RP1-CS*, respectively.

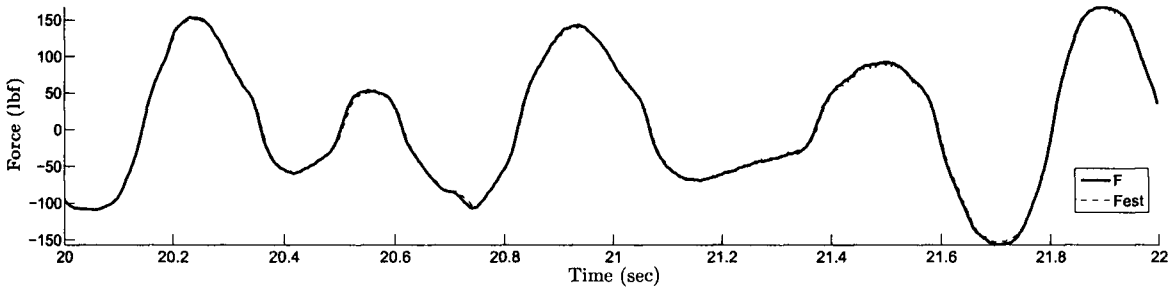

Figure. 5.1. Experimental and estimated damper force by the selected *ARX* model. Experimental data taken from experiment *RP-APRBS*.

It can be noticed from the time comparison plot that the *ARX* model very accurately matches the experimental force, with only slight differences at the lower peaks. The force-velocity plots reveal that at the lower electric current values, the *ARX* structure struggles to model the non-linearities of the *MR* damper. As the electric current increases, the *ARX* model starts to almost perfectly model the behavior of the damper. If analyzed in detail, a minor shift can

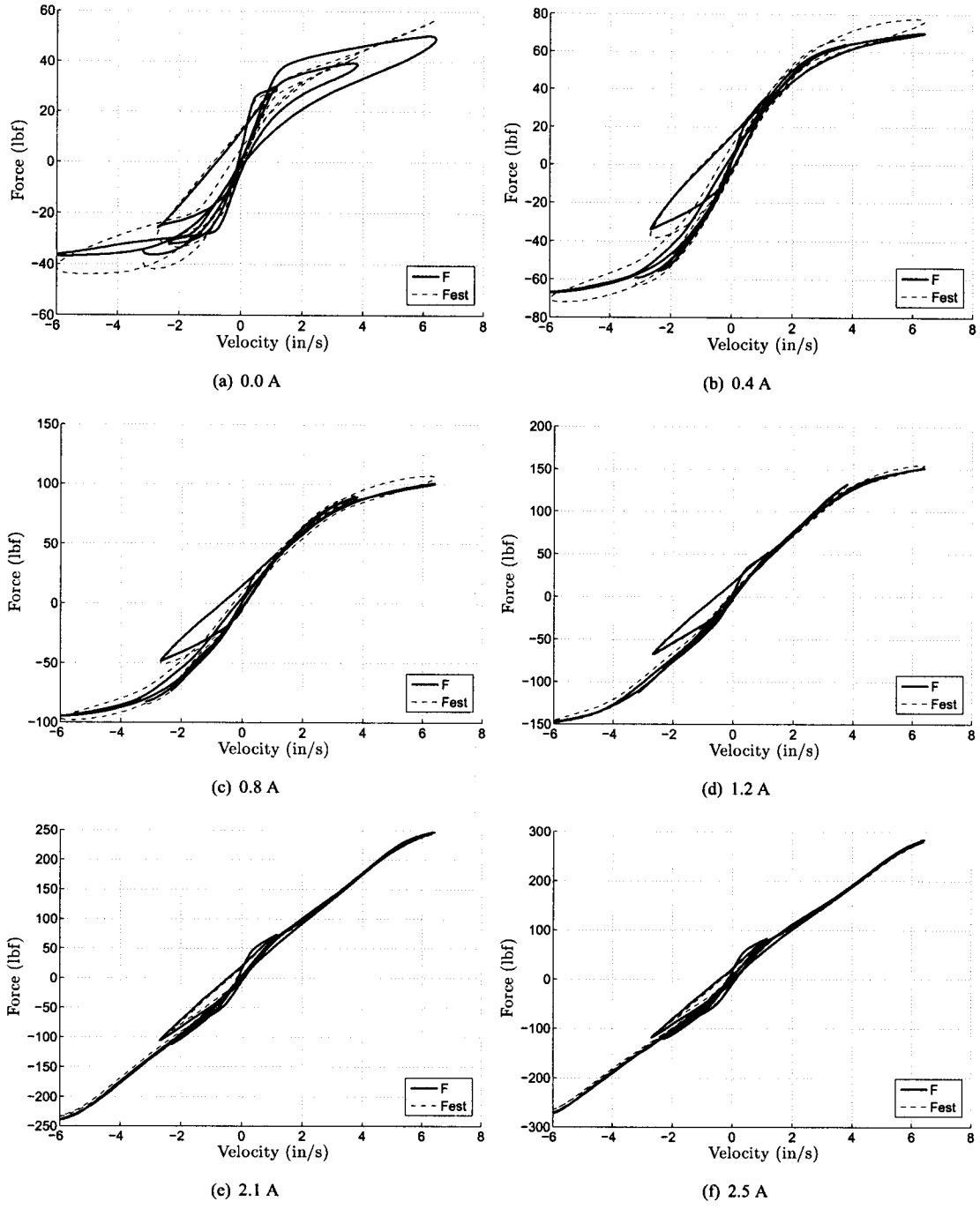

Figure. 5.2. Experimental and estimated F-v behavior of the selected *ARX* model. Each of the figures presents the behavior at a constant value of the electric current using the data from experiment *RP1-CS*.

be noticed between the experimental and predicted forces. This shift may be due to the fact that the *ARX* structure is highly dependent on the previous values of the damping force. Moreover, the model may be merely expecting for the future value of the force to be equal to the previous one and hence the observed shift.

5.1.2 S-P Model

It was observed that the *S-P* model performed uniformly for all the experimental data sets. The inclusion of the electric current to the model significantly diminished the *RSSE* and *ESR* values by approximately 15 lbf and 0.15, respectively. Nonetheless, this inclusion of the electric current incremented considerably the number of parameters. Based on the average error calculations, the semi-active *S-P* model trained with experiment *RP-ICPS-L* was selected as the best *S-P* model, with *RSSE* and *ESR* values of 24.5619 lbf and 0.0771, respectively.

Fig. 5.3 presents a two second window that compares the experimental force and the force estimated by the model. Fig. 5.4 compares the force-velocity behavior for the experimental and estimated damper force at six different constant electric current values. Once again, the experimental data was taken from experiments *RP-APRBS* and *RP1-CS*, respectively.

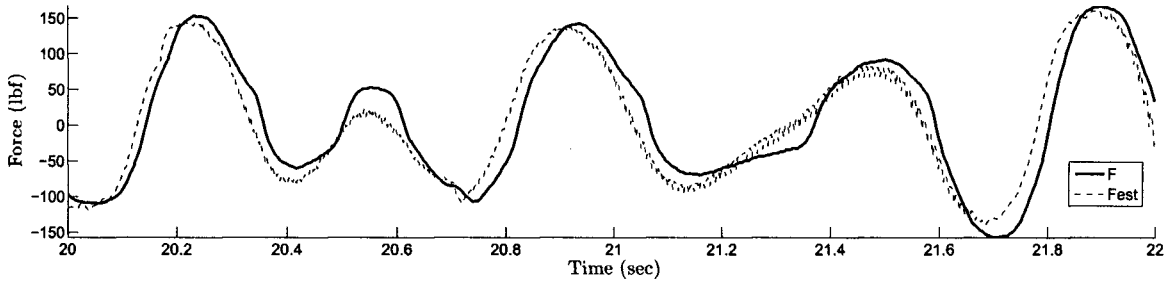

Figure. 5.3. Experimental and estimated damper force by the selected *S-P* model. Experimental data taken from experiment *RP-APRBS*.

It can be seen from the force-time plot that the *S-P* model follows the pattern of the experimental force with a minor lead time. On the other hand, the force-velocity plots confirm that the *S-P* model correctly follows the non-linearities of the MR damper, but overly exaggerates the width of the hysteresis loop. As for the *ARX* one, the *S-P* model seems to improve its performance as the electric current is increased, but never reaches an acceptable performance.

5.1.3 P Model

The *P* model was observed to perform almost constantly for all the experimental data sets. The addition of the electric current to the model was not seen to significantly improve its performance. Moreover, the *RSSE* and *ESR* values were seen to significantly increase for five experimental data sets when the semi-active *P* model was employed. As for the *ARX* model, this phenomenon is due to the fact that the model places greater importance on the force inputs than on the electric current. Based on the average error calculations, the *P* model trained with the *RP-ICPS* data set was selected as the best *P* model, with *RSSE* and *ESR* values of 23.9550 lbf and 0.0723, respectively.

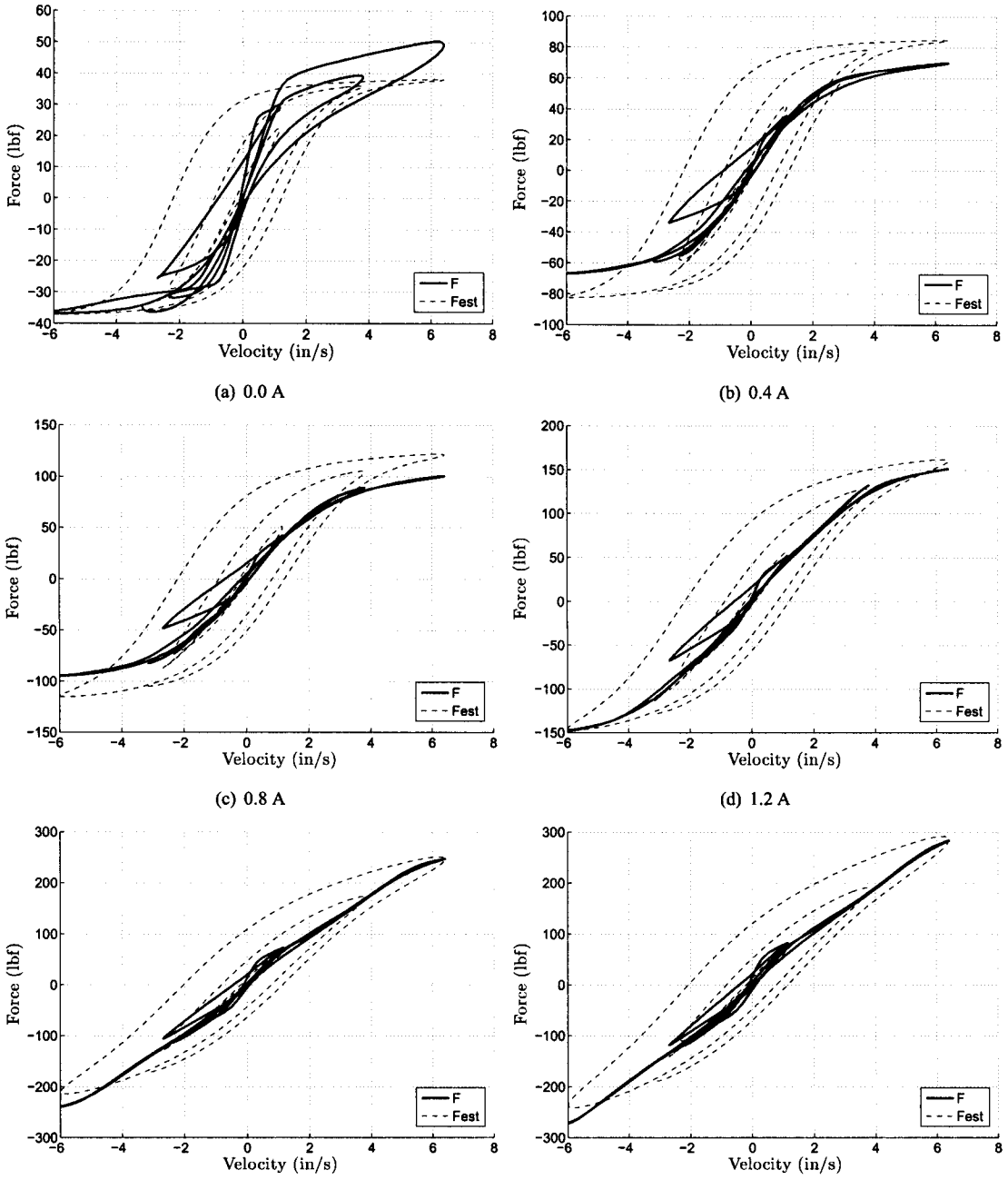

(a) 0.0 A (b) 0.4 A

(c) 0.8 A (d) 1.2 A

(e) 2.1 A (f) 2.5 A

Figure. 5.4. Experimental and estimated F-v behavior of the selected *S-P* model. Each of the figures presents the behavior at a constant value of the electric current using the data from experiment *RP1-CS*.

Fig. 5.5 presents a two second window that compares the experimental force and the force estimated by the model. Fig. 5.6 compares the force-velocity behavior for the experimental and estimated damper force at six different constant electric current values.

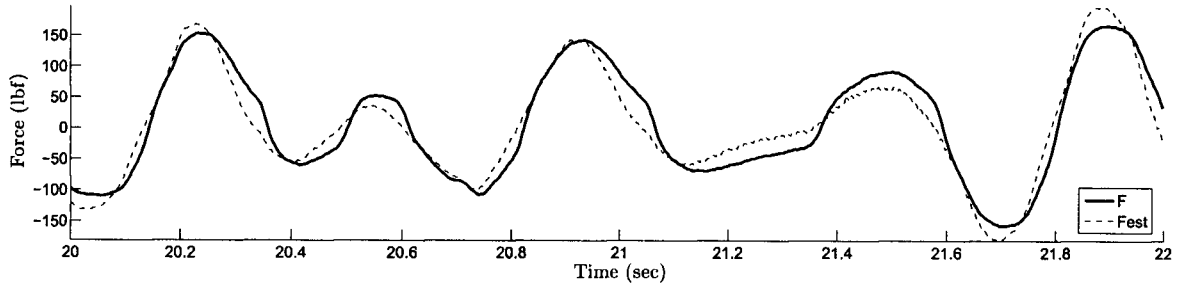

Figure. 5.5. Experimental and estimated damper force by the selected *P* model. Experimental data taken from experiment *RP-APRBS*.

It can be noticed from the force-time plot that the *P* model follows the experimental damping force with slight variations. On the other hand, the force-velocity plots depict that the *P* model is not able to closely resemble the non-linearities of the *MR* damper. For all electric current values, the models appears rigid and struggles at the extreme velocity values. Contrary to other models, the *P* structure was not seen to improve as the electric current increased.

5.1.4 Fuzzy-Based Model

The fuzzy-based model identified using *ANFIS* showed considerably lower error values when trained using experimental data sets with constant steps of the electric current. When those experiments were employed, the *RSSE* and *ESR* were observed to drop by more than 10 lbf and 0.08, respectively. Based on the average error calculations, the fuzzy-based model identified with experiment *RP1-CS* was selected as the best fuzzy-based structure, with *RSSE* and *ESR* values of 25.9376 lbf and 0.0864, respectively.

Fig. 5.7 presents a two second window that compares the experimental force and the force estimated by the model. Fig. 5.8 compares the force-velocity behavior for the experimental and estimated damper force at six different constant electric current values.

It can be observed from the force-time figure that the fuzzy-based model follows the experimental force with lead time. Additionally, at instants the predicted force seems to be affected by noise, which may be due to the form in which the various membership functions of the model interact. From the force-velocity plots, it is noted that while the fuzzy-based model correctly mimics the non-linearities of the *MR* damper, the hysteresis loop is exaggerated for all electric current values.

5.1.5 Non-Linear Fuzzy-Based Model

The proposed non-linear fuzzy-based model was observed to obtain almost constant error values for the three experimental data sets with which it was trained. Based on the average error calculations, the non-linear fuzzy-based

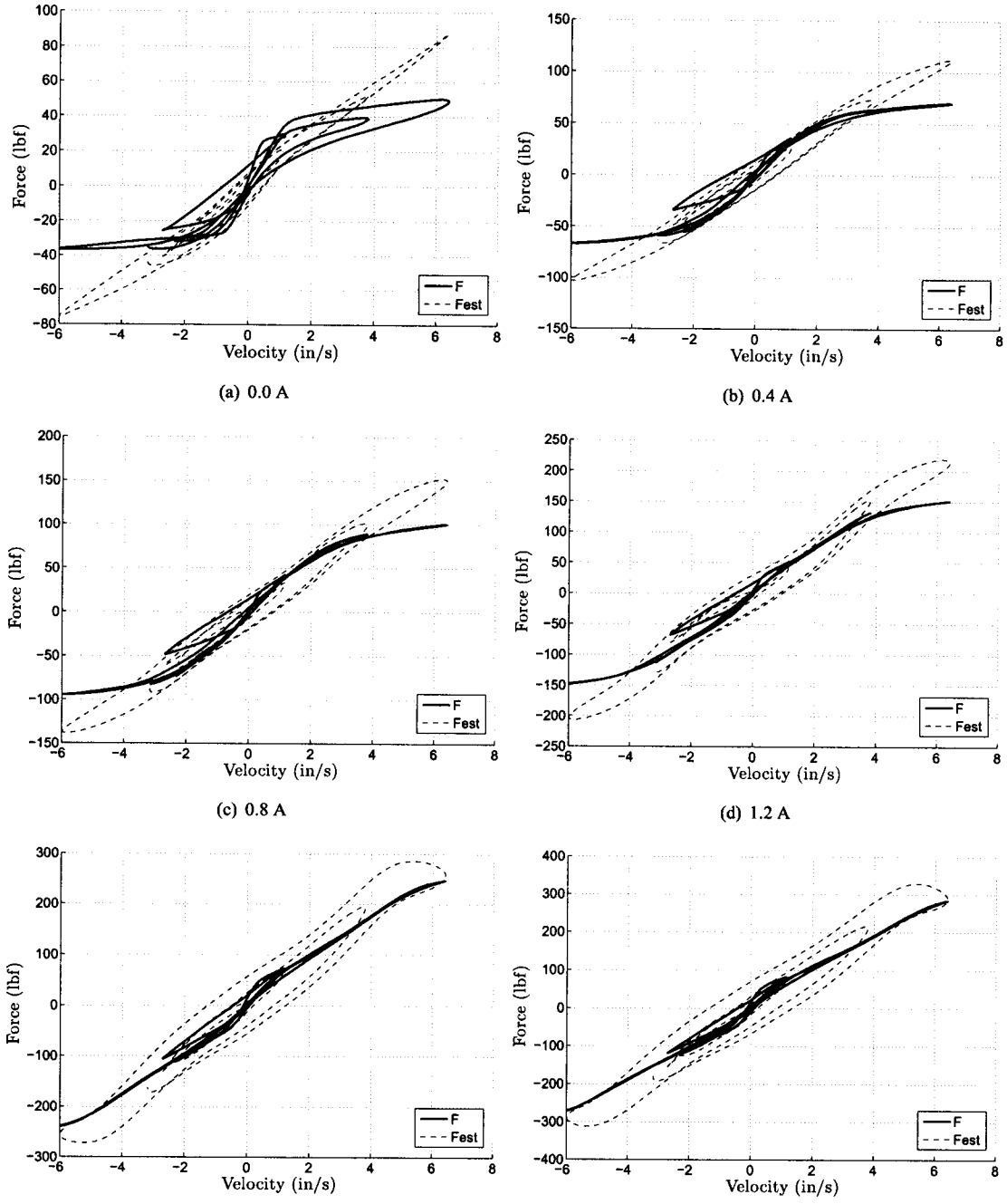

Figure. 5.6. Experimental and estimated F-v behavior of the selected *P* model. Each of the figures presents the behavior at a constant value of the electric current using the data from experiment *RP1-CS*.

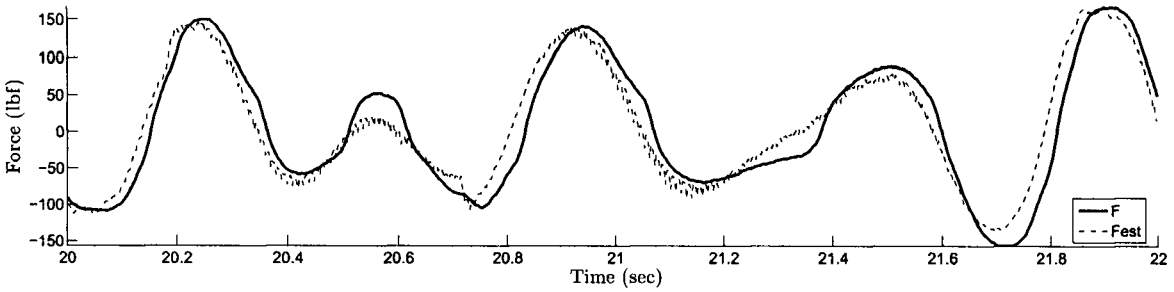

Figure. 5.7. Experimental and estimated damper force by the selected fuzzy-based model. Experimental data taken from experiment *RP-APRBS*.

structure trained with experiment *RP3-CS* was selected as the best structure, with *RSSE* and *ESR* values of 27.8199 *lbf* and 0.0993, respectively.

Fig. 5.9 presents a two second window that compares the experimental force and the force estimated by the model. Fig. 5.10 compares the force-velocity behavior for the experimental and estimated damper force at six different constant electric current values.

It can be noted from the force-time figure that the proposed non-linear fuzzy-based model acceptably follows the experimental force. Nonetheless, minor noise is observed at at certain moments, which may be produced by the shifting dynamics of membership functions. The force-velocity plots confirm that the non-linear fuzzy-based model accurately follows the non-linear behavior of the *MR* damper. Nevertheless, the hysteresis loops can be observed to be slightly wide in comparison to the experimental force. Moreover, as the electric current increases the proposed structure is seen to improve its performance.

5.2 Discussion

After selecting the best models based on the average error values, the force-time and force-velocity plots greatly allowed for a more in depth comparison of the results. Overall, the *ARX* structure was seen to outperform the other structures and closely mimic the dynamics of the *MR* damper. The best ARX model obtained *RSSE* and *ESR* values that were 10 *lbf* and 0.06 lower than those of the other models, respectively. Nonetheless, with 12 parameters and a high dependency on past values of the damping force, the model may not be adequate for an implementation where the experimental force is not being measured. As it was noted, if the initial conditions were not set properly, the *ARX* model would not predict correctly the damping force during the first sampling periods. In addition, it was proven that as the experimental sampling period increased, the *RSSE* and *ESR* values for the *ARX* model also increased. This confirmed that the great performance of the structure is highly based on the damping force regressors. On the other hand, the use of the model for the design of controllers may not be practical.

It took 15 parameters for the *S-P* model to obtain low *RSSE* and *ESR* values. Nevertheless, as it was observed in the force-velocity plots, the model could not accurately predict the non-linear and hysteretic behavior of the *MR* damper. This performance may be in part due to the restrictive way in which the electric current dependency was introduced to the model, as linear functions. Performance aside, the 15 parameters, along with the *tanh* function

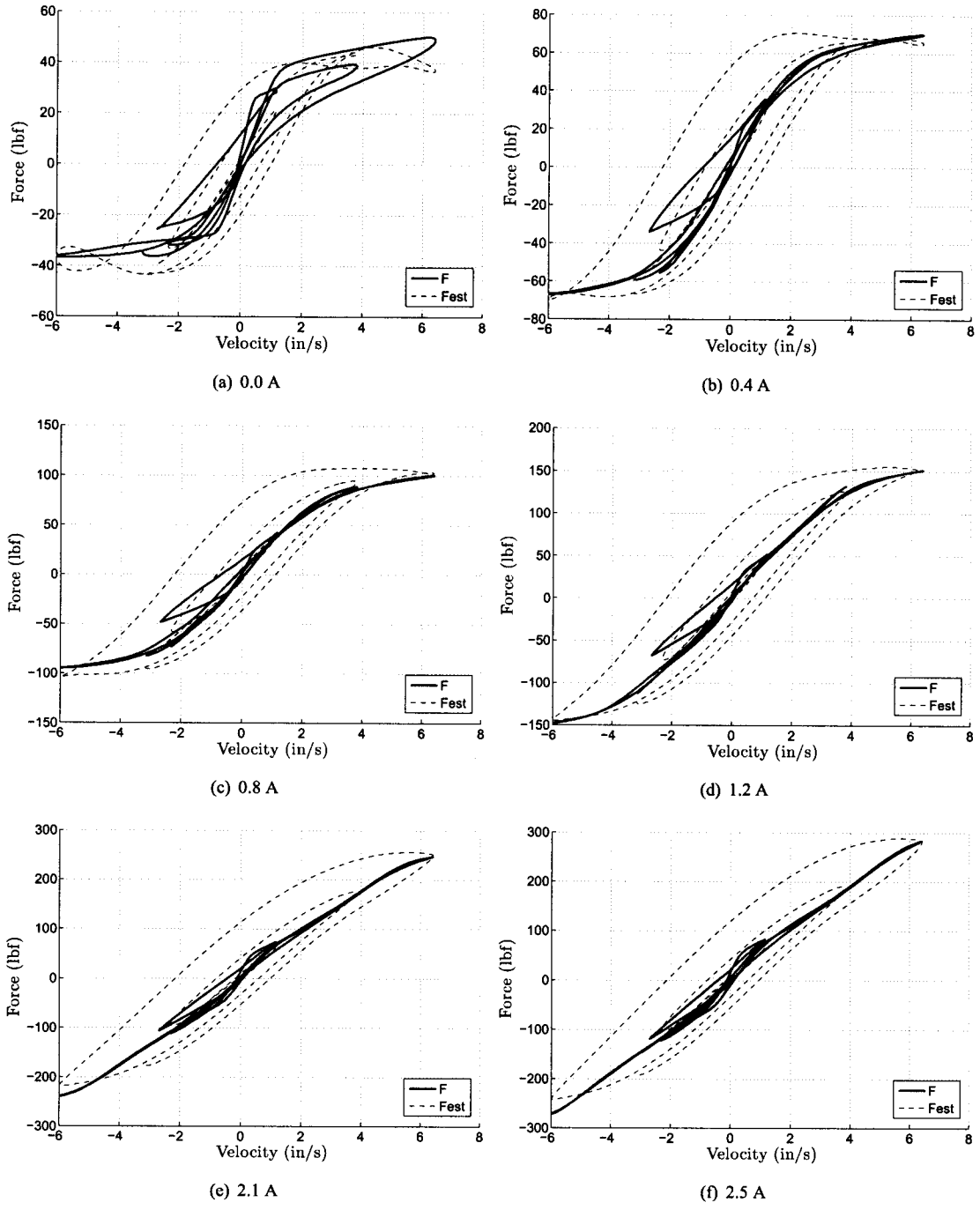

Figure. 5.8. Experimental and estimated F-v behavior of the selected fuzzy-based model. Each of the figures presents the behavior at a constant value of the electric current using the data from experiment *RP1-CS*.

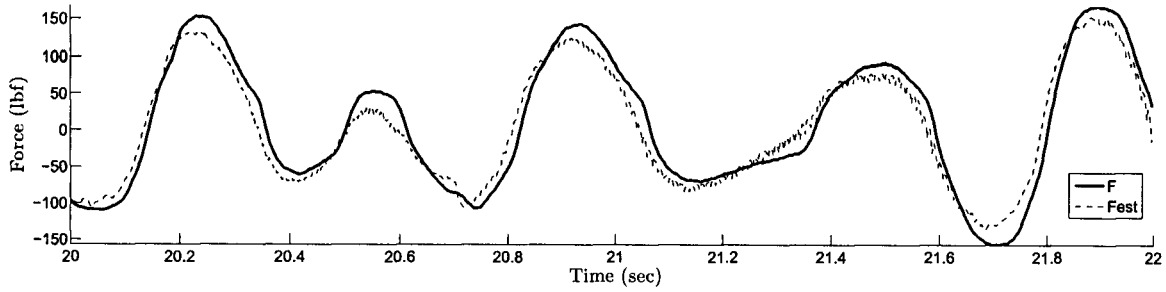

Figure. 5.9. Experimental and estimated damper force by the selected non-linear fuzzy-based model. Experimental data taken from experiment *RP-APRBS*.

on the *S-P* model, make it impractical for online implementation. On the controller design side, the model may be promising for the synthesis of non-linear control strategies.

The analyzed *P* model was observed to have acceptable average *RSSE* and *ESR* values. Nevertheless, the force-velocity plots revealed that the model is too rigid when it comes to modeling the non-linearities of the *MR* damping system. Moreover, the 15 parameters and high complexity of the *P* structure make it greatly impractical for online implementation. When it comes to designing controllers, the third and fifth powers of the damping force on which the *P* model depends, make it hard to utilize even for space-state strategies.

The fuzzy-based model trained with *ANFIS* obtained average *RSSE* and *ESR* values comparable to those obtained by other structures. However, the force-velocity plots showed that the model struggled to resemble the hysteretic behavior of the *MR* damper. On the other hand, the fuzzy-based structure may be well suited for online implementation, as it can be regarded as 27 *if* statements and simple sums. In regard to the potential for the design of controllers, the fuzzy-based model may be utilized to design linear control strategies based on the output functions of the structure. These controllers may be combined according to the membership functions of the model.

Finally, the proposed non-linear fuzzy based model was observed to obtain *RSSE* and *ESR* values slightly higher than to those of the *S-P* and fuzzy-based models. Nonetheless, the force-velocity plots allowed to see that the model very closely mimics the non-linear and hysteretic behavior of the *MR* damper. When it comes to implementation, the non-linear fuzzy-based structure consists of simple *if* statements, and the only consideration may be the *tanh* function of the seven output equations. As for the fuzzy-based model trained with *ANFIS*, the proposed model may be employed to design individual control strategies based on the output functions of the structure. In addition, if the model was trained using more closely spaced steps of the electric current, the performance may see a significant improvement.

5.3 Summary

This chapter presented an analysis of the modeling results. First, the best *MR* damper models were selected according to the average *RSSE* and *ESR* values. Then, each of the selected models was analyzed in detail by mean of force-time and force-velocity plots. At the end, the overall performance of the models, as well as their suitability for online implementation and control, was discussed.

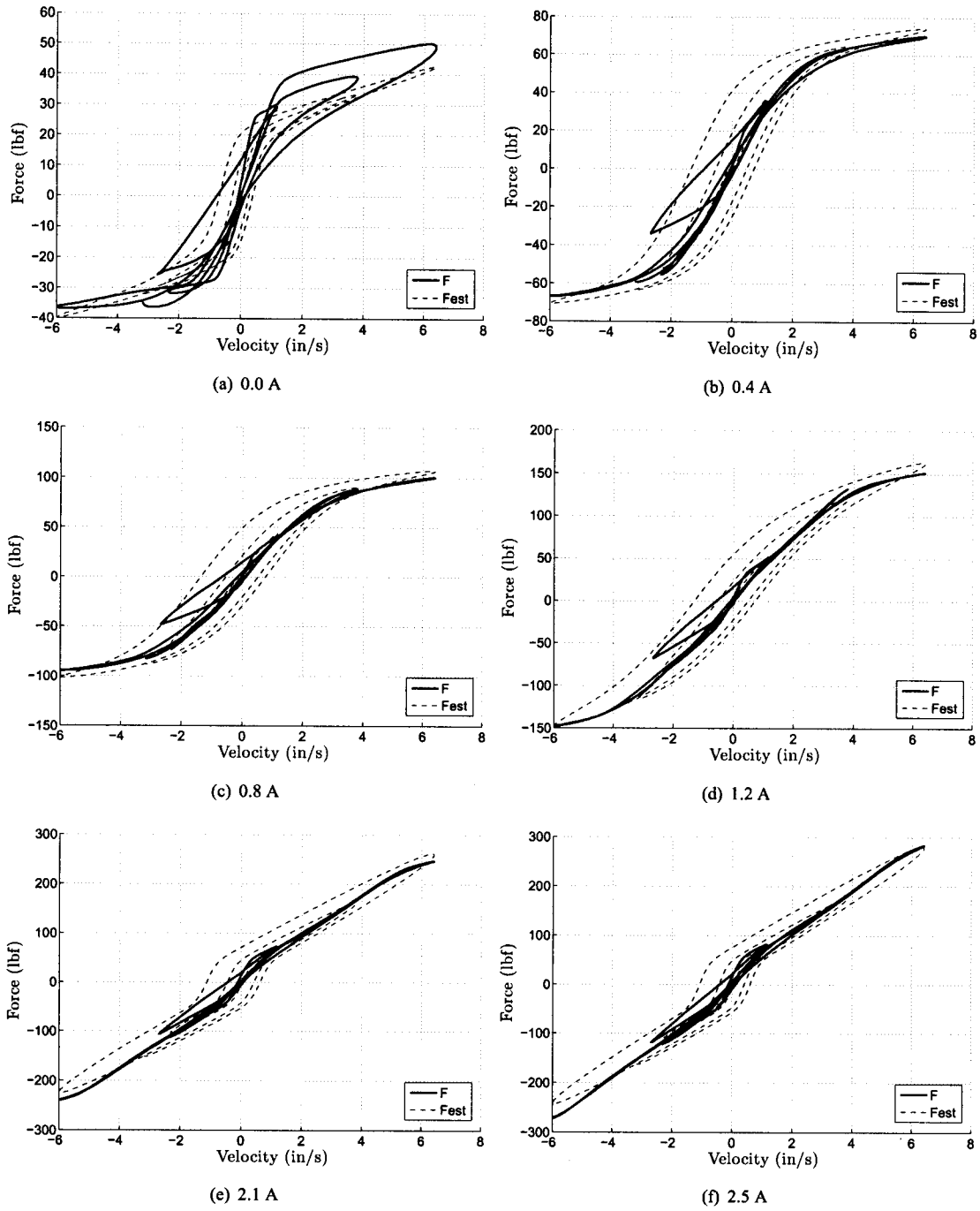

Figure. 5.10. Experimental and estimated F-v behavior of the selected non-linear fuzzy-based model. Each of the figures presents the behavior at a constant value of the electric current using the data from experiment *RP1-CS*.

Chapter 6

Conclusions

6.1 Final Conclusions

The present research work was aimed to answer the question of what type of model of an *MR* can accurately predict the highly non-linear and hysteretic behavior of the system and be suitable for online implementation of a control system. In order to obtain an answer, a literature review allowed for an in depth investigation of current models and modeling techniques. Out of the state of the art, 16 models of an *MR* damper were reviewed and four models were selected according to their reported performance and overall complexity. Each of the four models was selected from a specific modeling approach: phenomenological, semi-phenomenological, black-box, and fuzzy-based. Eight experiments were designed to test the models and experimental data was obtained from an industrial *MR* damper. The experimental data sets were selected in order to emulate the dynamics of a damper for automotive applications. From there, an extensive comparison and analysis of the four selected models was done. Each model was trained separately with the eight experimental data sets, and their performances were measured by means of the *RSSE* and *ESR* indexes. Based on the obtained results, a new model for an *MR* damper was proposed, which employed fuzzy-based methods in order to include the electric current dependency into a semi-phenomenological function. The models that obtained the lowest average validation errors were selected and then further compared by means of force-time and force-velocity plots.

It was proven from the analysis of the results that there are models for an *MR* damper that can precisely describe its behavior. An *ARX* black-box structure that depended on the displacement, velocity, electric current, and old values of the damping force was seen to accurately mimic the non-linear and hysteretic behavior of the *MR* damper. Phenomenological, semi-phenomenological, and fuzzy-based models were observed to be able to resemble the non-linearities of the *MR* damper, but struggled greatly to predict the hysteresis loops. On the other hand, the proposed non-linear fuzzy-based model was observed to acceptably follow the hysteretic behavior of the *MR* damper and accurately predict its non-linearities.

Concerning the modeling techniques, black-box modeling was noticed to outperform all the other analyzed techniques. Nonetheless, black-box models had to include old values of the damping force in order to succeed. This fact made the developed structures not optimal for online implementation when the damping force was not directly measured. For the phenomenological technique, its high complexity and poor performance were seen as reasons for which the analyzed structures were not suitable for online implementation. The semi-phenomenological approach was observed to produce acceptable models. Nevertheless, these models required a high number of parameters and

complex mathematical functions in order to correctly predict the damping force. On the other hand, linear fuzzy-based modeling techniques were observed to be highly suitable for online implementation, as they were comprised of simple *if* statements and linear output functions. Finally, when fuzzy-based and semi-phenomenological techniques were combined, the resulting non-linear structure was seen as viable for online implementation. The only drawback was identified on the non-linear form of its output functions.

Regarding experimental input patterns, a marked difference was seen for the *ARX* and fuzzy-based structures. For the first, the experimental data sets with highly variant electric current were seen to facilitate the identification of the structures. When these patterns were employed, the average *RSSE* and *ESR* values were significantly lower than those obtained with other training patterns. On the other hand, fuzzy-based structures saw a considerable improvement when trained with experimental data sets with stepped increments of the electric current. Said experimental data sets permitted the fuzzy-based model to identify the various operational zones of the *MR* damper. Concerning training patterns, no significant difference was observed for the phenomenological and semi-phenomenological models.

The proposed non-linear fuzzy-based model was seen as the model with best compromise between modeling precision and ease of implementation. Individual non-linear controllers may be developed according to the selected output functions of the structure. Moreover, the proposed structure may be improved by employing more closely spaced steps of the electric current. In this manner, more non-linear output functions would allow the model to characterize the behavior of the *MR* damper on a greater number of operational zones. In general terms, the research results are greatly applicable to the automotive industry, where better comfort and handling control systems can be developed based on the analyzed models of *MR* dampers. In addition, based on the results, experimental patterns may be designed according to a desired modeling technique.

6.2 Future Work

Along the same line of investigation, the following specific areas could be studied:

- Other modeling techniques, such as *Linear Parameter-Varying (LPV)* systems, may be explored for better characterization of the behavior of an *MR* damper.
- Different methods of introducing the electric current dependency to phenomenological and semi-phenomenological models may be explored. These methods may include complex mathematical representations or other fuzzy-based techniques.
- Various output functions may be tested for the proposed non-linear fuzzy-based model. These functions may include *MR* damper models that work correctly under constant electric current inputs.
- *MR* damper controllers may be developed based on the results obtained for the fuzzy-based and non-linear fuzzy-based models. These controllers could be individually designed according to output functions and combined by employing fuzzy sets.

Bibliography

[1] B. F. Spencer, S. J. Dyke, M. K. Sain, and J. D. Carlson. Phenomenological Model of a MR Damper. *ASCE Journal of Engineering Mechanics*, 123:230–238, March 1997.

[2] S. Guo, S. Li, and S. Yang. Semi-active Vehicle Suspension Systems with Magnetorheological Dampers. In *Vehicular Electronics and Safety, 2006. ICVES 2006. IEEE International Conference on*, pages 403–406, 2006.

[3] N. M. Kwok, Q. P. Ha, T. H. Nguyen, J. Li, and B. Samali. A Novel Hysteretic Model for Magnetorheological Fluid Dampers and Parameter Identification using Particle Swarm Optimization. *Sensors and Actuators A: Physical*, 132(2):441–451, 11/20 2006.

[4] I.A. Brigadnov and A. Dorfmann. Mathematical Modeling of Magnetorheological Fluids. *Continuum Mech. Thermodyn.*, 17:29–42, 2005.

[5] L. X. Wang and H. Kamath. Modelling Hysteretic Behaviour in MR Fluids and Dampers using Phase-Transition theory. *Smart Mater. Struct.*, 15:1725–1733, 2006.

[6] G. Jin, M. K. Sain, and B. E. Spencer Jr. Nonlinear Blackbox Modeling of MR-Dampers for Civil Structural Control. *Control Systems Technology, IEEE Transactions on*, 13(3):345–355, 2005.

[7] V. S. Atray and P. N. Roschke. Design, Fabrication, Testing, and Fuzzy Modeling of a Large Magnetorheological Damper for Vibration Control in a Railcar. In *Proceedings of the 2003 IEEE/ASME Joint Rail Conference*, pages 223 – 229, 2003.

[8] F. Li and L. Xianzhuo. The Modeling Research of Magnetorheological Damper in Advanced Intelligent Prosthesis. In *Chinese Control and Decision Conference*, pages 781 – 784, 2009.

[9] F. Li, H. Xie, W. Yuan, and Y. Liu. The Application Research of MR Damper in Intelligent Bionic Leg. In *Control and Decision Conference, 2009. CCDC '09. Chinese*, pages 1327 –1331, jun. 2009.

[10] S. M. Savaresi, S. Bittanti, and M. Montiglio. Identification of Semi-Physical and Black-Box Non-Linear Models: the Case of MR-Dampers for Vehicles Control. *Automatica,*, 41(1):113–127, 1 2005.

[11] W. W. Chooi and S. O. Oyadiji. Design, Modelling and Testing of Magnetorheological (MR) Dampers using Analytical Flow Solutions. *Computers and Structures*, 86(3-5):473 – 482, 2008. Smart Structures.

[12] K. C. Schurter and P. N. Roschke. Fuzzy Modeling of a Magnerorheological Damper using ANFIS. In *Fuzzy Systems, 2000. FUZZ IEEE 2000. The Ninth IEEE International Conference on*, volume 1, pages 122–127 vol.1, 2000.

[13] S. Çesmeci and T. Engin. Modeling and Testing of a Field-Controllable Magnetorheological Fluid Damper. *International Journal of Mechanical Sciences*, 52(8):1036 – 1046, 2010.

[14] S. B. Choi, S. K. Lee, and Y. P. Park. A Hysteresis Model for the Field-Dependent Damping Force of a Magnetorheological Damper. *Journal of Sound and Vibration*, 245(2):375 – 383, 2001.

[15] H. Nguyen, N. Prasad, C. Walker, and E. Walker. *A First Course in Fuzzy and Neural Control.* Chapman and Hall/CRC, Boca Raton, Florida 33431, first edition, 2003.

[16] D. H. Wang and W. H. Liao. Neural Network Modeling and Controllers for Magnetorheological Fluid Dampers. In *Fuzzy Sys.. The 10th IEEE Int. Conf. on*, volume 3, pages 1323–1326, 2001.

[17] M. J. L. Boada, J. A. Calvo, B. L. Boada, and V. Díaz. Modeling of a Magnetorheological Damper by Recursive Lazy Learning. *International Journal of Non-Linear Mechanics*, In Press, Corrected Proof:–, 2008.

[18] E. L. Chen, C. D. Si, M. M. Yan, and B. Y. Ma. Dynamic Characteristics Identification of Magnetic Rheological Damper Based on Neural Network. In *Artificial Intelligence and Computational Intelligence, 2009. AICI '09. International Conference on*, volume 2, pages 525 –529, nov. 2009.

[19] K. M. Passino and S. Yurkovich. *Fuzzy Control.* Addison Wesley Longman, Inc., 1998.

[20] H. Wang and H. Hu. The Neuro-fuzzy Identification of MR Damper. In *Fuzzy Systems and Knowledge Discovery, 2009. FSKD '09. Sixth International Conference on*, volume 6, pages 464 –468, aug. 2009.

[21] H. Du and N. Zhang. Evolutionary Takagi-Sugeno Fuzzy Modelling for MR Damper. In *Hybrid Intelligent Systems, 2006. HIS '06. Sixth International Conference on*, pages 69 –69, dec. 2006.

[22] K. K. Ahn, M.A. Islam, and D.Q. Truong. Hysteresis Modeling of Magneto-Rheological (MR) Fluid Damper by Self Tuning Fuzzy Control. In *Control, Automation and Systems, 2008. ICCAS 2008. International Conference on*, pages 2628 –2633, oct. 2008.

[23] S. Kern. Modelling and Control of a Magneto-Rheological Damper for Automobile Vehicles. Master's thesis, Grenoble INP, 2007.

[24] R. Richards. Comparison of Linear, Nonlinear, Hysteretic, and Probabilistic MR Damper Models. Master's thesis, Virginia Polytechnic Institute and State University, 2 2007. type: Master Thesis.

[25] J. de-J. Lozoya-Santos, R. Morales-Menendez, J. A. Ruiz-Cabrera, V. Diaz-Salas, and Ricardo Ramirez-Mendoza. Building Training Patterns for Modelling MR Dampers. In *6th International Conference on Informatics in Control, Automation, and Robotics*, 2009.

[26] J. Lozoya-Santos, R. Morales-Menendez, and R. A. Ramirez-Mendoza. Design of Experiments for MR Damper Modelling. In *17th International Joint Conference on Neural Networks*, pages 1915–1922, 2009.

[27] T. Söderström and P. Stoica. *System Identification.* Prentice Hall, 1989.

[28] J. Y. Wong. *Theory of ground vehicles.* John Wiley, 2001.

[29] S. Park, A. A. Popov, and D. J. Cole. Influence of Soil Deformation on Off-Road Heavy Vehicle Suspension Vibration. *Journal of Terramechanics*, 41:41–68, 2004. Road Profiles.

[30] J. G. S. da Silva. Dynamical Performance of Highway Bridge Decks with Irregular Pavement Surface. *Computers and Structures*, 82:871–881, 2004.

[31] D. Kowalski and M. D. Rao. The Effects of Different Input Excitations on the Dynamic Characterization of an Automotive Shock Absorber. *SAE Transactions*, 2001.

[32] S. Guo, S. Yang, and C. Pan. Dynamical Modeling of Magneto-Rheological Damper Behaviors. *Intelligent Material Systems and Structures*, 17:3–14, 2006.

[33] E. Niño-Juarez, R Morales-Menendez, R Ramirez-Mendoza, and L Dugard. Minimizing the Frecuency in a Black Box Model of a Magneto-Rheological Damper. In *11th Mini Conf on Vehicle Sys. Dyn., Ident. and Anomalies*, 2008.

Appendix A

Experiments

A.1 Experimental Setup

A.1.1 Experimental System

The employed experimental system consisted of three main blocks: actuation, control, and data acquisition. An *HMI* was created to interact with the control and acquisition systems. The acquisition system captured six signals from the experiment: the displacement; the generated force; the commanded reference from the *MR* damper piston position control system; a voltage, from the electric current driver, proportional to the electric current through the coil of the *MR* damper; the temperature of the case of the damper; and the room temperature.

A.1.2 Actuation System

The actuation system installed on the laboratory was an MTS^{TM} system that included: an actuator of 3000 psi with a 15 Hz bandwidth, the controller hardware unit *Flextest GT*, the software *Station Manager*^{TM} and the *MultiPurpose TestWare*^{TM}. The controller hardware unit was operated through the MTS^{TM} *Station Manager*^{TM} which was located on a control room. The computer and controller were communicated via a 100 Mb/sec ethernet connection.

The *Station Manager*^{TM} and the *MultiPurpose TestWare*^{TM} softwares were utilized before the experimentation in order to calibrate the signal levels. During the experimentation, the main tasks of the *Station Manager*^{TM} software were the MTS^{TM} hardware startup and the monitoring of the generated force and displacement.

The hardware components of the position control system were: an actuator, a 3,000 psi hydraulic pump, a load control unit, a servovalve, a hydraulic manifold, a work station, a load cell, a linear variable differential transformer (*LVDT*), and various signal conditioners. The actuator was a hydraulic *Instron*^{TM} piston, double action, controlled by the servovalve. The load capacity of the system was 5620 lbf at 3000 psi, with a maximum stroke of 6 in.

A.1.3 Control System

The employed control system was based on two slave controllers: the position controller (MTS^{TM} system) and the electric current driver with a proportional integral control. Then, a supervisory system was in charge of commanding the slave controllers.

The supervisory system consisted of an *HMI* programmed in *LabView*^{TM}. The *HMI* would read the desired displacement and electric current values from a file with the extension *.txt*. Then, the information was sent to a *National Instruments*^{TM} (*NI*) analog output card. The *Flextest GT*^{TM} and the electric current driver *High Country Tek*^{TM} were commanded via two analog outputs. The commanding signals were utilized in voltage units. The number of replicates were specified on the *HMI* before each of the experimental tests. During each experiment, the *HMI* displayed the displacement and electric current commanded to the controllers.

The displacement control was done by the *MTS*^{TM} *Flextest GT*^{TM} controller. The *Flextest GT*^{TM} was set to receive an external set point, which defined the position of the *MR* damper piston. The span of the position command was set to ± 0.25 V, which was equivalent to ± 0.3 in. The electric current control adjusted the electric current in the coil of the *MR* damper according to the received voltage signal. The span of the electric current was set from 0 to 9 V, which were linearly proportional to 0 and 2.5 A.

A.1.4 Data Acquisition System

The employed data acquisition system consisted of a *HMI* programmed in *LabView*^{TM}, two signal conditioner circuits, one analog input *NI* card, and one thermocouple *NI* card. The captured information was visualized in real time on the *HMI*. The measured information was recorded in a file with a *.txt* extension with a sampling frequency of 512 Hz. The order of the columns in the files was: sampling time stamp, piston displacement, generated force, electric current on the coil, environment laboratory temperature, damper case temperature, and the position set point commanded to the *Flextest GT*^{TM}.

The displacement measurement was done via an *LVDT*. The *LVDT* was located over the actuator piston and served as feedback to the position controller. An *Instron*^{TM} load cell delivered the generated force in voltage units. A peak detector converted the *LVDT* signal into a corresponding voltage. The electric current measurement was done via a 1 Ω resistor in series with the coil of the *MR* damper. The voltage from the resistor was conditioned by means of an industrial instrumentation amplifier. Finally, two type *J* thermocouples provided the damper case and laboratory room temperatures.

A.2 Experimental Data Sets

Figures A.1 - A.6 show 20 and 100 second windows of the patterns employed for the experiments that complement the ones described in the report. In addition, 30 and 60 second windows present the frequency content of the experiments.

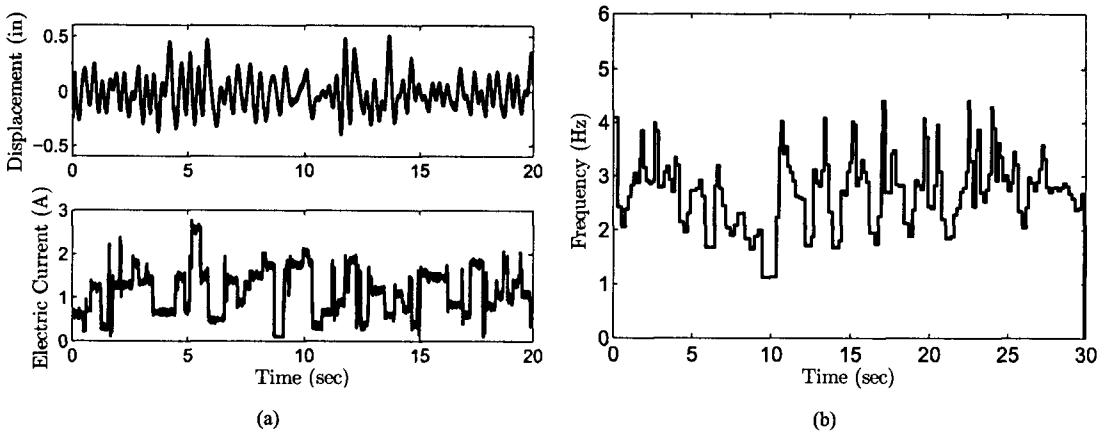

(a) (b)

Figure. A.1. Description of experiment *RP-APRBS*. Displacement and electric current patterns (left). Frequency content (right).

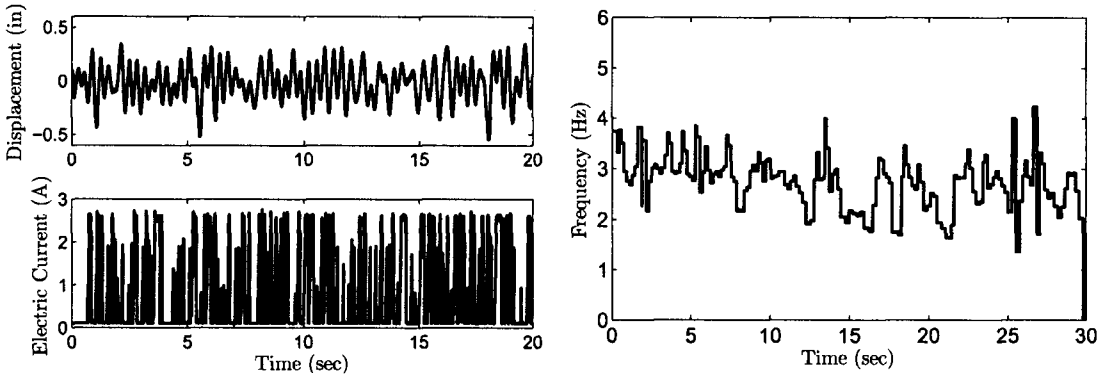

(a) (b)

Figure. A.2. Description of experiment *RP-PRBS*. Displacement and electric current patterns (left). Frequency content (right).

A.3 Discrete Derivative

In order to compute de velocity of the *MR* damper, a discrete derivative was employed. Fig. A.7 presents the calculation of the velocity of the *MR* damper using *Simulink*.

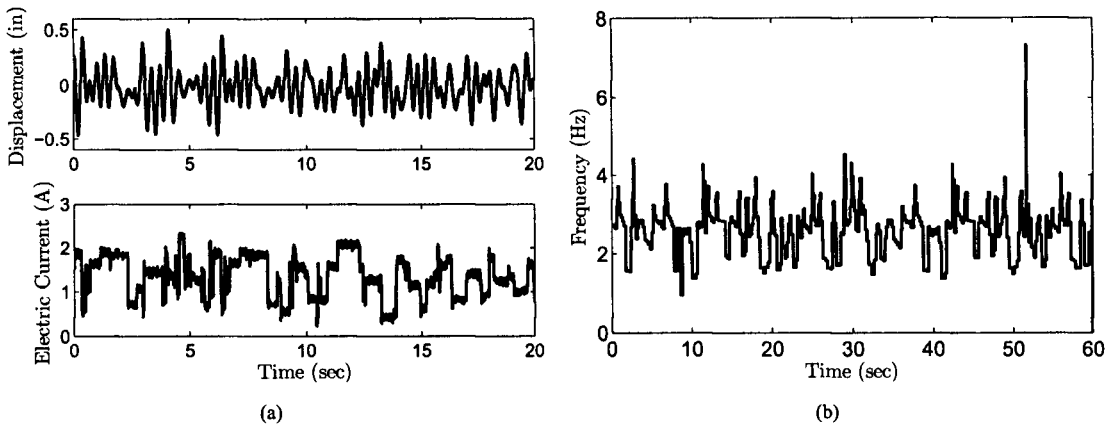

Figure. A.3. Description of experiment *RP-APRBS-L*. Displacement and electric current patterns (left). Frequency content (right).

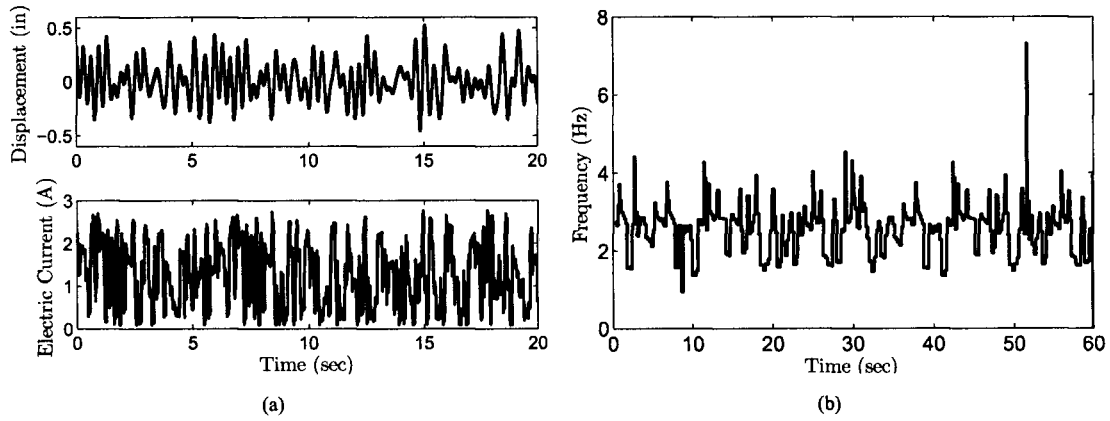

Figure. A.4. Description of experiment *RP-ICPS*. Displacement and electric current patterns (left). Frequency content (right).

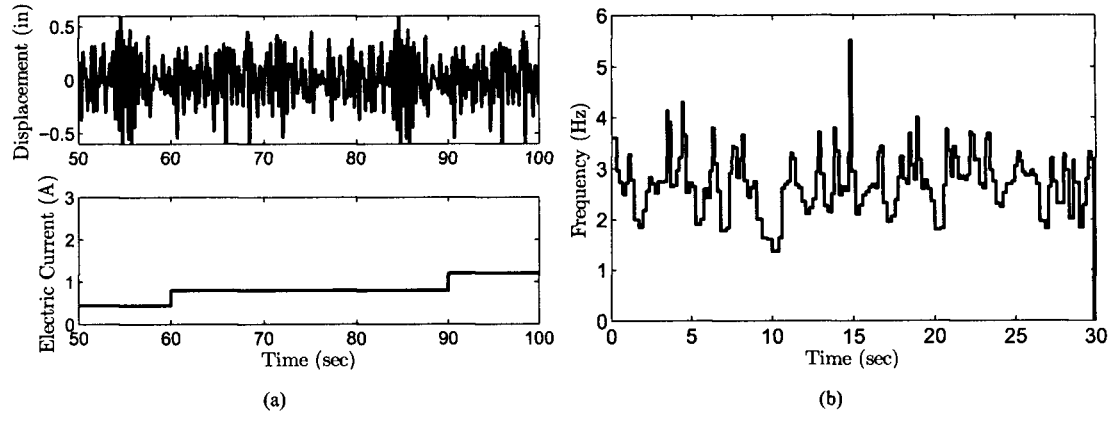

Figure. A.5. Description of experiment *RP1-CS*. Displacement and electric current patterns (left). Frequency content (right).

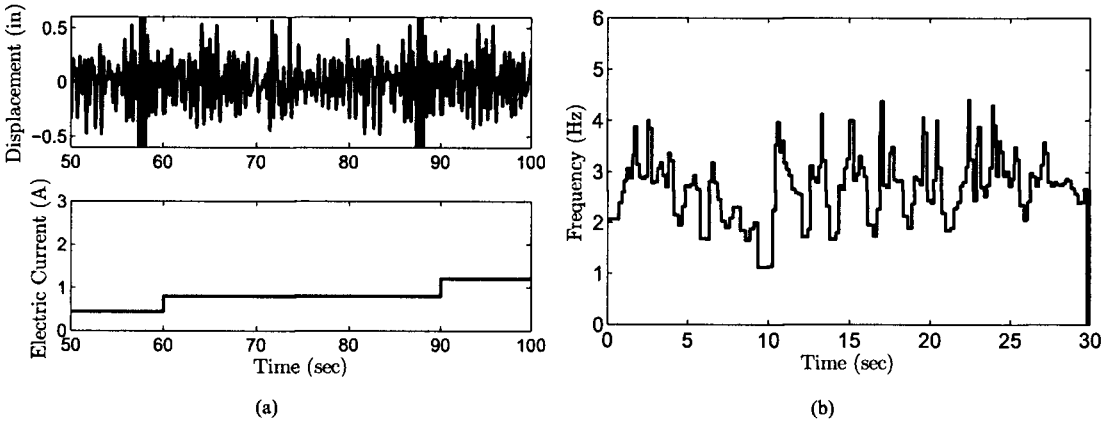

Figure. A.6. Description of experiment *RP2-CS*. Displacement and electric current patterns (left). Frequency content (right).

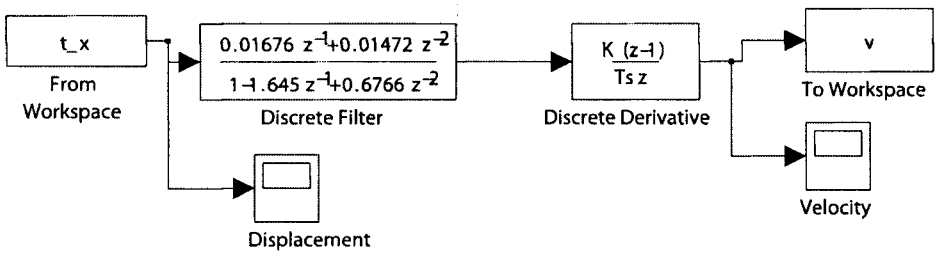

Figure. A.7. Velocity calculation using *Simulink*. The time and displacement patterns are read from the workspace and low-pass filtered. Then, a discrete derivative block is used to calculate the respective velocity. The results are saved to the workspace and plotted.

Appendix B

Identified Coefficients

The coefficients for the passive and semi-active *ARX*, *S-P*, and *P* models were calculated using the *Optimization Toolbox* from *MATLAB*^{TM}. The selected identification function was *lsqcurvefit*. The full identification process is specified in the block diagram of Fig. B.1.

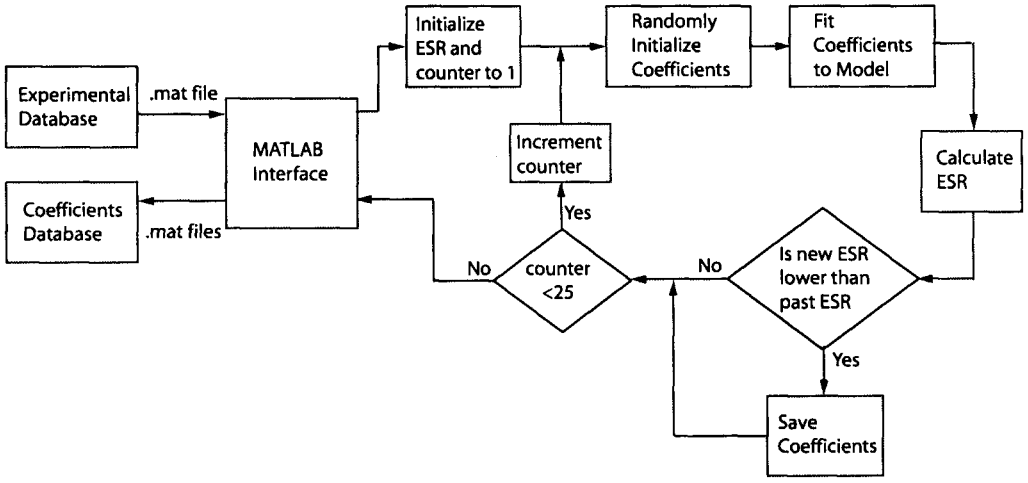

Figure. B.1. Identification of the coefficients for the models. The experimental data is loaded from a file into *MATLAB*^{TM}. Then, the identification algorithm begins. Once the identification has been done 25 times, the coefficients with which the model obtained the lowest *ESR* are recorded. Finally, the coefficients are saved to a .mat file.

B.1 *ARX* Model

For the *ARX* structure, the three regressors of the damping force required the experimental data to be utilized from the fourth sampling interval. Table B.1 shows the identified coefficients for the passive *ARX* model.

* In order to include the semi-active action to the model, three regressors of the electric current were added to the structure. Tables B.2 and B.2 show the identified coefficients for the semi-active *ARX* model.

Table B.1. Identified coefficients for the passive *ARX* model.

Model	a_1	a_2	a_3	a_4	a_5	a_6	a_7	a_8	a_9
RP-ICPS	1.308	-0.543	0.198	38.484	-0.447	-49.072	8.956	-4.039	-3.938
RP-APRBS	1.335	-0.625	0.253	34.932	4.319	-52.095	7.987	-2.939	-4.030
RP-PRBS	1.261	-0.401	0.108	25.777	2.602	-35.203	7.811	-5.430	-1.788
RP-APRBS-L	1.238	-0.501	0.196	91.372	-4.248	-98.815	15.834	-3.737	-10.159
RP-ICPS-L	1.199	-0.366	0.118	67.708	-3.602	-74.215	12.371	-3.587	-7.504
RP1-CS	1.965	-1.111	0.144	508.236	-464.142	-44.018	-83.719	159.628	-77.020
RP2-CS	2.182	-1.466	0.283	-58.581	42.815	14.460	-0.142	1.271	-0.998
RP3-CS	2.160	-1.461	0.299	-306.676	851.727	-545.478	-13.986	26.319	-12.804

Table B.2. Identified coefficients for the semi-active *ARX* model.

Model	a_1	a_2	a_3	a_4	a_5	a_6	a_7	a_8	a_9
RP-ICPS	1.308	-0.542	0.197	38.632	0.784	-50.360	9.028	-3.971	-4.079
RP-APRBS	1.333	-0.620	0.250	35.256	4.891	-52.948	7.995	-2.847	-4.123
RP-PRBS	1.260	-0.399	0.106	26.065	3.503	-36.247	7.962	-5.398	-1.973
RP-APRBS-L	1.236	-0.497	0.194	90.876	-3.479	-99.061	15.764	-3.650	-10.187
RP-ICPS-L	1.198	-0.365	0.117	67.767	-2.459	-75.441	12.450	-3.520	-7.627
RP1-CS	1.978	-1.129	0.148	-154.514	936.415	-781.942	-86.508	164.171	-78.931
RP2-CS	2.201	-1.521	0.317	-285.952	689.071	-403.801	-0.861	1.429	-0.771
RP3-CS	2.248	-1.639	0.389	679.039	-1037.871	358.646	-18.202	31.743	-14.151

Table B.3. Identified coefficients for the semi-active *ARX* model continued.

Model	a_{10}	a_{11}	a_{12}
RP-ICPS	-7.187	17.996	-10.832
RP-APRBS	-13.694	26.577	-12.827
RP-PRBS	-2.930	7.580	-4.665
RP-APRBS-L	-18.968	30.806	-11.821
RP-ICPS-L	-6.254	14.783	-8.397
RP1-CS	241.241	-497.047	255.806
RP2-CS	265.862	-805.376	539.518
RP3-CS	533.283	-1058.675	525.392

B.2 *S-P* Model

Following the procedure described in Fig. B.1, the coefficients for the passive *S-P* model were obtained. Table B.4 shows the identified coefficients for the passive *S-P* model.

Table B.4. Identified coefficients for the passive *S-P* model.

Model	A_1	A_2	A_3	A_4	A_5
RP-ICPS	88.202	11.979	0.536	3552.743	-902.233
RP-APRBS	120.052	9.870	0.355	-2530.261	619.071
RP-PRBS	107.343	-1.821	0.401	-2883.556	695.050
RP-APRBS-L	142.550	5.803	0.334	-998.157	250.701
RP-ICPS-L	132.229	5.491	0.343	-317.049	81.463
RP1-CS	46.273	18.442	0.832	-1921.658	507.945
RP2-CS	191.281	-2.534	0.229	1226.437	-344.231
RP3-CS	77.860	12.458	0.435	2591.915	-657.758

In order to include the electric current into the model, each of the coefficients was made equal to a second order polynomial dependent on the electric current. This resulted in 15 coefficients for the semi-active *S-P* model. Tables B.5 and B.6 show the identified coefficients for the semi-active *S-P* model.

Table B.5. Identified coefficients for the semi-active *S-P* model.

Model	A_{11}	A_{12}	A_{13}	A_{21}	A_{22}	A_{23}	A_{31}	A_{32}	A_{33}
RP-ICPS	37.988	123.952	-36.383	1.599	-3.412	4.943	0.735	-0.450	0.131
RP-APRBS	42.478	120.899	-17.201	-4.189	3.088	0.532	0.631	-0.347	0.084
RP-PRBS	17.290	98.788	-34.664	3.206	-2.856	6.968	1.564	-1.529	0.501
RP-APRBS-L	40.070	130.526	-45.922	-0.772	-1.141	5.751	0.645	-0.392	0.127
RP-ICPS-L	35.103	118.359	-37.528	0.456	-1.703	5.400	0.634	-0.330	0.091
RP1-CS	31.400	41.576	-16.041	0.688	9.649	2.573	1.275	-1.305	0.600
RP2-CS	38.620	106.225	78.733	-0.132	-8.257	-1.976	0.384	-0.187	0.032
RP3-CS	25.296	83.500	-29.651	0.573	4.796	4.021	0.788	-0.542	0.209

B.3 *P* Model

The coefficients for the passive *P* model were obtained as described in Fig. B.1. Table B.7 shows the identified coefficients for the passive *P* model.

In order to make the model dependent on the electric current, each coefficient was replaced by a second order polynomial electric current equation. Tables B.8 and B.9 show the identified coefficients for the semi-active *P* model.

Table B.6. Identified coefficients for the semi-active *S-P* model continued

Model	X_{01}	X_{02}	X_{03}	V_{01}	V_{02}	V_{03}
RP-ICPS	6768.989	10812.271	12336.201	-2009.267	-2418.549	-3192.612
RP-APRBS	-19856.177	-11012.135	-22001.331	2616.040	11090.042	775.668
RP-PRBS	-29880.883	-22690.407	2330.089	7027.813	3583.264	472.563
RP-APRBS-L	2162.089	1530.477	539.615	-425.214	-593.572	-57.766
RP-ICPS-L	-3331.536	3234.184	-861.446	823.845	-800.106	214.594
RP1-CS	-1566.455	-5291.779	-1747.241	485.379	1075.238	612.818
RP2-CS	64.254	1292.078	1515.348	-38.002	-242.847	-428.805
RP3-CS	108.218	13577.953	201.927	-45.504	-2983.101	-207.646

Table B.7. Identified coefficients for the passive *P* model.

Model	C_1	C_2	C_3	C_4	C_5
RP-ICPS	19.049	0.017	-0.0003	2.53E-05	-2.63E-10
RP-APRBS	22.503	0.018	-0.00024	2.31E-05	-3.05E-10
RP-PRBS	13.089	0.014	-0.00021	3.68E-05	-4.22E-10
RP-APRBS-L	25.043	0.017	-0.00019	2.21E-05	-3.38E-10
RP-ICPS-L	21.261	0.017	-0.00025	2.39E-05	-2.65E-10
RP1-CS	16.395	0.018	-0.00039	1.90E-05	-1.48E-10
RP2-CS	14.236	0.020	-0.0005	1.96E-05	-1.44E-10
RP3-CS	14.903	0.019	-0.0005	2.00E-05	-1.56E-10

Table B.8. Identified coefficients for the semi-active *P* model.

Model	C11	C12	C13	C21	C22	C23	C31	C32
RP-ICPS	11.834	4.090	1.634	0.0120	0.0015	0.0007	-0.0001	-0.00016
RP-APRBS	11.548	12.648	-2.426	0.0161	0.0030	-0.0011	-0.00015	-4.56E-05
RP-PRBS	8.282	1.055	3.021	0.0073	0.0094	-0.0025	-0.00015	-1.88E-05
RP-APRBS-L	9.505	3.519	1.806	0.0085	0.0056	-0.0018	-0.00016	-0.00022
RP-ICPS-L	9.689	13.204	-0.838	0.0140	0.0036	-0.0011	-0.00014	-8.91E-05
RP1-CS	3.743	4.212	8.070	0.0281	-0.0127	0.0057	-0.00054	0.000221
RP2-CS	4.687	3.416	5.055	0.0243	-0.0091	0.0036	-0.00041	2.99E-05
RP3-CS	6.604	15.716	0.148	0.0256	-0.0035	0.0010	-0.00031	-4.24E-05

Table B.9. Identified coefficients for the semi-active P model continued.

Model	C33	C41	C42	C43	C51	C52	C53
RP-ICPS	2.88E-05	7.32E-05	-3.52E-05	4.75E-06	-1.44E-09	7.75E-10	-1.06E-10
RP-APRBS	-2.35E-06	5.76E-05	-2.42E-05	3.11E-06	-1.48E-09	7.17E-10	-7.68E-11
RP-PRBS	2.12E-05	0.000153	-0.0001	2.05E-05	-4.53E-09	3.34E-09	-6.48E-10
RP-APRBS-L	0.000109	8.61E-05	-4.82E-05	9.18E-06	-1.36E-09	7.00E-10	-1.04E-10
RP-ICPS-L	4.50E-05	9.48E-05	-5.84E-05	1.03E-05	-4.40E-09	3.55E-09	-7.51E-10
RP1-CS	-4.04E-05	0.000188	-0.00014	2.28E-05	-6.74E-09	5.53E-09	-1.13E-09
RP2-CS	1.04E-05	0.000142	-9.38E-05	1.51E-05	-5.08E-09	4.12E-09	-8.37E-10
RP3-CS	4.08E-05	2.81E-05	-1.08E-05	-3.26E-07	-2.07E-09	1.62E-09	-3.18E-10

Appendix C

Fuzzy-Based Model

A fuzzy-based model was identified using the *ANFIS* toolbox in *MATLAB*^{TM}. For the eight experimental data sets, one model was trained for 50 epochs or until de identification error decreased by less than 0.01. After the training, a *FIS* file was obtained for each data set. The experimental data were first normalized by subtracting the mean and dividing by the standard deviation. The normalizing constants were recorded for future use in the error calculations.

With each of the *FIS* files, the corresponding error was calculated using the *Simulink* diagram presented in Fig. C.1.

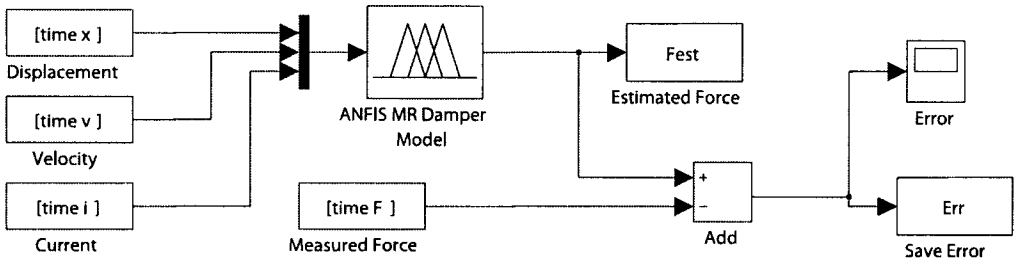

Figure. C.1. Fuzzy-based model validation. The displacement, velocity, and electric current are connected to the fuzzy-based model. The model predicts the damping force, and this force is compared with the experimental force. Finally, the estimated force and error calculations are saved.

In order to calculate the *RSSE* and *ESR* values, the resulting validation error values were denormalized using the normalizing constants respective to each model. The following *MATLAB*^{TM} code describes in detail the *FIS* files obtained for the fuzzy-based models trained with the eight experimental data sets. The inputs were ordered as: displacement, velocity, and electric current.

```
%MRDamperANFIS_expRP_ICPS.FIS
[System]
Name='MRDamperANFIS_expRP_ICPS'
Type='sugeno'
Version=2.0
NumInputs=3
NumOutputs=1
NumRules=27
AndMethod='prod'
OrMethod='probor'
```

```
ImpMethod='prod'
AggMethod='sum'
DefuzzMethod='wtaver'

[Input1]
Name='displacement__(x)'
Range=[-3.07646220933282 3.42434553818148]
NumMFs=3
MF1='in1mf1':'gaussmf',[1.36890460739573 -3.10651988064284]
MF2='in1mf2':'gaussmf',[1.39020527161337 0.129201710845673]
MF3='in1mf3':'gaussmf',[1.34055648552855 3.44818226667927]

[Input2]
Name='velocity__(v)'
Range=[-3.80656224325263 3.32105057454475]
NumMFs=3
MF1='in2mf1':'gaussmf',[1.58499823382204 -3.73340989649714]
MF2='in2mf2':'gaussmf',[1.62165663339208 -0.251911183353459]
MF3='in2mf3':'gaussmf',[1.57163636811725 3.26353672277654]

[Input3]
Name='electric__current__(i)'
Range=[-1.52237296227663 1.91405546737931]
NumMFs=3
MF1='in3mf1':'gaussmf',[0.760280896727532 -1.52187637402028]
MF2='in3mf2':'gaussmf',[0.774521446528792 0.20151054545624]
MF3='in3mf3':'gaussmf',[0.546317498760088 2.04304075703716]

[Output1]
Name='Force'
Range=[-3.47772985404031 3.21627620909248]
NumMFs=27
MF1='out1mf1':'linear',[0.464023100928815 0.800584499096287 -2.71471727958833 0.870788281334411]
MF2='out1mf2':'linear',[-2.0764761048272 0.921350431740111 -1.89132650018032 -3.54752537349722]
MF3='out1mf3':'linear',[2.14173055233575 -4.90224585264209 -6.55165019840417 -5.69595446591223]
MF4='out1mf4':'linear',[-0.425362113910831 2.77533497507699 -0.225469799728866 0.735915973973611]
MF5='out1mf5':'linear',[-0.566896242439656 2.04968617779207 -0.514527774104327 0.0832789574189921]
MF6='out1mf6':'linear',[-0.00078570604959441 2 -3.97700403136401 1.1980576822134 -0.791744475212608]
MF7='out1mf7':'linear',[0.861288287978477 6.67448381125321 5.840629852607161 -4.04428646094623]
MF8='out1mf8':'linear',[2.716106059373321 -0.214636487994583 6.156363173710374 4.306003356420621]
MF9='out1mf9':'linear',[10.90550034023201 -9.111657680557951 3.431594607629628 8.320104724242671]
MF10='out1mf10':'linear',[0.4549540783737691 3.441490103047831 -1.727032367097681 9.536165280615491]
MF11='out1mf11':'linear',[-1.208163262198131 -0.412702896403016 -0.005910473281082 04 -1.130594428207571]
MF12='out1mf12':'linear',[1.134391912551241 5.694567843234741 4.296647600784911 7.258746000642111]
MF13='out1mf13':'linear',[-0.253925091306101 2.726503822462021 0.132342977099077 0.3109078005548361]
MF14='out1mf14':'linear',[-0.484808059692907 1.505855033936631 0.166478400682325 0.0543734356922698]
MF15='out1mf15':'linear',[0.8519174728782231 3.580506990168021 0.374337455233831 -1.245168308392111]
MF16='out1mf16':'linear',[0.436012834150991 1.847671966560291 1.133419259304851 -4.839164477233811]
MF17='out1mf17':'linear',[1.204604130930261 0.6665286137639431 0.144985154553262 -0.426363800597523]
MF18='out1mf18':'linear',[4.232271185823911 1.788310864487541 0.145539762461671 -3.393586351995521]
MF19='out1mf19':'linear',[2.147827005978321 18.03993215826221 -7.370517345664511 25.63161207950571]
MF20='out1mf20':'linear',[-1.888611239575831 2.080571780207051 -9.407421531123971 18.628898719307211]
MF21='out1mf21':'linear',[16.16647929512511 -15.56606360151591 -40.12986212902791 -1.427256053047481]
MF22='out1mf22':'linear',[-0.492228747283104 3.271382979403071 0.057901271287288 1 -2.150280765343261]
MF23='out1mf23':'linear',[-0.831061870159931 3.112969475231541 0.222326873050761 0.846458527687652]
MF24='out1mf24':'linear',[3.384621092774541 -2.561838007004401 0.636621872417981 -11.30112942993121]
MF25='out1mf25':'linear',[0.176335555166731 0.144692429521921 -0.735536213985421 -2.771398918731461]
MF26='out1mf26':'linear',[2.050144093625281 3.315411969129421 -0.011723878958761 8 -12.83474605729811]
MF27='out1mf27':'linear',[15.33338052554761 -5.910169326975461 1.966976171068371 -21.76752292626661]

[Rules]
1 1 1, 1 (1) : 1
1 1 2, 2 (1) : 1
1 1 3, 3 (1) : 1
1 2 1, 4 (1) : 1
1 2 2, 5 (1) : 1
1 2 3, 6 (1) : 1
1 3 1, 7 (1) : 1
1 3 2, 8 (1) : 1
1 3 3, 9 (1) : 1
2 1 1, 10 (1) : 1
2 1 2, 11 (1) : 1
2 1 3, 12 (1) : 1
2 2 1, 13 (1) : 1
2 2 2, 14 (1) : 1
2 2 3, 15 (1) : 1
2 3 1, 16 (1) : 1
2 3 2, 17 (1) : 1
2 3 3, 18 (1) : 1
3 1 1, 19 (1) : 1
3 1 2, 20 (1) : 1
3 1 3, 21 (1) : 1
3 2 1, 22 (1) : 1
3 2 2, 23 (1) : 1
3 2 3, 24 (1) : 1
3 3 1, 25 (1) : 1
3 3 2, 26 (1) : 1
3 3 3, 27 (1) : 1
```

```
%=========================================================================

%MRDamperANFIS_expRP_APRBS.FIS
[System]
Name='MRDamperANFIS_expRP_APRBS'
Type='sugeno'
Version=2.0
NumInputs=3
NumOutputs=1
NumRules=27
AndMethod='prod'
OrMethod='probor'
ImpMethod='prod'
AggMethod='sum'
DefuzzMethod='wtaver'

[Input1]
Name='input1'
Range=[-3.11977176557615 3.5215050174981]
NumMFs=3
MF1='in1mf1':'gaussmf',[1.43983971404427 -3.12932806807909]
MF2='in1mf2':'gaussmf',[1.47820058141561 0.196627169824823]
MF3='in1mf3':'gaussmf',[1.56014888937955 3.43141921729424]

[Input2]
Name='input2'
Range=[-4.12599812765608 3.97906349835775]
NumMFs=3
MF1='in2mf1':'gaussmf',[1.82821174758 69 -4.06085276747947]
MF2='in2mf2':'gaussmf',[1.85214228419147 -0.0415869024152758]
MF3='in2mf3':'gaussmf',[1.78278034139502 3.98245841511505]

[Input3]
Name='input3'
Range=[-2.13969686934153 2.84962693872519]
NumMFs=3
MF1='in3mf1':'gaussmf',[1.04422805803326 -2.15946952102991]
MF2='in3mf2':'gaussmf',[0.998784474616955 0.347339155099881]
MF3='in3mf3':'gaussmf',[0.974116886743692 2.90324498532764]

[Output1]
Name='output'
Range=[-3.15048990465981 2.79948915309713]
NumMFs=27
MF1='out1mf1':'linear',[-3.14609080754551 -8.26663292865714 6.60341194767937 -23.1354080278521]
MF2='out1mf2':'linear',[-0.123840893800529 1.52875388968008 4.11604522926384 1.75690176065151]
MF3='out1mf3':'linear',[3.29238953773353 1.9029349095295 5.40986629224824 -1.33820287855715]
MF4='out1mf4':'linear',[-0.5444621341379 -1.30885798851467 -0.733744077403974 -0.219684525010343]
MF5='out1mf5':'linear',[-1.37074788859097 2.37393355414971 -1.65575877425715 -1.70109574296999]
MF6='out1mf6':'linear',[-1.60072028014755 2.31358771690997 -4.4096183401404 7.56317503154458]
MF7='out1mf7':'linear',[-3.48064889693448 2.0415020442426 5.47596232607809 -2.33872198854525]
MF8='out1mf8':'linear',[1.24609366358969 3.03974593402286 4.99087754431372 -7.07971139795016]
MF9='out1mf9':'linear',[-13.2734219234199 4.93628344769851 9.28800076181109 -63.2467632373648]
MF10='out1mf10':'linear',[-4.62210226467023 2.62885140010742 -3.81841397244968 1.85494765412574]
MF11='out1mf11':'linear',[-0.102905187896383 0.0493283820630618 -3.38246972309652 0.0978063367081735]
MF12='out1mf12':'linear',[1.65150701133439 0.198247244217839 -5.59290045522168 10.8036249469334]
MF13='out1mf13':'linear',[-0.302449421111 95 3.24922635874948 0.007373707639147 0.496382706052 55]
MF14='out1mf14':'linear',[-0.890255165309091 1.70622217446658 0.742246628688991 0.364334519747 91]
MF15='out1mf15':'linear',[-2.61564773599254 2.52340896563666 2.85886787042512 -6.38960613274879]
MF16='out1mf16':'linear',[-4.11142915310134 2.13430267988121 4.06556173965928 -6.88232978199353]
MF17='out1mf17':'linear',[0.920704440311778 1.20300425685797 -0.348665887666673 -3.21094413070036]
MF18='out1mf18':'linear',[-3.3982910231731 1.39188284173855 -3.32463815117878 6.7514148089238]
MF19='out1mf19':'linear',[-19.3580347885022 37.2522033662086 11.1032173151037 159.482731479266]
MF20='out1mf20':'linear',[-0.404080240533533 2.80624525588877 3.99715061734 7.68596684686588]
MF21='out1mf21':'linear',[-5.62085382512167 -1.96768924673728 12.925292057719 -27.1442289649474]
MF22='out1mf22':'linear',[1.23401517708275 9.23778978346199 -1.41502862900106 -11.9149029776414]
MF23='out1mf23':'linear',[-1.00724861009389 1.79329743018673 -1.37780369665483 0.975856108073192]
MF24='out1mf24':'linear',[-4.41656211753792 0.912692264169717 -8.47303550350362 28.6527343773058]
MF25='out1mf25':'linear',[-9.44322019496194 5.17192937169913 -1.02696203820349 5.05865574376337]
MF26='out1mf26':'linear',[0.703656728116056 -0.373864341475067 1.099677583282 -0.181534636232511]
MF27='out1mf27':'linear',[0.117187057741692 2.25832016544275 10.0038029587821 -18.5672968177061]

[Rules]
1 1 1, 1 (1) : 1
1 1 2, 2 (1) : 1
1 1 3, 3 (1) : 1
1 2 1, 4 (1) : 1
1 2 2, 5 (1) : 1
1 2 3, 6 (1) : 1
1 3 1, 7 (1) : 1
1 3 2, 8 (1) : 1
1 3 3, 9 (1) : 1
2 1 1, 10 (1) : 1
2 1 2, 11 (1) : 1
2 1 3, 12 (1) : 1
2 2 1, 13 (1) : 1
2 2 2, 14 (1) : 1
2 2 3, 15 (1) : 1
```

```
2 3 1, 16 (1) : 1
2 3 2, 17 (1) : 1
2 3 3, 18 (1) : 1
3 1 1, 19 (1) : 1
3 1 2, 20 (1) : 1
3 1 3, 21 (1) : 1
3 2 1, 22 (1) : 1
3 2 2, 23 (1) : 1
3 2 3, 24 (1) : 1
3 3 1, 25 (1) : 1
3 3 2, 26 (1) : 1
3 3 3, 27 (1) : 1
%=============================================================================

%MRDamperANFIS_expRP_PRBS.FIS
[System]
Name='MRDamperANFIS_expRP_PRBS'
Type='sugeno'
Version=2.0
NumInputs=3
NumOutputs=1
NumRules=27
AndMethod='prod'
OrMethod='probor'
ImpMethod='prod'
AggMethod='sum'
DefuzzMethod='wtaver'

[Input1]
Name='input1'
Range=[-3.08899881674069 4.27266398753162]
NumMFs=3
MF1='in1mf1':'gaussmf',[1.57163487312992 -3.08622325968734]
MF2='in1mf2':'gaussmf',[1.56438802771854 0.581655449085396]
MF3='in1mf3':'gaussmf',[1.58713383840115 4.25748392564793]

[Input2]
Name='input2'
Range=[-3.56221312793547 3.65135519869651]
NumMFs=3
MF1='in2mf1':'gaussmf',[1.59480190420293 -3.47805496879854]
MF2='in2mf2':'gaussmf',[1.65323061417955 0.0527288519016438]
MF3='in2mf3':'gaussmf',[1.59912232362747 3.55798116275664]

[Input3]
Name='input3'
Range=[-0.842039836019602 1.88506482625885]
NumMFs=3
MF1='in3mf1':'gaussmf',[0.517881147681429 -0.955684437623483]
MF2='in3mf2':'gaussmf',[0.656461203307079 0.431814237076301]
MF3='in3mf3':'gaussmf',[0.476832476358521 1.95161045404253]

[Output1]
Name='output'
Range=[-4.08928856525157 3.57237566398979]
NumMFs=27
MF1='out1mf1':'linear',[-0.459149593222616 0.0103349587759533 -3.6941339464557 -3.69003125562649]
MF2='out1mf2':'linear',[0.892463775171511 0.814123493057967 -1.6663757152562 6.06478968453631]
MF3='out1mf3':'linear',[4.46450815789651 7.38857318649154 -2.24741214161923 39.900242883408]
MF4='out1mf4':'linear',[-0.147084812432798 1.57325747656983 1.31189800017712 2.10103873088827]
MF5='out1mf5':'linear',[-1.6002636729019 4.34156311498157 0.612751158701448 -0.914725543348957]
MF6='out1mf6':'linear',[-0.895289776326591 7.66890195014895 -0.07526899483472 -0.142438385811191]
MF7='out1mf7':'linear',[0.233911538816112 4.23980253437635 8.69754682048171 -2.777773613516581]
MF8='out1mf8':'linear',[4.60429711592359 13.7790916778962 3.82141406628982 -22.9583043725211]
MF9='out1mf9':'linear',[1.63843111500868 15.4057788073321 5.9083612548749 -45.8293387124856]
MF10='out1mf10':'linear',[-0.13434291837106 1.99440817888553 -5.76928333308192 1.696704280436271]
MF11='out1mf11':'linear',[1.68432664810292 -1.01773526755709 -2.78278679640451 -2.53113245438421]
MF12='out1mf12':'linear',[11.0169938406171 8.27287106377984 -4.67966781239967 33.7664790765351]
MF13='out1mf13':'linear',[-0.158727416315939 1.98512612843651 -0.204880450741457 -0.176415152326665]
MF14='out1mf14':'linear',[-2.35670376361328 1.11887768051863 0.0825334298299887 -0.0230232820504858]
MF15='out1mf15':'linear',[-1.4527262728624 6.77815139663204 1.48176809227898 -1.89750096123261]
MF16='out1mf16':'linear',[-0.0368623248816352 2.03093373473336 4.81611212352669 -2.93939069935904]
MF17='out1mf17':'linear',[4.9476659733669 -1.65759178486 6 2.15517969484213 2.84740363655221]
MF18='out1mf18':'linear',[-0.25517306878742 11.9574640169524 0.919131560562099 -31.079297416671]
MF19='out1mf19':'linear',[1.24341146368114 2.40602029884503 -8.93443841018205 -2.43704673855514]
MF20='out1mf20':'linear',[-16.9050612058123 22.0223561084158 -6.17322622245426 69.1252821036377]
MF21='out1mf21':'linear',[151.26245496037 61.1594977456149 4.92720140841521 -160.880050104673]
MF22='out1mf22':'linear',[0.14336991839493 -0.861006539340023 -0.0851492911619035 -2.77688275663818]
MF23='out1mf23':'linear',[-3.9732391192274 8.55206599382727 0.753172378806062 14.2665077716653]
MF24='out1mf24':'linear',[-9.30494035998815 19.5194116615351 -4.32981091554839 10.6630374346038]
MF25='out1mf25':'linear',[-2.26367783666519 -4.6908237208472 -2.56638583994964 18.4404480458475]
MF26='out1mf26':'linear',[11.0890175038562 12.0860020094769 -4.47648668190052 -76.0154217674246]
MF27='out1mf27':'linear',[6.61719165350706 2.4211938759423 0.229816605148412 -32.7849297904517]

[Rules]
1 1 1, 1 (1) : 1
1 1 2, 2 (1) : 1
1 1 3, 3 (1) : 1
```

```
1 2 1, 4 (1) : 1
1 2 2, 5 (1) : 1
1 2 3, 6 (1) : 1
1 3 1, 7 (1) : 1
1 3 2, 8 (1) : 1
1 3 3, 9 (1) : 1
2 1 1, 10 (1) : 1
2 1 2, 11 (1) : 1
2 1 3, 12 (1) : 1
2 2 1, 13 (1) : 1
2 2 2, 14 (1) : 1
2 2 3, 15 (1) : 1
2 3 1, 16 (1) : 1
2 3 2, 17 (1) : 1
2 3 3, 18 (1) : 1
3 1 1, 19 (1) : 1
3 1 2, 20 (1) : 1
3 1 3, 21 (1) : 1
3 2 1, 22 (1) : 1
3 2 2, 23 (1) : 1
3 2 3, 24 (1) : 1
3 3 1, 25 (1) : 1
3 3 2, 26 (1) : 1
3 3 3, 27 (1) : 1
%=========================================================================================

%MRDamperANFIS_expRP_APRBS_L.FIS
[System]
Name='MRDamperANFIS_expRP_APRBS_L'
Type='sugeno'
Version=2.0
NumInputs=3
NumOutputs=1
NumRules=27
AndMethod='prod'
OrMethod='probor'
ImpMethod='prod'
AggMethod='sum'
DefuzzMethod='wtaver'

[Input1]
Name='input1'
Range=[-2.65425169055877 3.1545115947056]
NumMFs=3
MF1='in1mf1':'gaussmf',[1.24165315146706 -2.63942716569738]
MF2='in1mf2':'gaussmf',[1.22327362112448 0.2464731712215621
MF3='in1mf3':'gaussmf',[1.23801334273052 3.13705436064304]

[Input2]
Name='input2'
Range=[-2.86296208086463 3.503732153751821
NumMFs=3
MF1='in2mf1':'gaussmf',[1.40012635228044 -2.79796532774504]
MF2='in2mf2':'gaussmf',[1.52952190086198 0.364525207694143]
MF3='in2mf3':'gaussmf',[1.51406656246153 3.4236975164607]

[Input3]
Name='input3'
Range=[-2.53577487519009 2.77157538581688]
NumMFs=3
MF1='in3mf1':'gaussmf',[1.20540786735098 -2.474063556331]
MF2='in3mf2':'gaussmf',[1.11628267184873 0.1297818325078061
MF3='in3mf3':'gaussmf',[1.05687318987525 2.79954641243359]

[Output1]
Name='output'
Range=[-2.74459419317953 2.830150118977071
NumMFs=27
MF1='out1mf1':'linear',[1.880231851509272.83353218226612-2.433889608915425.27571258779132]
MF2='out1mf2':'linear',[0.0750668856464077 1.37900474298103-1.868874891125552.783964524956061
MF3='out1mf3':'linear',[-2.213847454448290.162858372303207-3.585756011733711-0.1627949384269551
MF4='out1mf4':'linear',[-0.830588587769736 5.53661809758396 1.111961765987994.935300362860631
MF5='out1mf5':'linear',[-1.027711154312782.504740395018141.279706515634660-0.801501870479681
MF6='out1mf6':'linear',[-0.585836196412626-0.174910844045921 3.123003481004530-7.215361381541191
MF7='out1mf7':'linear',[4.320414197008861 3.844582399795900.529280377079838-35.8713866214357]
MF8='out1mf8':'linear',[-0.5400215366150911 5.3134190917018-3.623876615450741-12.4656578917068]
MF9='out1mf9':'linear',[9.243545718752531-4.619724491328241-14.7551158049782 72.7207322964814]
MF10='out1mf10':'linear',[1.016513317931353.16967577083318-0.6083578882922030 6.878065932527891
MF11='out1mf11':'linear',[-0.028641723484256300.078859110854338701-0.1835816096664631-1.372358371831781
MF12='out1mf12':'linear',[-2.690817314752960.993693908509220.365474050514646 4.289193759917591
MF13='out1mf13':'linear',[-0.2908544419035154.164081956079971-0.5610911519295151-1.219587602337281
MF14='out1mf14':'linear',[-0.7513148869967931.348409367793560-0.5083346791401520.4258105465541141
MF15='out1mf15':'linear',[0.9402310453257052.798820473957781-0.6596117123631531.144842788770331
MF16='out1mf16':'linear',[0.001777888166023915.872683318179851.494153248150941-14.3630817420456]
MF17='out1mf17':'linear',[0.5304607677274731-0.1553510014041361.118982308616970.6394168882247181
MF18='out1mf18':'linear',[-0.8847215706759632.600281753506900.05436009536617741-6.106632795228911
MF19='out1mf19':'linear',[2.252540039505794.425269098923156.015452755472241616.5516825424732]
MF20='out1mf20':'linear',[-1.643809672845860.3856213248409572.820503451034880.5467756961215651
```

```
MF21='out1mf21':'linear',[-3.17992101634451 -6.1911798498391 -2.87559153196718 -8.16137940943252]
MF22='out1mf22':'linear',[-1.15017672734899 3.17440692879354 -0.818597581067691 -0.625672033180652]
MF23='out1mf23':'linear',[-0.10402834286188 0.505672131295S1 -0.318029357887557 -0.831710473203268]
MF24='out1mf24':'linear',[0.5551740026883335 -2.71710323197307 -0.379085882946192 -1.62062586969276]
MF25='out1mf25':'linear',[0.38882378023508 2.49695365130154 -0.0928281241650904 -8.58840778901096]
MF26='out1mf26':'linear',[0.00119336098940395 -2.51039747772265 0.402150754051726 8.68297471391425]
MF27='out1mf27':'linear',[1.62184869066052 -1.89677774402824 4.29014592564396 0.968698615751689]

[Rules]
1 1 1, 1 (1) : 1
1 1 2, 2 (1) : 1
1 1 3, 3 (1) : 1
1 2 1, 4 (1) : 1
1 2 2, 5 (1) : 1
1 2 3, 6 (1) : 1
1 3 1, 7 (1) : 1
1 3 2, 8 (1) : 1
1 3 3, 9 (1) : 1
2 1 1, 10 (1) : 1
2 1 2, 11 (1) : 1
2 1 3, 12 (1) : 1
2 2 1, 13 (1) : 1
2 2 2, 14 (1) : 1
2 2 3, 15 (1) : 1
2 3 1, 16 (1) : 1
2 3 2, 17 (1) : 1
2 3 3, 18 (1) : 1
3 1 1, 19 (1) : 1
3 1 2, 20 (1) : 1
3 1 3, 21 (1) : 1
3 2 1, 22 (1) : 1
3 2 2, 23 (1) : 1
3 2 3, 24 (1) : 1
3 3 1, 25 (1) : 1
3 3 2, 26 (1) : 1
3 3 3, 27 (1) : 1
%=============================================================================

%MRDamperANFIS_expRP_ICPS_L.FIS
[System]
Name='MRDamperANFIS_expRP_ICPS_L'
Type='sugeno'
Version=2.0
NumInputs=3
NumOutputs=1
NumRules=27
AndMethod='prod'
OrMethod='probor'
ImpMethod='prod'
AggMethod='sum'
DefuzzMethod='wtaver'

[Input1]
Name='input1'
Range=[-2.85364935661455 3.11213420022853]
NumMFs=3
MF1='in1mf1':'gaussmf',[1.19070241452016 -2.90325106575453]
MF2='in1mf2':'gaussmf',[1.26327129587382 0.0979932488126096]
MF3='in1mf3':'gaussmf',[1.38517632850882 3.00798454103428]

[Input2]
Name='input2'
Range=[-2.97291027771105 4.89826510788298]
NumMFs=3
MF1='in2mf1':'gaussmf',[1.63496914270118 -2.95728259424643]
MF2='in2mf2':'gaussmf',[1.60764719207885 1.04178271397505]
MF3='in2mf3':'gaussmf',[1.64034253553537 4.95792755824252]

[Input3]
Name='input3'
Range=[-1.65891316527171 1.94813003677832]
NumMFs=3
MF1='in3mf1':'gaussmf',[0.748572159826103 -1.68354209313507]
MF2='in3mf2':'gaussmf',[0.688346037868495 0.0421638943644091]
MF3='in3mf3':'gaussmf',[0.631446021815979 2.00216646592816]

[Output1]
Name='output'
Range=[-3.32161549336933 3.84442316556507]
NumMFs=27
MF1='out1mf1':'linear',[-0.3027146314l4606 -0.146111078533192 -1.99128216493503 -4.51645636978976]
MF2='out1mf2':'linear',[-1.23657343754S2 0.269231111072439 -1.72410950444132 -3.96922213768335]
MF3='out1mf3':'linear',[-0.140357582404287 2.77278223632195 -2.61325397393101 9.18128230681905]
MF4='out1mf4':'linear',[-0.368358447507383 1.18181241101792 0.920738769629458 2.06366300237189]
MF5='out1mf5':'linear',[-0.255898690742313 1.00552117217617 0.928084861555202 0.919160543002961]
MF6='out1mf6':'linear',[-1.87058892445021 5.31162772881458 1.95258100427507 -5.11227214924362]
MF7='out1mf7':'linear',[13.0508433594659 18.1458126954487 -4.16621886912418 -34.0481712956766]
MF8='out1mf8':'linear',[-8.72049224252168 12.3032794819756 -5.67785167673918 -39.603681943878]
```

```
MF9='out1mf9':'linear',[117.388864257209 15.1075349131033 -30.0644033456656 149.593287171889]
MF10='out1mf10':'linear',[0.0434871145528278 0.0582108373694941 -1.04679657209577 -1.59877185171209]
MF11='out1mf11':'linear',[-1.09300313009335 0.342924453255439 -0.776452717537719 -1.26263189827236]
MF12='out1mf12':'linear',[-0.368651367191627 0.0416288010465347 -1.4050036763901 -1.1774132857246]
MF13='out1mf13':'linear',[-0.310932847835641 1.18525049722989 0.430687081123609 1.17204900191858]
MF14='out1mf14':'linear',[-0.485170671741205 1.51741726064017 0.274637553003176 0.304220297473731]
MF15='out1mf15':'linear',[-0.432991230981821 0.193820779823074 0.332053375488135 0.182467426317327]
MF16='out1mf16':'linear',[3.88490561283527 9.53320884307946 1.09606502692787 -26.7812793013309]
MF17='out1mf17':'linear',[2.9981719865101 2.72746993746066 0.142732299304472 -8.58091434415445]
MF18='out1mf18':'linear',[17.9110777229967 -5.99222704752003 0.541104272871395 18.6690480408163]
MF19='out1mf19':'linear',[0.605246879664748 1.45329132715723 -0.69336580022614 1.14419650835221]
MF20='out1mf20':'linear',[-2.47646766311216 -0.173215091663222 -0.470020875456371 4.13778158597918]
MF21='out1mf21':'linear',[2.01478737496411 -3.46368698038775 3.47225675639151 -15.4791167392812]
MF22='out1mf22':'linear',[-0.268141841029581 2.52139484203645 -0.304521193445016 -1.25792666100287]
MF23='out1mf23':'linear',[-0.28685256040318 1.07483328276321 -0.841745776717022 0.0622554079074232]
MF24='out1mf24':'linear',[-0.905054138756031 0.854690519737901 -1.84396826361204 5.32391969148911]
MF25='out1mf25':'linear',[4.74296902510491 7.11536505906416 8.86033192248125 -24.2689722326039]
MF26='out1mf26':'linear',[3.27391823514808 -3.36448260603902 13.3834894736389 -2.10469109705929]
MF27='out1mf27':'linear',[24.2975426021798 3.26452615789596 34.7533494568471 -127.461718069331]

[Rules]
1 1 1, 1 (1) : 1
1 1 2, 2 (1) : 1
1 1 3, 3 (1) : 1
1 2 1, 4 (1) : 1
1 2 2, 5 (1) : 1
1 2 3, 6 (1) : 1
1 3 1, 7 (1) : 1
1 3 2, 8 (1) : 1
1 3 3, 9 (1) : 1
2 1 1, 10 (1) : 1
2 1 2, 11 (1) : 1
2 1 3, 12 (1) : 1
2 2 1, 13 (1) : 1
2 2 2, 14 (1) : 1
2 2 3, 15 (1) : 1
2 3 1, 16 (1) : 1
2 3 2, 17 (1) : 1
2 3 3, 18 (1) : 1
3 1 1, 19 (1) : 1
3 1 2, 20 (1) : 1
3 1 3, 21 (1) : 1
3 2 1, 22 (1) : 1
3 2 2, 23 (1) : 1
3 2 3, 24 (1) : 1
3 3 1, 25 (1) : 1
3 3 2, 26 (1) : 1
3 3 3, 27 (1) : 1
%=========================================================================

%MRDamperANFIS_expRC1_CS.FIS
[System]
Name='MRDamperANFIS_expRC1_CS'
Type='sugeno'
Version=2.0
NumInputs=3
NumOutputs=1
NumRules=27
AndMethod='prod'
OrMethod='probor'
ImpMethod='prod'
AggMethod='sum'
DefuzzMethod='wtaver'

[Input1]
Name='input1'
Range=[-3.42237630328106 3.29302845231913]
NumMFs=3
MF1='in1mf1':'gaussmf',[1.43098041010664 -3.42006790324062]
MF2='in1mf2':'gaussmf',[1.42752592504453 -0.0694193043394365]
MF3='in1mf3':'gaussmf',[1.42563340657259 3.28896509338191]

[Input2]
Name='input2'
Range=[-3.77188584123213 3.32767706994718]
NumMFs=3
MF1='in2mf1':'gaussmf',[1.56960210094698 -3.72428308874678]
MF2='in2mf2':'gaussmf',[1.55704933537479 -0.235136747602453]
MF3='in2mf3':'gaussmf',[1.49469230313653.3232000505409]

[Input3]
Name='input3'
Range=[-1.48599517330948 1.52383301336969]
NumMFs=3
MF1='in3mf1':'gaussmf',[0.6307524173606841.49739360082896]
MF2='in3mf2':'gaussmf',[0.662987909248046 0.00556822009380193]
MF3='in3mf3':'gaussmf',[0.63724068228087 1.52704203778426]
```

```
[Output1]
Name='output'
Range=[-3.91896012793866 3.96632822939564]
NumMFs=27
MF1='out1mf1':'linear',[-0.186579417882172 0.367909438418147 -0.94763776359529 -0.57763853704613]
MF2='out1mf2':'linear',[0.0287861790954439 0.428225362571167 -1.17835391682051 0.563054769051825]
MF3='out1mf3':'linear',[-1.57456226369366 0.519480300857278 -0.831551707100836 -4.3559681675606]
MF4='out1mf4':'linear',[-0.117073942693168 1.22895651689925 0.59381905340063 1.52444359969549]
MF5='out1mf5':'linear',[-0.553622540925557 1.88513959262909 0.383304140113207 0.142641518505961
MF6='out1mf6':'linear',[-0.48713164628898 1.68197559918357 0.211443773238603 -0.103852154212855]
MF7='out1mf7':'linear',[0.491311305879797 3.75557224220391 0.294623399867962 -6.32496258788094]
MF8='out1mf8':'linear',[1.42915186851999 2.41301046439345 1.52880979506194 -1.61250308748698]
MF9='out1mf9':'linear',[1.76669684798766 0.622940985138066 1.18104067892594 4.32704684885671
MF10='out1mf10':'linear',[0.0954506523563329 1.49778828722862 -1.43498595322659 3.00330208448305]
MF11='out1mf11':'linear',[0.456751883395579 0.687013126716324 -1.73829833095625 1.45901177789304]
MF12='out1mf12':'linear',[-0.851339153583837 1.49475916224489 -1.20538712499199 3.32734502470224]
MF13='out1mf13':'linear',[-0.182877013372773 1.37018436913156 0.0723874535517321 0.0110297489079504]
MF14='out1mf14':'linear',[-0.468774547490662 1.49165668047238 0.0103838537253853 -0.155757961749541]
MF15='out1mf15':'linear',[-0.472557958279048 1.92382735909387 -0.00147615163915287 -0.176533798750336]
MF16='out1mf16':'linear',[0.351394155978173 1.05277512173513 0.630802439327103 -2.08081577703127]
MF17='out1mf17':'linear',[0.526068098604245 0.324192492274885 1.26070289368083 0.283205858006584]
MF18='out1mf18':'linear',[0.577031573606015 1.15767665870399 0.905112739700874 -1.48145372203829]
MF19='out1mf19':'linear',[-0.917085097828929 8.42180147871158 -0.899854973995931 22.0245390530826]
MF20='out1mf20':'linear',[2.14360280410234 3.37133282745394 -3.22332680719515 4.02030539058575]
MF21='out1mf21':'linear',[0.716080733684552 3.39065791707091 -1.85148070841108 10.4319648229879]
MF22='out1mf22':'linear',[-0.366076082644453 2.11405568680143 -0.373882246168311 -1.42128303373222]
MF23='out1mf23':'linear',[-0.944248715576832 1.97439048182686 -0.275750973799191 0.590048899181359]
MF24='out1mf24':'linear',[-1.32184179272466 3.49394036391433 -0.197204709978259 1.82274521818196]
MF25='out1mf25':'linear',[0.348679313808849 0.473815760175479 0.319300494819747 -2.04305536194827]
MF26='out1mf26':'linear',[0.546338938093462 0.773296379144569 0.777719742511295 -2.65035690982666]
MF27='out1mf27':'linear',[1.16547413435979 2.91373903498176 0.643576755854014 -10.7395029488658]

[Rules]
1 1 1, 1 (1) : 1
1 1 2, 2 (1) : 1
1 1 3, 3 (1) : 1
1 2 1, 4 (1) : 1
1 2 2, 5 (1) : 1
1 2 3, 6 (1) : 1
1 3 1, 7 (1) : 1
1 3 2, 8 (1) : 1
1 3 3, 9 (1) : 1
2 1 1, 10 (1) : 1
2 1 2, 11 (1) : 1
2 1 3, 12 (1) : 1
2 2 1, 13 (1) : 1
2 2 2, 14 (1) : 1
2 2 3, 15 (1) : 1
2 3 1, 16 (1) : 1
2 3 2, 17 (1) : 1
2 3 3, 18 (1) : 1
3 1 1, 19 (1) : 1
3 1 2, 20 (1) : 1
3 1 3, 21 (1) : 1
3 2 1, 22 (1) : 1
3 2 2, 23 (1) : 1
3 2 3, 24 (1) : 1
3 3 1, 25 (1) : 1
3 3 2, 26 (1) : 1
3 3 3, 27 (1) : 1
%=============================================================================

%MRDamperANFIS_expRC2_CS.FIS
[System]
Name='MRDamperANFIS_expRC2_CS'
Type='sugeno'
Version=2.0
NumInputs=3
NumOutputs=1
NumRules=27
AndMethod='prod'
OrMethod='probor'
ImpMethod='prod'
AggMethod='sum'
DefuzzMethod='wtaver'

[Input1]
Name='input1'
Range=[-3.78501984696143 3.51707372823506]
NumMFs=3
MF1='in1mf1':'gaussmf',[1.77049561379651 -3.69286420665269]
MF2='in1mf2':'gaussmf',[1.61391677496437 -0.163980624459519]
MF3='in1mf3':'gaussmf',[1.50215773500331 3.56351575625551]

[Input2]
Name='input2'
Range=[-4.03792384181093 8.17518309181665]
NumMFs=3
```

```
MF1='in2mf1':'gaussmf',[2.346515020815O2  -4.0159237165299]
MF2='in2mf2':'gaussmf',[2.38595521629585  2.35709222180533]
MF3='in2mf3':'gaussmf',[2.76446400308016  8.10370129964483]

[Input3]
Name='input3'
Range=[-1.48599517330948  1.52383301336969]
NumMFs=3
MF1='in3mf1':'gaussmf',[0.533870387633702  -1.59026043932265]
MF2='in3mf2':'gaussmf',[0.731761837010892  -0.0738724854514102]
MF3='in3mf3':'gaussmf',[0.777215985175257  1.43024516304312]

[Output1]
Name='output'
Range=[-4.03561773965864  4.21865734197246]
NumMFs=27
MF1='out1mf1':'linear',[-0.119735144031826  0.383106485936537  -1.16273022865113  -0.914237051711183]
MF2='out1mf2':'linear',[0.258639915426856  1.85835889366686  -0.91472147938745  6.77493531661756]
MF3='out1mf3':'linear',[-1.98880747439853  0.975119325767678  -0.654473454169569  -4.72284441079215]
MF4='out1mf4':'linear',[0.138136317359431  2.46190151306421  1.99419857821335  6.85209108789825]
MF5='out1mf5':'linear',[-4.01467774886967  13.0529727392936  0.886045556422097  13.4221657345197]
MF6='out1mf6':'linear',[-2.38050709366913  3.01749314631757  0.544943613372273  -1.32875335318484]
MF7='out1mf7':'linear',[-2.04421030252989  43.4852347711311  17.0561671331322  -150.475488232]
MF8='out1mf8':'linear',[49.2437571071434  287.758080578973  28.2887600868844  -997.431835963485]
MF9='out1mf9':'linear',[-62.1756480977556  60.3172729250696  19.9919239294315  -384.989278373912]
MF10='out1mf10':'linear',[-0.0636513202352946  0.111423906199018  -1.63893300840553  -2.43441594245695]
MF11='out1mf11':'linear',[0.207912639330152  -0.647829614622377  -1.61132482083016  -3.88805332547265]
MF12='out1mf12':'linear',[-1.24739809403138  0.155129841877754  -1.124866442423  -1.21951481911021]
MF13='out1mf13':'linear',[-0.153802638512727  0.826075378490769  1.00079985530848  2.03181730991807]
MF14='out1mf14':'linear',[-1.95622887578243  0.120789282005797  0.693675349664146  1.33006422180051]
MF15='out1mf15':'linear',[-1.37630348460951  0.816408627518816  0.50445473045055  0.349596986310587]
MF16='out1mf16':'linear',[4.33496099964384  5.32982155753832  -5.43517607848781  -39.0138778857031]
MF17='out1mf17':'linear',[22.5985629065376  -16.3520554790002  -0.749395647190257  36.0829141100679]
MF18='out1mf18':'linear',[-11.0507241403943  -8.69228585228252  -1.0740928702198  46.1463226883637]
MF19='out1mf19':'linear',[-0.00642597948629535  -2.37463434751046  -2.16833820734759  -10.4132943111732]
MF20='out1mf20':'linear',[-0.165211026541312  1.71471632282884  -2.17752222741916  4.14732811953654]
MF21='out1mf21':'linear',[-2.34638783067784  1.23543337264077  -1.54254471168516  8.67702817221895]
MF22='out1mf22':'linear',[-0.0820232989920042  -3.25068760459041  0.358634727349S4  -0.164813905838952]
MF23='out1mf23':'linear',[-1.53809064970565  4.86163369664884  0.252763994084335  6.60882598992046]
MF24='out1mf24':'linear',[-1.22318567304467  2.73283400445242  0.200326766581652  2.85948590190795]
MF25='out1mf25':'linear',[0.453201960389842  -30.6331809419151  11.2881800481532  165.336024735383]
MF26='out1mf26':'linear',[12.2137582823273  39.9143493295616  6.94032559234475  -239.358594245961]
MF27='out1mf27':'linear',[-10.2019793741768  8.24105639195665  4.81865804632485  -19.6745448360813]

[Rules]
1 1 1, 1 (1) : 1
1 1 2, 2 (1) : 1
1 1 3, 3 (1) : 1
1 2 1, 4 (1) : 1
1 2 2, 5 (1) : 1
1 2 3, 6 (1) : 1
1 3 1, 7 (1) : 1
1 3 2, 8 (1) : 1
1 3 3, 9 (1) : 1
2 1 1, 10 (1) : 1
2 1 2, 11 (1) : 1
2 1 3, 12 (1) : 1
2 2 1, 13 (1) : 1
2 2 2, 14 (1) : 1
2 2 3, 15 (1) : 1
2 3 1, 16 (1) : 1
2 3 2, 17 (1) : 1
2 3 3, 18 (1) : 1
3 1 1, 19 (1) : 1
3 1 2, 20 (1) : 1
3 1 3, 21 (1) : 1
3 2 1, 22 (1) : 1
3 2 2, 23 (1) : 1
3 2 3, 24 (1) : 1
3 3 1, 25 (1) : 1
3 3 2, 26 (1) : 1
3 3 3, 27 (1) : 1
%=============================================================================

%MRDamperANFIS_expRC3_CS.FIS
[System]
Name='MRDamperANFIS_expRC3_CS'
Type='sugeno'
Version=2.0
NumInputs=3
NumOutputs=1
NumRules=27
AndMethod='prod'
OrMethod='probor'
ImpMethod='prod'
AggMethod='sum'
DefuzzMethod='wtaver'
```

```
[Input1]
Name='input1'
Range=[-3.04464377265303 4.63593933027745]
NumMFs=3
MF1='in1mf1':'gaussmf',[1.65208604654202 -3.02250188879322]
MF2='in1mf2':'gaussmf',[1.64997458656274 0.81167241427774]
MF3='in1mf3':'gaussmf',[1.68450110836318 4.61075299098043]

[Input2]
Name='input2'
Range=[-5.03739828228762 3.63758745739507]
NumMFs=3
MF1='in2mf1':'gaussmf',[1.96276258184005 -4.96454249943251]
MF2='in2mf2':'gaussmf',[1.87464149617569 -0.756733966373629]
MF3='in2mf3':'gaussmf',[1.76320905389868 3.65401618259546]

[Input3]
Name='input3'
Range=[-1.48599517330948 1.52383301336969]
NumMFs=3
MF1='in3mf1':'gaussmf',[0.572976626855999 -1.55220695273178]
MF2='in3mf2':'gaussmf',[0.697583917911525 -0.0347036834334241]
MF3='in3mf3':'gaussmf',[0.675793490457244 1.50379816692398]

[Output1]
Name='output'
Range=[-3.58006417685791 3.87803992022025]
NumMFs=27
MF1='out1mf1':'linear',[0.596619931809332 -4.28064598198994 -2.95080784645972 -15.3950589810284]
MF2='out1mf2':'linear',[0.250409922284571 3.32133294495946 -2.56031430472386 14.5961334371417]
MF3='out1mf3':'linear',[-0.681520850965558 4.91374332838383 -1.76273390442241 18.9770039684258]
MF4='out1mf4':'linear',[-0.16001954201733 0.0426372500566457 0.268774027095029 1.01021022864873]
MF5='out1mf5':'linear',[-0.522888979901607 3.24873751394576 0.100910225734164 0.192925926924864]
MF6='out1mf6':'linear',[-0.543653833681936 4.17220396321092 0.076663095966418 0.525526105821637]
MF7='out1mf7':'linear',[0.5379156742327 0.306346521570586 2.15502807296773 3.5287112163105]
MF8='out1mf8':'linear',[0.432654961162901 4.06228697990035 2.77437875694369 -8.63376956004433]
MF9='out1mf9':'linear',[-0.487759494213583 6.95773208985185 1.64443975718811 -17.1928895784703]
MF10='out1mf10':'linear',[0.939227885651517 3.22785320564162 0.0882151573031469 11.21559637395]
MF11='out1mf11':'linear',[0.560017662290975 3.44994597776871 -2.53776384964873 12.6950620482471]
MF12='out1mf12':'linear',[-0.92413255476826 1.983154623021 -1.70602199810054 8.44492364367583]
MF13='out1mf13':'linear',[-0.168296570366654 1.05392426958813 -0.795741526450922 -1.38015749318591]
MF14='out1mf14':'linear',[-0.894441805242348 1.96496444781168 -0.324158029883774 -0.673000721280061]
MF15='out1mf15':'linear',[-1.05084713043718 2.21513078821604 -0.242286882627146 0.0829413747679325]
MF16='out1mf16':'linear',[0.212664004277602 0.482017129865981 2.13873170296643 1.47559536072342]
MF17='out1mf17':'linear',[0.483349102443477 0.249456183065072 1.68791855674717 -0.0122544578842006]
MF18='out1mf18':'linear',[-0.206985383808439 1.07913854439829 1.29793737666999 -2.44808927577674]
MF19='out1mf19':'linear',[0.692431827816262 7.49816923130044 -7.66723177186487 8.02157198432951]
MF20='out1mf20':'linear',[-6.79908183301994 25.7606868772409 -2.24656105414705 86.7184688452328]
MF21='out1mf21':'linear',[-10.5124933317734 16.8426954476949 -0.272847928339462 78.0116639395749]
MF22='out1mf22':'linear',[-0.0189949879433825 1.07411992327657 -0.650486085695143 -2.10398683688076]
MF23='out1mf23':'linear',[-1.40932840845209 2.47658593568019 -0.945453783056805 1.29284535108196]
MF24='out1mf24':'linear',[-1.86215497690313 3.395504106105 -0.712105222515327 5.16000828123044]
MF25='out1mf25':'linear',[-0.0741522813087878 0.140150879909878 0.507341053203205 0.606543804550321]
MF26='out1mf26':'linear',[0.55093417198326 0.410544384644308 1.15469301664704 -2.21249446195775]
MF27='out1mf27':'linear',[-0.459489140619349 1.82053459349413 0.896501322961647 -2.99968367513259]

[Rules]
1 1 1, 1 (1) : 1
1 1 2, 2 (1) : 1
1 1 3, 3 (1) : 1
1 2 1, 4 (1) : 1
1 2 2, 5 (1) : 1
1 2 3, 6 (1) : 1
1 3 1, 7 (1) : 1
1 3 2, 8 (1) : 1
1 3 3, 9 (1) : 1
2 1 1, 10 (1) : 1
2 1 2, 11 (1) : 1
2 1 3, 12 (1) : 1
2 2 1, 13 (1) : 1
2 2 2, 14 (1) : 1
2 2 3, 15 (1) : 1
2 3 1, 16 (1) : 1
2 3 2, 17 (1) : 1
2 3 3, 18 (1) : 1
3 1 1, 19 (1) : 1
3 1 2, 20 (1) : 1
3 1 3, 21 (1) : 1
3 2 1, 22 (1) : 1
3 2 2, 23 (1) : 1
3 2 3, 24 (1) : 1
3 3 1, 25 (1) : 1
3 3 2, 26 (1) : 1
3 3 3, 27 (1) : 1
%=============================================================================
```

Appendix D

Non-Linear Fuzzy-Based Model

The proposed non-linear fuzzy model was trained using the three sets of experimental data for which the electric current was held constant. Each data set was divided into seven equal parts, each corresponding to a constant step of the electric current (0.0, 0.4, 0.8, 1.2, 1.6, 2.1, and 2.5 A). For each value of the electric current, one non-linear equation, as the one presented in equation 4.9, was identified using non-linear least squares in *MATLAB*^{TM}. Table D.1 presents the identified coefficients for the each of output functions of the non-linear fuzzy based model.

Table D.1. Identified coefficients for the non-linear fuzzy-based model.

Model	Output Function	d_1	d_2	d_3	d_4	d_5
$RC1-SC$	$f_1(t)$	25.2265	3.0650	4.6028	-3200.0681	2109.8135
	$f_2(t)$	52.1981	3.0503	0.6770	415.0016	-183.1820
	$f_3(t)$	81.5221	3.2595	0.4783	629.8635	-272.7241
	$f_4(t)$	171.6249	0.2753	0.2504	714.7907	-317.1429
	$f_5(t)$	48.3849	24.2010	0.7565	-148.0621	68.6384
	$f_6(t)$	34.6003	34.5981	4.0249	-26.3173	13.9835
	$f_7(t)$	38.5583	37.7723	4.2741	-23.6473	13.2332
$RC2-SC$	$f_1(t)$	17.0918	3.2781	2.7087	-1.4775	1.8047
	$f_2(t)$	54.4845	2.6434	0.6610	-708.1935	301.5387
	$f_3(t)$	87.0530	2.3311	0.4572	-719.4389	303.4493
	$f_4(t)$	197.3649	-2.2904	0.2292	808.5372	-353.0962
	$f_5(t)$	64.9750	20.2574	0.5609	70.4272	-31.7165
	$f_6(t)$	39.5097	32.6552	3.2390	1054.1195	-541.9325
	$f_7(t)$	43.2435	35.7863	3.5948	11.8777	-6.4219
$RC3-SC$	$f_1(t)$	17.0222	3.3977	2.6617	-2929.4556	2468.9527
	$f_2(t)$	53.8456	2.6965	0.6524	-766.0747	300.3521
	$f_3(t)$	83.8162	3.2644	0.4669	1423.8401	-559.0957
	$f_4(t)$	99.6419	10.2792	0.3517	-76.7070	31.5043
	$f_5(t)$	35.9105	28.2310	1.2507	-866.9619	378.8263
	$f_6(t)$	31.8596	35.6241	3.5689	-378.2586	178.2317
	$f_7(t)$	36.6054	38.4434	3.6598	-480.9478	238.9911

Once the output functions had been obtained, ***Simulink*** was employed to create the non-linear fuzzy-based model as shown in Fig. D.1. The input fuzzy sets were selected as seven Gaussian functions with variance equal to 0.2 and means of 0, 0.4, 0.8, 1.2, 1.6, 2.1, and 2.5 A.

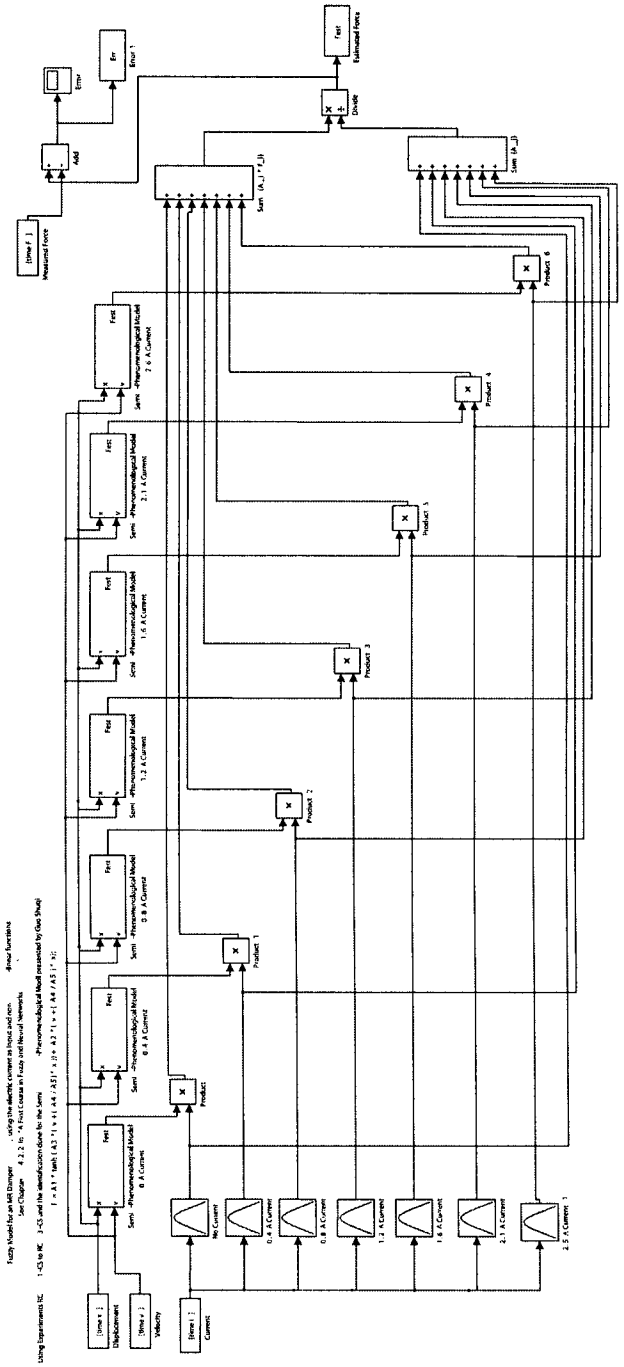

Figure. D.1. Non-linear fuzzy-based model validation. The electric current pattern is connected to the seven membership functions. The fuzzy conclusions are then connected to the non-linear output functions, and their output is summed in order to obtain the final estimated force. The model saves the error and estimated force values.

Appendix E

Published Works

18th Mediterranean Conference on Control & Automation
Congress Palace Hotel, Marrakech, Morocco
June 23-25, 2010

Comparison of MR Damper Models

Javier A. Ruiz-Cabrera, Vicente A. Díaz-Salas, Ruben Morales-Menendez,
Luis Garza-Castañón, and Ricardo A. Ramírez-Mendoza.
Tecnológico de Monterrey, Campus Monterrey
Av. Eugenio Garza Sada 2501
64,849 Monterrey NL, México

Abstract— **A Magneto-Rheologial (*MR*) damper exhibits a hysteretic and non-linear behavior. This behavior makes it a challenge to develop a model for the system. The present research is centered on analyzing and comparing three state-of-the-art models for *MR* dampers. *NARX*, *Semi-Phenomenological*, and *Phenomenological* models were selected. Experimental data was obtained using different input patterns. The models were identified for both constant and variant electric current scenarios. The results showed that *road profile* patterns allow a better identification of the models. The *phenomenological* model was found to obtain the best compromise between performance and simplicity.**

I. MOTIVATION

Magneto-Rheological (*MR*) fluids are non-colloidal suspensions of particles with a size on the order of a few microns [1]. These fluids are unique due to their ability to change its properties reversibly between fluid and solid-like states in milliseconds upon the application of a magnetic field.

Among a broad spectrum of applications, *MR* fluids have been widely utilized for vibration damping systems. *MR* fluids can operate at temperatures ranging from 40 to 150 °C with only slight variations in the yield stress. They are almost insensitive to impurities and can be controlled with low voltages and a current driven power supply outputting 1-2 amperes [2].

An *MR* damper can be part of a semi-active suspension system. These systems offer the reliability of passive devices, but maintain the versatility and adaptability of active systems. A semi-active *MR* damper is a non-linear dynamical system, where the inputs can be selected to be the elongation speed and the electric current. The current is the control input that modulates damping characteristic of the *MR* fluid through the variation of a magnetic field. The output is the force delivered by the damper.

The major drawback of *MR* dampers lies on their non-linear and hysteretic force-velocity response, Fig. 1. The design of a controller generally demands a model of the actuator which becomes a non-trivial task when it comes to *MR* dampers [3].

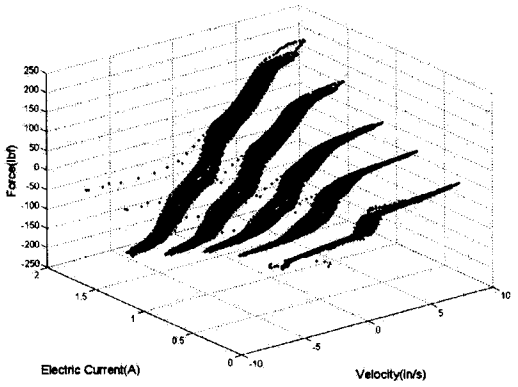

Fig. 1. *MR* damper behavior at constant electric currents. The force delivered by a MR damper is plotted for different electric current inputs.

Different modelling techniques have been studied for *MR* dampers. In [3], [4], and [5] phenomenological modelling techniques have been explored. In [6], semi-phenomenological techniques were used to develop a mathematical model able to describe the hysteretic behavior of the *MR* damper. In [2] and [7] black-box models based on Non-linear Autoregressive with eXogenous terms (*NARX*) structures have been studied.

This study is motivated on the aforementioned challenge that involves the correct modelling of an *MR* damping system. Among the state of the art, the selected models were the ones presented in [5], [6] and a black-box model structure used in [2] and [7]. Experimental data sets were obtained at the mechanical testing laboratory of Metalsa[1]. Section II presents a literature review of *MR* damper models. Section III discusses the experimental setup. Section IV describes the design of experiments. Section V presents the modelling results. Section VI compares the models and the results obtained. Finally, section VII concludes the research. Table I defines the variables that will be used through the paper.

[1] www.metalsa.com.mx

J. A. Ruiz-Cabrera is an MSc student at Tecnológico de Monterrey, Monterrey, NL, México. A00804994@itesm.mx
V. A. Díaz-Salas is an MSc student at Tecnológico de Monterrey, Monterrey, NL, México. A00790521@itesm.mx
R. Morales-Menendez is a full professor at Tecnológico de Monterrey, Monterrey, NL, México rmm@itesm.mx
L. Garza-Castañón is a full professor at Tecnológico de Monterrey, Monterrey, NL, México legarza@itesm.mx
R. A. Ramírez-Mendoza is a full professor at Tecnológico de Monterrey, Ciudad de México, México ricardo.ramirez@itesm.mx

978-1-4244-8092-0/10/$26.00 ©2010 IEEE

TABLE I
VARIABLES

Variable	Description
F_{MR}, f	*MR* damper force
$\dot{f}$	First derivative of *MR* damper force
$\ddot{f}$	Second derivative of *MR* damper force
I, i	Electric current
X, x	Damper piston position
$\dot{x}$	Damper piston velocity
f_0	Damper force offset
a_i	Regressor coefficients
c_i	Model coefficients in [5]
A_1	Dynamic yield force of the *MR* fluid
A_2	Post-yield viscous damping coefficient
A_3	Pre-yield viscous damping coefficient
V_0	Hysteretic critical velocity
X_0	Hysteretic critical displacement

II. LITERATURE REVIEW

A. Previous Work

The research done in [2] compared the semi-physical modified Bouc-Wen model presented in [4] and a black-box *NARX* model structure. The selected *NARX* model structure consisted of two regressors for each input (displacement, velocity) and two regressors for the output force. The performance index utilized for comparing the results was the Error to Signal Ratio (*ESR*), (1). The *ESR* is the ratio of the error estimation (experimental force minus estimated force) and the variance of the experimental force. The index value is 1 if the model is trivial and 0 if the model is perfect.

$$ESR = \frac{\frac{1}{T}\sum_{t=1}^{T}\left(f(t) - \hat{f}(t;v)\right)}{\frac{1}{T}\sum_{t=1}^{T}\left(f(t) - \left(\frac{1}{T}\sum_{i=1}^{T} f(i)\right)\right)^2} \quad (1)$$

Three experiments were made at three different constant input current values of 0.0A (no magnetic field), 0.6A (mid-excitation of the magnetic field, corresponding to a high-viscosity fluid), and 1.2A (high magnetic field, corresponding to a semi-solid fluid). The authors first compared the models using the three experimental data sets in which the electrical current was held constant. Both models were reported to obtain *ESR* values of less than 3%.

In addition, one experiment with varying current was performed. For the semi-physical model, each coefficient was made equal to a time varying linear function of the electric current. For the *NARX* model, two regressors for the input electric current were added. The reported results showed that the semi-physical model was not able to predict the behavior of the damper and obtained an *ESR* value of 22%. On the other hand, the *NARX* model obtained an *ESR* of 4%.

B. State-of-the-art

The model presented in [5] represents a phenomenological model based on the phase shifting dynamics of *MR* dampers. Equation 2 shows the non-linear differential equation, where five parameters need to be determined under a given loading velocity $\dot{x}$.

$$\dot{x} = c_1\ddot{f} + c_2\dot{f} + c_3 f + c_4 f^3 + c_5 f^5 \quad (2)$$

The authors commented that all the coefficients should be functions of the applied magnetic field. This dependency is to be approximated by a polynomial of order 2 and must be identified from experimental data. The parameters for the model were identified using nonlinear least-squares approximation. The model captured the hysteretic behavior of the damper. In addition, hysteresis loops with various loading frequencies, applied field intensities, and excitation amplitudes were all modeled successfully by this model.

Among semi-phenomenological models, the one presented in [6] has been greatly analyzed in the past years. The proposed model shown in (3) is said to describe the bi-viscous and hysteretic behaviors of the *MR* damper with high precision. Nonetheless, the model was not tested for different electric current patterns.

$$f = A_1 tanh\left(A_3(\dot{x} + \frac{V_0}{X_0}x)\right) + A_2\left(\dot{x} + \frac{V_0}{X_0}x\right) \quad (3)$$

In [2], a *NARX* model for an *MR* damper is proposed as shown in (4).

$$\begin{aligned} f_k &= a_1 f_{k-1} + a_2 f_{k-2} + a_3 x_{k-1} + a_4 x_{k-2} \\ &\quad + a_5 \dot{x}_{k-1} + a_1 \dot{x}_{k-2} \end{aligned} \quad (4)$$

The experimentation showed that the most important regressors of the model were the ones for $\dot{x}$ and the old values of f. Two extra regressors were used for electric current consideration.

The results obtained showed that the proposed *NARX* model was able to predict, with high precision, the behavior of the *MR* damper. Furthermore, for the varying current case the *NARX* model was said to outperform by far other phenomenological models.

III. EXPERIMENTAL SETUP

An *MR* damper from a Delphi MagneRide™suspension system was used to perform a total of 28 tests. An MTS™GT controller testing system was used to control the position of the damper, Fig. 2. A Flextest™data acquisition system commanded the controller and recorded the position and force from the *MR* damper. A sampling frequency of 512 Hz was utilized. The bandwidth of displacement was 0.5-14.5 Hz, which lies within normal automotive applications. The displacement and electric current ranges were: 0 - 0.04 m and 0 - 4 A, respectively.

IV. DESIGN OF EXPERIMENTS

A series of training patterns were proposed to be used as position and current inputs for the *MR* damper [8]. As position patterns, Amplitude-Modulated (AM), Frequency-Modulated (FM), Triangular wave with Positive and Negative Variable Slopes (TPNVS), Stepped Frequency Sinusoidal (SFS), Sinusoidal Chirp (CHS), and Road Profile (RP) waves

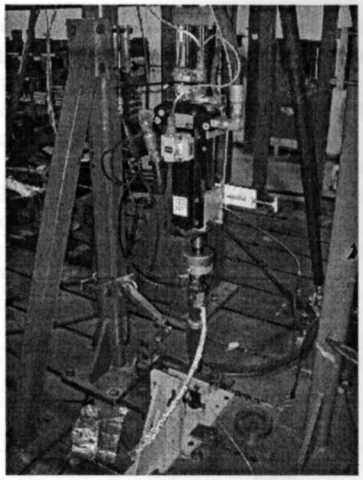

Fig. 2. Experimental system.

TABLE II
DESCRIPTION OF EXPERIMENTAL TESTS

Experiment	Displacement Pattern	Current Pattern	Replicates
1	AM	SC	11
2	TPNVS	SC	11
3	SFS	SC	7
4	FM	ICPS	10
5	RP	APRBS	11
6	SFS	constant	7
7	AM	constant	7
8	TPNVS	constant	7
9	FM	constant	7
10	RP	constant	7

were used. As electric current patterns, Stepped Increments (SC), Increased Clock Period Signal (ICPS), and Amplitude Pseudo Random Binary Signal (APRBS) waves were used. A total of twenty eight tests were performed. Also, various replicates of each test were done.

Ten of these tests were chosen to analyze the performance of a group of models and to make a comparison, Table II.

V. MODELLING RESULTS

Three models were tested to characterize the dynamical behavior of the damper by the performance index *ESR*. Additional modifications were incorporated to the models.

A. NARX Model

The *NARX* model in (4) was modified to consider three regressors for each input variable instead of two. The nine parameters of the model were identified using a recursive least squares method. For each replicate of each experiment, the best parameters for the model were obtained and the *ESR* index was computed. The results are shown in Fig 3. The figure presents a box and whisker plot with one box for each experiment. The boxes have lines at the lower quartile, median, and upper quartile values. The whiskers are lines extending from each end of the boxes to show the extent of the rest of the data. Outliers are data with values beyond the ends of the whiskers.

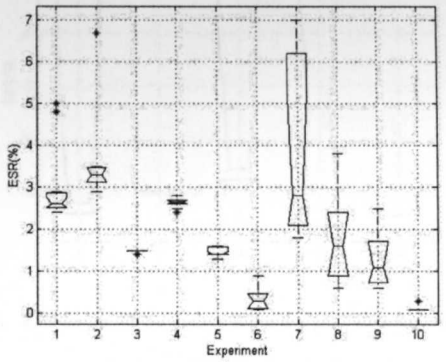

Fig. 3. *ESR* results for the *NARX* model.

Notice that the average *ESR* is less than 5% for every experiment. Experiment ten was observed to obtain the best results.

The *NARX* model was modified by including the dependency on the electric current by adding three regressor, eqn. (5).

$$\begin{aligned} f_k &= a_1 f_{k-1} + a_2 f_{k-2} + a_3 f_{k-3} \\ &\quad + a_4 x_{k-1} + a_5 x_{k-2} + a_6 x_{k-3} \\ &\quad + a_7 \dot{x}_{k-1} + a_8 \dot{x}_{k-2} + a_9 \dot{x}_{k-3} \\ &\quad + a_{10} i_{k-1} + a_{11} i_{k-2} + a_{12} i_{k-3} \end{aligned} \tag{5}$$

The obtained *ESR* values by each experiment are shown in Fig 4.The current dependent model also generated excellent results, with *ESR* averages of less than 3.5%.

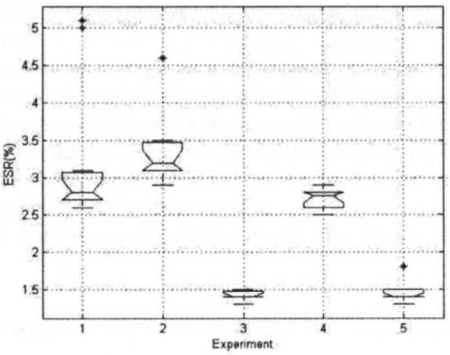

Fig. 4. *ESR* results for the current dependent NARX model.

B. Semi-Phenomenological (S-P) Model

The model shown in (3) was identified for the ten sets of experiments abovementioned. The resulting *ESR* values for

each experiment were observed to be about 50% for all the experiments. Nonetheless the fifth and tenth ones obtained values below 10%.

The *semi-phenomenological* model was not able to predict the damping force in an accurate manner. Then, each of the parameters of the model (A_1, A_2, A_3, V_0, and X_0) was made equal to an second order polynomial dependent on the electric current. For example, A1 = A_{11} + A_{12} I + $A_{13}I^2$. The *ESR* values for the current dependent experiments are shown in Fig 5.

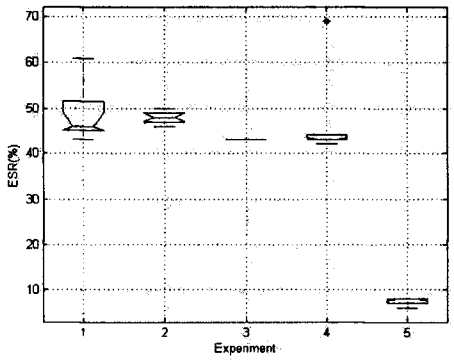

Fig. 5. *ESR* results for the current dependent *semi-phenomenological* model.

Adding the electric current dependency to the *semi-phenomenological* model improved its performance. Nonetheless, the improvements seen may not be worth the inclusion of 10 additional parameters to the model.

C. Phenomenological (P) Model

The model shown in (2) was identified using an optimization algorithm. The relationship shown in (6) was utilized as the objective function in order to capture the dynamics of the damper.

$$f = \frac{1}{c_3}\dot{x} - \frac{c_2}{c_3}\dot{f} - \frac{c_1}{c_3}\ddot{f} - \frac{c_4}{c_3}f^3 - \frac{c_5}{c_3}f^5$$
$$f = C_1\dot{x} + C_2\dot{f} + C_3\ddot{f} + C_4f^3 + C_5f^5 \quad (6)$$

The *ESR* index was used to measure the performance of the model.The results for the ten tests showed that most of the *ESR* values obtained were near 8%.

In order to make the model dependent on the electric current, a modification as in section V-B was included.The *ESR* results are shown in Fig 6.

It can be observed that the variation was increased. Experiments 2 and 5 showed lower *ESR* values, and variance.

VI. COMPARISON

Tables III and IV compare the average *ESR* values obtained by the non-current dependent and current dependent models, respecively. The *NARX* model can be observed to outperform the other models by far. The fifth and tenth

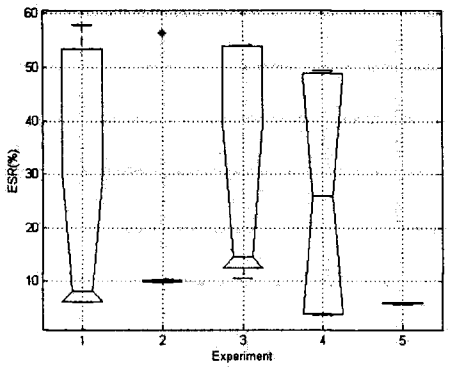

Fig. 6. *ESR* results for the current dependent *phenomenological* model.

TABLE III
COMPARISON OF *ESR*(%) BY EXPERIMENT FOR NON-CURRENT DEPENDENT MODELS

	Experiment									
Model	1	2	3	4	5	6	7	8	9	10
NARX	3	4	2	3	1	0.4	4	2	1	0.1
S-P	52	51	53	49	10	37	38	49	44	3
P	8	13	16	7	7	9	9	10	4	4

experiments were found to consistently obtain the lowest *ESR* values for all models. For the *NARX* model, the addition of the dependency on the electric current improved the average of the *ESR*. Nonetheless, the improvements on the indexes did not surpass 1%.

On the other hand, the *semi-phenomenological* model obtained acceptable results only for the experiments where an *RP* displacement pattern was used. The addition of the electric current dependency to the model was seen to improve its performance, but only slightly. It is to be remembered that ten additional parameters were included to the model for this purpuse.

The *phenomenological* model was seen to obtain low *ESR* values for most of the experiments. Notable results were met for the *FM* and *RP* profile displacement patterns. It was also seen that the inclusion of the electric current dependency improved the results obtained by the model, but increased the variation on the index results.

Fig 7 shows experimental and estimated forces compared

TABLE IV
COMPARISON OF *ESR* (%) BY EXPERIMENT FOR CURRENT DEPENDENT MODELS

	Experiment				
Model	1	2	3	4	5
NARX	3	3	1	3	1
S-P	49	48	43	46	7
P	6	10	13	4	6

by each current dependent model. The data belongs to experiment five and it is shown for a two second window.For experiment five, the *phenomenological* model can be seen to exceed the amplitude of the experimental data at the positive and negative peaks, while the *NARX* and *semi-phenomenological* models fall short most of the time.

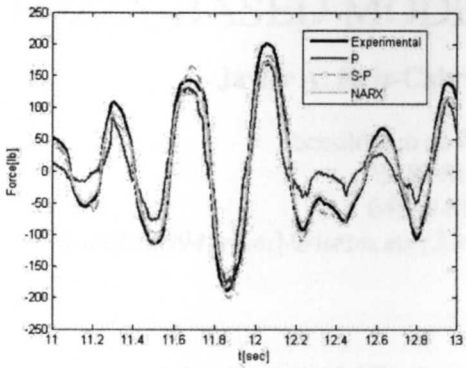

Fig. 7. Comparison of experimental and estimated forces by model for experiment five.

In Fig 8 and 9, the experimental and estimated force-velocity dynamics are shown for the *semi-phenomenological* and *phenomenologicalv* models, respectively. The data used corresponds to experiment four and the models are dependent on the electric current.

Notice that while the *phenomenological* model is able to closely mimic the dynamics of the *MR* damper, the *semi-phenomenological* model struggles to resemble the hysteretic behavior at the cero velocity line.

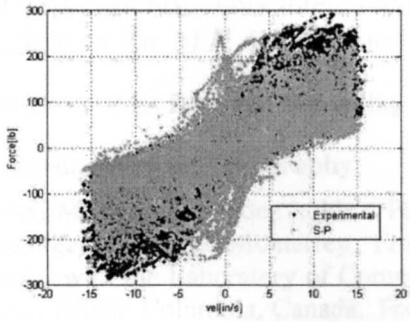

Fig. 8. Comparison of experimental and estimated forces by the current dependent *semi-phenomenological* model for experiment four.

VII. CONCLUSIONS

It can be concluded that the *road profile* displacement signals allow a lower *ESR* index because the bandwidth of the pattern is in the automotive operational zone of the damper. For the constant current experiments, the *phenomenological* model had the best compromise between performance and

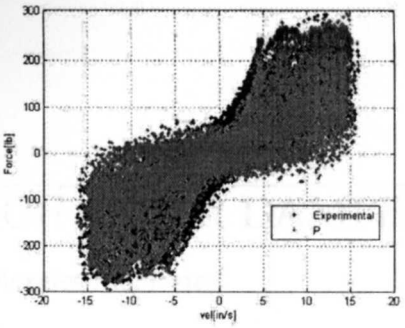

Fig. 9. Comparison of experimental and estimated force by the current dependent *phenomenological* model for experiment four.

simplicity. The model had an average *ESR* 30% less than that of the *semi-phenomenological* model and only 6% greater than that of the *NARX* one. Also, using only five coefficients the *phenomenological* model obtained results comparable to those of the nine coefficient *NARX* model.

The addition of the dependancy on the current was seen to improve the performance of the three models. Nonetheless, the minimum improvement may not be worth the addition of extra parameters to the models.

VIII. ACKNOWLEDGMENTS

Authors thank J. Lozoya-Santos for providing the experimental data. Also thank the Autotronics and Supervision and Advanced Control research chairs at Tecnológico de Monterrey for their partial support.

REFERENCES

[1] I.A. Brigadnov and A. Dorfmann. Mathematical Modeling of Magnetorheological Fluids. *Continuum Mech. Thermodyn.*, 17:29–42, 2005.

[2] S. M. Savaresi, S. Bittanti, and M. Montiglio. Identification of Semi-Physical and Black-Box Non-Linear Models: the Case of MR-Dampers for Vehicles Control. *Automatica,*, 41(1):113–127, 1 2005.

[3] N. M. Kwok, Q. P. Ha, T. H. Nguyen, J. Li, and B. Samali. A Novel Hysteretic Model for Magnetorheological Fluid Dampers and Parameter Identification using Particle Swarm Optimization. *Sensors and Actuators A: Physical*, 132(2):441–451, 11/20 2006.

[4] BF Spencer, SJ Dyke, MK Sain, and JD Carlson. Phenomenological Model of a MR Damper. *ASCE Journal of Engineering Mechanics*, 1996.

[5] L X Wang and H Kamath. Modelling Hysteretic Behaviour in MR Fluids and Dampers using Phase-Transition theory. *Smart Mater. Struct.*, 15:1725–1733, 2006.

[6] Shuqi Guo, Shapou Yang, and Cunzhi Pan. Dynamical Modeling of Magneto-Rheological Damper Behaviors. *Intelligent Material Systems and Structures*, 17:3–14, 2006.

[7] E. Niño-Juarez, R Morales-Menendez, R Ramirez-Mendoza, and L Dugard. Minimizing the Frecuency in a Black Box Model of a Magneto-Rheological Damper. In *11th Mini Conf on Vehicle Sys. Dyn., Ident. and Anomalies*, 2008.

[8] J. Lozoya-Santos, R. Morales-Menendez, and R. A. Ramirez-Mendoza. Design of Experiments for MR Damper Modelling. In *17th International Joint Conference on Neural Networks*, pages 1915–1922, 2009.

FUZZY-BASED MODELLING OF AN MR DAMPER

Javier A. Ruiz-Cabrera[1], Ruben Morales-Menendez[2]

Tecnológico de Monterrey, campus Monterrey
[1]MSc Student, [2]Full Professor
64849 Monterrey, NL., Mexico
{a00804994, rmm}@itesm.mx (Javier A. Ruiz-Cabrera, Ruben Morales-Menendez)

Abstract

A Magneto-Rheologial (MR) damper exhibits a hysteretic and non-linear behavior. This behavior makes it a challenge to develop a model for this system. The present research is centered on proposing and analyzing two different fuzzy models of an MR damper based on experimental data. The first model uses an Adaptive Neuro-Fuzzy Inference System ($ANFIS$) and the second combines fuzzy methods with semi-phenomenological models. The results showed that fuzzy modelling can be a powerful framework to capture the behavior of highly non-linear systems. Among the various input patterns analized, stepped electric current signals allowed a better training of the $ANFIS$ model. Both proposed structures obtained Error to Signal Ratio (ESR) values of less than 0.1 for the majority of the experiments. This intensive experimental study confirmed previous theoretic work done for MR damper model fitting.

Keywords: MR Damper, Modelling, Fuzzy, ANFIS, Non-Linear Systems.

Presenting Author's Biography

Ruben Morales-Menendez holds a PhD Degree in Artificial Intelligence from Tecnológico de Monterrey. From 2000 to 2003, he was a visiting scholar with the Laboratory of Computational Intelligence at the University of British Columbia, Canada. For more than 23 years, he has been a consultant specializing in the analysis and design of automatic control systems for continuous processes. He is a member of the National Researchers System of Mexico (Level I) and a member of IFAC TC 9.3.

1 Introduction

Magneto-Rheological (MR) fluids are non-colloidal suspensions of particles with a size on the order of a few microns [1]. These fluids are unique due to their ability to change their properties reversibly between fluid and solid-like states in milliseconds upon the application of a magnetic field.

Among a broad spectrum of applications, MR fluids have been widely utilized for vibration damping systems. In the past decade, there has been an increasing interest of scientists and engineers on these MR fluid dampers and their applications [2]. MR fluids are appealing for damping systems since they can operate at temperatures ranging from 40 to 150 °C with only slight variations in the yield stress. Additionally, MR fluids are almost insensitive to impurities and can be controlled with low voltages (12-24 V) and an electric current driven power supply outputting 1-2 A [3].

An MR damper can be regarded as a semi-active suspension system. These systems offer the reliability of passive devices, but maintain the versatility and adaptability of active systems. A semi-active MR damper is a non-linear dynamical system, where the inputs can be the elongation speed and the electric current. The current is the control input that modulates the damping characteristic of the MR fluid through the variation of a magnetic field. The output is the force delivered by the damper.

Although MR dampers are greatly promising for control scenarios, their major drawback lies on their nonlinear and hysteretic behavior, Fig. 1. Furthermore, the design of a controller generally requires to model the system, which becomes a non-trivial task when it comes to MR dampers [4].

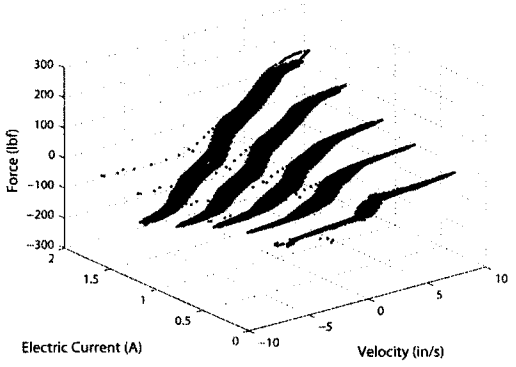

Fig. 1 MR damper behavior. Force is plotted against velocity at five electric current inputs.

In [5], an Adaptive Neuro-Fuzzy Inference System ($ANFIS$) was explored for fitting simulated data obtained with the Spencer model, [2]. The $ANFIS$ was proven to fit the simulated data to an acceptable degree. Similar results can be observed in [6] and [7].

The present study is motivated on the aforementioned challenge that involves the correct modelling of an MR damping system. Two fuzzy models are proposed and analyzed. Experimental data sets were obtained at the mechanical testing laboratory of Metalsa [1]. Section 2 presents a literature review. Section 3 discusses the experimental setup and design of experiments (DoE). Sections 4 and 5 describe the models proposed and the results. Section 6 discusses the results. Finally, section 7 concludes the research.

Tab 1 defines the variables that will be used through the paper.

Tab. 1 Variables.

Variable	Description
x(t)	Linear displacement, in
v(t)	Linear velocity, in/s
i(t)	Electric current, A
F(t)	MR Damper output force, lbf
$\hat{F}$(t)	Estimated MR damper force, lbf
T	Total number of discrete samples

2 Literature Review

2.1 MR Damper Modelling

Different modelling techniques have been studied for MR dampers. In [2], [8], and [4] phenomenological modelling techniques have been explored in order to obtain MR damper models. In [9], semi-phenomenological techniques were used to develop a mathematical model able to describe the hysteretic behavior of the MR damper. The research done in [3] compared three different model structures for the MR damper including a black-box one based on Non-linear ARX ($NARX$) models. The performance index selected by the author for comparing the results was the Error to Signal Ratio (ESR). The index value is one if the model is trivial and zero if the model is perfect. The definition for the ESR is shown in Eq. 1 taken from [3], where T indicates the total number of discrete samples.

$$ESR = \frac{\frac{1}{T}\sum_{t=1}^{T}\left(F(t) - \hat{F}(t)\right)}{\frac{1}{T}\sum_{t=1}^{T}\left(F(t) - \left(\frac{1}{T}\sum_{j=1}^{T}F(j)\right)\right)^2} \quad (1)$$

2.2 Fuzzy Modelling

A Takagi-Sugeno-Kang (TSK) fuzzy model can be selected for modelling complex systems. The fuzzy rules of the model can be determined by adaptively generating them based on input and output data or by selecting them by hand. The inputs of the model are fuzzy and the outputs are crisp. The total output of the system is calculated using the weighted average of the output functions [6]. The system can use a hybrid learn-

[1] www.metalsa.com.mx

ing algorithm that combines the backpropagation gradient descent and least squares methods. A TSK fuzzy model trained in this manner is often named Adaptive Neuro-Fuzzy Inference System ($ANFIS$).

If a first-order $ANFIS$ consists of three inputs and one output (each input with three possible membership functions), and only three fuzzy rules are selected as shown in Eqs. 2 - 4,

$$\begin{aligned} &If\ x(t)\ is\ A_1\ and\ v(t)\ is\ B_1\ and\ i(t)\ is\ C_1 \\ &then\ f_1(t) = p_1x(t) + q_1v(t) + r_1i(t) + s_1 \end{aligned} \tag{2}$$

$$\begin{aligned} &If\ x(t)\ is\ A_2\ and\ v(t)\ is\ B_2\ and\ i(t)\ is\ C_2 \\ &then\ f_2(t) = p_2x(t) + q_2v(t) + r_2(t) + s_2 \end{aligned} \tag{3}$$

$$\begin{aligned} &If\ x(t)\ is\ A_3\ and\ v(t)\ is\ B_3\ and\ i(t)\ is\ C_3 \\ &then\ f_3(t) = p_3x(t) + q_3v(t) + r_3i(t) + s_3 \end{aligned} \tag{4}$$

where $x(t)$, $v(t)$, and $i(t)$ are input language variables; A_j, B_j, and C_j are fuzzy sets; $f_1(t)$, $f_2(t)$ and $f_3(t)$ are output language variables; p_j, q_j, r_1, and s_j are the output parameters of the fuzzy system, then Fig. 2 would represent the $ANFIS$ structure for the first-order fuzzy system. The W_j and Wn_j represent the degree of fitness and the normalized fitness of the fuzzy rules, respectively.

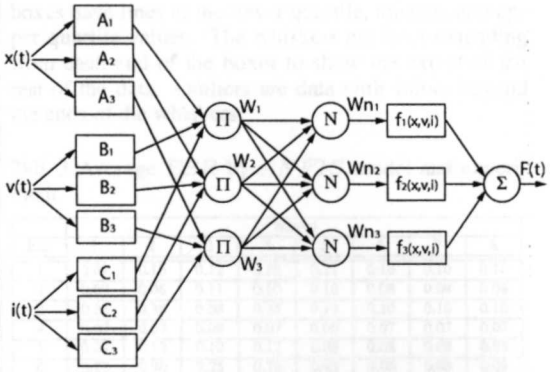

Fig. 2 $ANFIS$ structure of a first-order fuzzy model with three inputs and one output. For simplicity, only three fuzzy rules, out of the 27 possible combinations, are considered.

3 Experimental System

A Delphi MagneRide^{TM} MR damper was used to perform a total of 29 tests [10] . An MTS^{TM}GT controller testing system was used to control the position of the damper. A Flextest^{TM}data acquisition system commanded the controller and recorded the position and force of the MR damper, as well as the electric current on the coil. A sampling frequency of 512 hertz was used. The bandwidth of displacement was 0.5 - 14.5 Hz, which lies within normal automotive applications. The experimental setup is shown in Fig. 3.

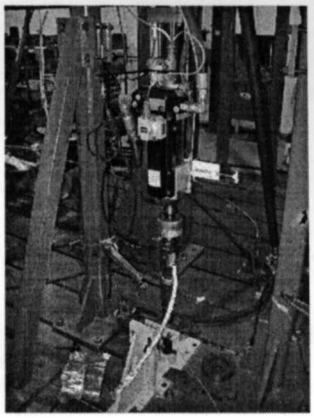

Fig. 3 Experimental setup.

Eight of the 29 tests were chosen for this study. In the experiments, the electric current, $i(t)$, patterns were Stepped Increments (SC), Increased Clock Period Signal ($ICPS$), Pseudo Random Binary Signal ($PRBS$), and Amplitude $PRBS$ ($APRBS$). Road Profile (RP) signals were used as the displacement, $x(t)$, input pattern. The RP signals reach a maximum amplitude of 0.5 in and emulate the dynamics of a damper used in automotive applications. Various replicates of the experiments were performed and used as validation data. The specific patterns of the eight experiments are shown in Tab. 2. Fig. 4 shows the patters used for experiments three and four. For experiments six to eight, stepped increments of 0, 0.4, 0.8, 1.2, 1.6, 2.1, and 2.5 A, each with a duration of 30 seconds, were utilized. The seven replicates for the last three experiments correspond to the seven constant current stepped increments.

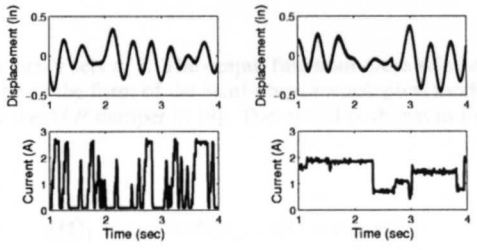

(a) Exp. 3. (b) Exp. 4.

Fig. 4 Displacement and electric current patterns for experiments 3 and 4. Both experiments were done using an RP displacement pattern and $PRBS$ and $APRBS$ electric current signals, respectively.

4 ANFIS Model

An $ANFIS$ structure was proposed for modelling the MR damper. Displacement, velocity, and electric cur-

Tab. 2 Experiments

Exp.	Displacement Pattern	E. Current Pattern	Replicates
1	Smooth Highway RP	ICPS	11
2	Smooth Highway RP	APRBS	11
3	Smooth Highway RP	PRBS	11
4	Long Duration RP	APRBS	3
5	Long Duration RP	ICPS	4
6	RP	SC	7
7	RP	SC	7
8	RP	SC	7

rent were used as inputs, and the damper force was the output. The model resembles the one in Fig. 2, but contains 27 fuzzy rules for all possible combinations of inputs. Three Gaussian membership functions were utilized to fuzzify each input. The outputs of the system were selected as linear functions.

One $ANFIS$ model was trained using the first replicate of each set of experimental data after being normalized. The training was done until the error decreased by less than a threshold. Then, the eight trained $ANFIS$ models were validated using the experimental data. The $ANFIS$ models were named after the experiment with which they were trained. Tab. 3 presents the average ESR obtained by the models when validated with the experimental data sets.

The box plots on Fig. 5 and 6 show the ESR obtained by models 1 and 7. The figures present a box and whisker plot with one box for each experiment. The boxes have lines at the lower quartile, median, and upper quartile values. The whiskers are lines extending from each end of the boxes to show the extent of the rest of the data. Outliers are data with values beyond the ends of the whiskers.

Tab. 3 Average ESR by $ANFIS$ model and experiment.

	Model							
Exp	1	2	3	4	5	6	7	8
1	0.07	0.15	0.12	0.22	0.21	0.10	0.10	0.10
2	0.09	0.06	0.11	0.10	0.10	0.08	0.08	0.08
3	0.33	0.36	0.08	0.35	0.19	0.10	0.10	0.10
4	0.07	0.07	0.09	0.07	0.06	0.07	0.07	0.07
5	0.09	0.12	0.10	0.12	0.08	0.08	0.08	0.08
6	0.22	0.90	0.25	0.78	0.45	0.06	0.08	0.09
7	0.53	1.69	0.68	2.04	1.99	0.09	0.07	0.12
8	1.02	8.96	1.07	1.47	0.62	0.11	0.07	0.05

5 Non-Linear Fuzzy Model

A TSK non-linear fuzzy model [11] was proposed for the MR damper. Using the electric current as input for the model, fuzzy rules were proposed as specified in Eq 5.

$$If\ i(t)\ is\ A_j\ then\ f(t)_j = g_j(x(t), v(t)) \quad (5)$$

Notice that each output function $f(t)_j$ depends on the displacement and the velocity of the MR damper. A_j are fuzzy sets of i. The output functions were selected to be of the form of the semi-phenomenological model for the MR damper in [9]. The model is shown in Eq. 6,

$$\begin{aligned} f(t)_j = c_{1j}\ tanh\left(c_{2j}\ (v(t) + c_{3j}\ x(t))\right) \\ + c_{4j}\ (v(t) + c_{3j}\ x(t)) \end{aligned} \quad (6)$$

where the coefficients c_{1j}, c_{2j}, c_{3j}, and c_{4j} are to be determined from experimental data.

The overall output force of the damper is computed as specified by Eq. 7,

$$F(t) = \frac{\sum_{j=1}^{7} W_j(i(t))\ f(t)_j}{\sum_{j=1}^{7} W_j(i(t))} \quad (7)$$

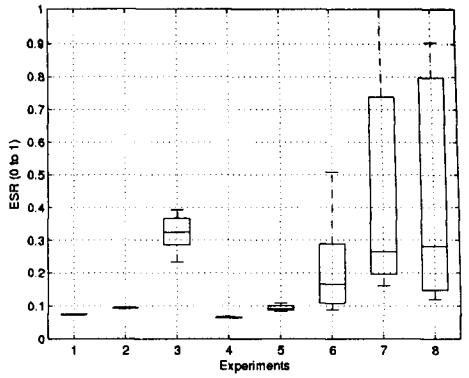

Fig. 5 ESR by experiment for $ANFIS$ model 1. The error of the model greatly increased when validated with experiments 3 and 6 to 8.

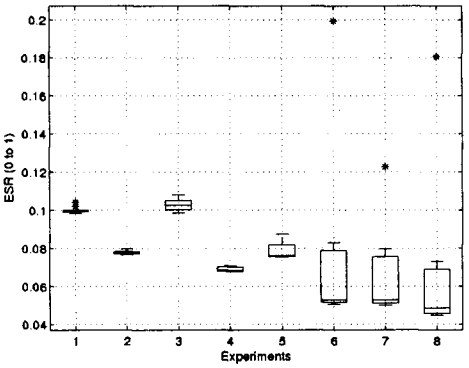

Fig. 6 ESR by experiment for $ANFIS$ model 7. The error of the model remained below 0.1 for all experiments. The outliers on the validation with experiments 6 to 8 correspond to zero input electric current.

where W_j represents the membership degree of $i(t)$ on each of the membership functions. As Eq. 6 only depends on the displacement and velocity of the damper, the coefficients were identified using experiments six to eight. The fitting algorithm selected was non-linear least squares and yielded one non-linear equation for each of the seven electric current stepped increments on the experiments. In this way, one non-linear fuzzy model was obtained from experiment 6, one from experiment 7, and one from experiment 8. The fuzzy models were labeled according to the experiments with which they were trained. Fig. 7 depicts the proposed fuzzy structure.

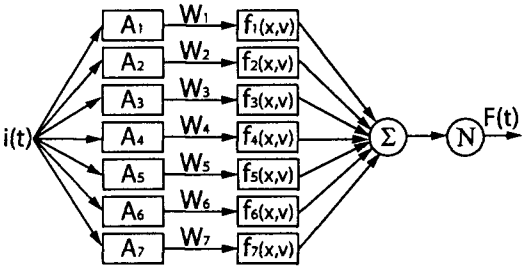

Fig. 7 Non-linear fuzzy model structure with one input and one output. Seven possible input membership functions are considered.

The input membership functions for each model were defined as seven Gaussian functions with a variance equal to 0.2 and means of 0, 0.4, 0.8, 1.2, 1.6, 2.1, and 2.5 A, respectively. Additionally, seven output functions were selected in the form of Eq. 6 with coefficients previously identified.

The proposed models were validated using the eight sets of experimental data. The box plots on Figs. 8 - 10 present the resulting ESR by experiment.

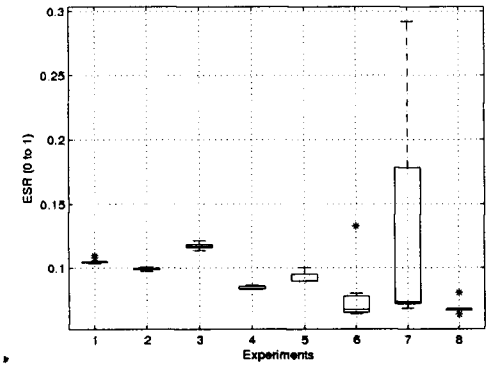

Fig. 8 ESR by experiment for fuzzy model 6. The error of the model remained below 0.12 for most of the experiments. The variance greatly increased for experiment 7.

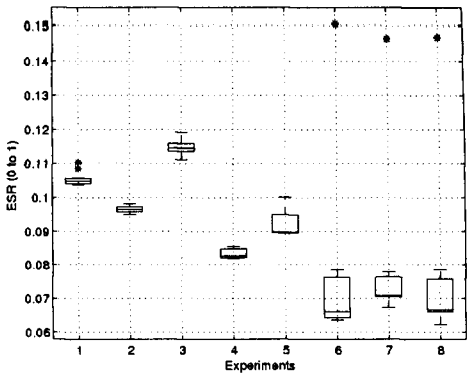

Fig. 9 ESR by experiment for fuzzy model 7. The error of the model constantly remained below 0.12. The outliers on the validation with experiments 6 to 8 correspond to zero input electric current.

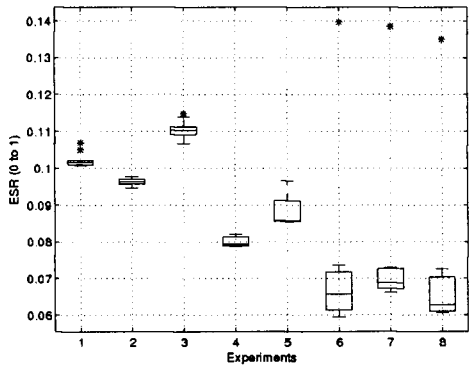

Fig. 10 ESR by experiment for fuzzy model 8. The error of the model constantly remained below 0.11. The outliers on the validation with experiments 6 to 8 correspond to zero input electric current.

6 Discussion

The $ANFIS$ structure obtanined ESR values of approximately 0.1 when trained using experimental data with constant electric current stepped increments. Nonetheless, the ESR variance increased considerably when validated with constant electric current experiments (Fig. 6). The outliers on the plot correspond to experiments with zero electric current. On the other hand, $ANFIS$ structures trained using experimental data with varying electric current could not predict the output force of the damper when validated with constant electric current inputs.

Surprisingly low ESR values were constantly obtained by the proposed non-linear fuzzy structure. Excelent results were seen with fuzzy model 6, except when validated with experiment 7. With fuzzy models 7 and 8

the outliers observed on the resulting ESR validation box plots correspond to experiments with zero electric current. Additionally, for both proposed structures, the ESR variance increased when validated with constant electric current experiments.

Tab. 4 presents the average ESR obtained by both the $ANFIS$ and non-linear fuzzy structures. Notice that, if classified by the average error, $ANFIS$ models 6 to 8 and the three fuzzy models are the best options for modelling the MR damper.

Tab. 4 Average ESR by model.

Model	Average ESR
$ANFIS$ 1	0.30
$ANFIS$ 2	1.44
$ANFIS$ 3	0.30
$ANFIS$ 4	0.62
$ANFIS$ 5	0.45
$ANFIS$ 6	0.09
$ANFIS$ 7	0.08
$ANFIS$ 8	0.09
Fuzzy 6	0.10
Fuzzy 7	0.09
Fuzzy 8	0.09

When comparing the complexity of the structures, the proposed non-linear fuzzy model is crearly less complex than the $ANFIS$ one. The first is composed of 27 rules, whereas the latter contains only seven. Nonetheless, the advantage of the $ANFIS$ structure lies in its use of simple linear output functions instead of non-linear ones.

The present study confirmed the work done in [5], [6], and [7] for model fitting and extended it to experimental data. As mentioned in [6], it was proved that an $ANFIS$ structure can succesfully capture the dynamics of an MR damper and can be a useful tool for control. In addition, the results obtained by the proposed non-linear fuzzy structure extended the capabilities of the model in [9] to varying electric current scenarios.

Further work may address the use of different phenomenological models of the MR damper as output functions for the non-linear fuzzy structure. Additionally, the non-linear fuzzy model may benefit from the inclusion of more input membership functions.

7 Conclusion

The results obtained showed that fuzzy-based modelling can be a powerful method for describing the behavior of highly non-linear systems. As opposed to phenomenological techniques, fuzzy methods do not requiere a profound knowledge of the dynamics of the system. After validating the $ANFIS$ structures, experiments with stepped increments of the electric current allowed for a better training of the models and obtained average ESR values of less than 0.1. The proposed non-linear fuzzy structure succesfully combined fuzzy methods with semi-phenomenological modelling. The three trained non-linear fuzzy models obtained average ESR values of less than 0.1.

8 Acknowledgments

The authors thank J. Lozoya-Santos for providing the experimental data. Also, thank the Autotronics and Supervision and Advanced Control research chairs at Tecnológico de Monterrey for their partial support.

9 References

[1] I.A. Brigadnov and A. Dorfmann. Mathematical Modeling of Magnetorheological Fluids. *Continuum Mech. Thermodyn.*, 17:29–42, 2005.

[2] B.F. Spencer, S.J. Dyke, M.K. Sain, and J.D. Carlson. Phenomenological Model of a MR Damper. *ASCE Journal of Engineering Mechanics*, 1996.

[3] S.M. Savaresi, E. Siciliani, and S. Bittanti. Acceleration Driven Damper (ADD): an Optimal Control Algorithm for Comfort Oriented Semi-Active Suspensions. *ASME Transactions: Journal of Dynamic Systems, Measurements and Control*, 127(2):218–229, 2005.

[4] N. M. Kwok, Q. P. Ha, T. H. Nguyen, J. Li, and B. Samali. A Novel Hysteretic Model for Magnetorheological Fluid Dampers and Parameter Identification Using Particle Swarm Optimization. *Sensors and Actuators A: Physical*, 132(2):441–451, 11/20 2006.

[5] K. C. Schurter and P. N. Roschke. Fuzzy Modeling of a Magnerorheological Damper Using ANFIS. *Fuzzy Systems, 2000. FUZZ IEEE 2000. The Ninth IEEE International Conference on*, 1:122–127, May 2000.

[6] H. Wang and H. Hu. The Neuro-Fuzzy Identification of MR Damper. *Fuzzy Systems and Knowledge Discovery, 2009. FSKD '09. Sixth International Conference on*, 6:464 – 468, 2009.

[7] H. Du and N. Zhang. Evolutionary Takagi-Sugeno Fuzzy Modelling for MR Damper. *Hybrid Intelligent Systems, 2006. HIS '06. Sixth International Conference on*, pages 69–69, 2006.

[8] L. X. Wang and H. Kamath. Modelling Hysteretic Behaviour in MR Fluids and Dampers Using phase-Transition theory. *Smart Mater. Struct.*, 15:1725–1733, 2006.

[9] S. Guo, S. Yang, and C. Pan. Dynamical Modeling of Magneto-rheological Damper Behaviors. *Intelligent Material Systems and Structures*, 17:3–14, 2006.

[10] J. Lozoya-Santos, R. Morales-Menendez, and R. A. Ramirez-Mendoza. Design of Experiments for MR Damper Modelling. *17th International Joint Conference on Neural Networks*, pages 1915–1922, 2009.

[11] H. T. Nguyen, N. R. Prasad, C. L. Walker, and E. A. Walker. *A First Course in Fuzzy and Neural Control*, volume 1. Chapman and Hall/CRC, November 2002.